Contract No:

This document was prepared in conjunction with work accomplished under Contract No. DE-AC09-08SR22470 with the U.S. Department of Energy (DOE) Office of Environmental Management (EM).

Disclaimer:

This work was prepared under an agreement with and funded by the U.S. Government. Neither the U. S. Government or its employees, nor any of its contractors, subcontractors or their employees, makes any express or implied:

1) warranty or assumes any legal liability for the accuracy, completeness, or for the use or results of such use of any information, product, or process disclosed; or
2) representation that such use or results of such use would not infringe privately owned rights; or
3) endorsement or recommendation of any specifically identified commercial product, process, or service.

Any views and opinions of authors expressed in this work do not necessarily state or reflect those of the United States Government, or its contractors, or subcontractors.

We put science to work.™

Savannah River National Laboratory™

OPERATED BY SAVANNAH RIVER NUCLEAR SOLUTIONS

A U.S. DEPARTMENT OF ENERGY NATIONAL LABORATORY • SAVANNAH RIVER SITE • AIKEN, SC

Corrosion Testing of Monofrax™ K-3 Refractory in Defense Waste Processing Facility (DWPF) Alternate Reductant Feeds

M. S. Williams

C. M. Jantzen

P. R. Burket

April 6, 2016

SRNL-STI-2016-00030, Revision 0

SRNL.DOE.GOV

DISCLAIMER

This work was prepared under an agreement with and funded by the U.S. Government. Neither the U.S. Government or its employees, nor any of its contractors, subcontractors or their employees, makes any express or implied:

1. warranty or assumes any legal liability for the accuracy, completeness, or for the use or results of such use of any information, product, or process disclosed; or
2. representation that such use or results of such use would not infringe privately owned rights; or
3. endorsement or recommendation of any specifically identified commercial product, process, or service.

Any views and opinions of authors expressed in this work do not necessarily state or reflect those of the United States Government, or its contractors, or subcontractors.

Printed in the United States of America

Prepared for
U.S. Department of Energy

SRNL-STI-2016-00030
Revision 0

Keywords: *corrosion, refractory, K-3, glass, alternate reductant, DWPF, materials of construction*

Retention: *Permanent*

Corrosion Testing of Monofrax™ K-3 Refractory in Defense Waste Processing Facility (DWPF) Alternate Reductant Feeds

M. S. Williams
C. M. Jantzen
P. R. Burket

April 6, 2016

Prepared for the U.S. Department of Energy under contract number DE-AC09-08SR22470.

Savannah River National Laboratory™
OPERATED BY SAVANNAH RIVER NUCLEAR SOLUTIONS

REVIEWS AND APPROVALS

AUTHORS:

_____
M. S. Williams, Environmental & Chemical Process Technology Research Programs Date

_____
C. M. Jantzen, Environmental & Chemical Process Technology Research Programs Date

_____
P. R. Burket, Environmental & Chemical Process Technology Research Programs Date

TECHNICAL REVIEW:

_____
K. J. Imrich, Materials Science and Technology, Reviewed per E7 2.60 Date

APPROVAL:

_____
F. M. Pennebaker, Manager Date
Environmental & Chemical Process Technology Research

_____
D. E. Dooley, Director, Environmental & Chemical Process Technology Research Date

_____
E. J. Freed, Manager Date
DWPF Engineering, Savannah River Remediation

ACKNOWLEDGEMENTS AND PREFACE

The authors would like to thank fellow researchers in the Environmental & Chemical Process Technology Research Programs (E&CPT), Analytical Development (AD) and Process Technology Programs of the Savannah River National Laboratory (SRNL) who assisted in performance and characterization of the corrosion tests and analyses. For assistance preparing feeds: Jon Duval and Frances Williams of E&CPT. For assistance cutting crucibles: Gary Dobos and Curt Sexton of the SRNL glass shop. For assistance with SEM analyses: Catherine Brown, Pat O'Rourke, and Henry Ajo of AD.

This research and report were prepared in connection with work done under Contract No. DE-AC09-08SR22470 with the U.S. Department of Energy.

EXECUTIVE SUMMARY

The Defense Waste Processing Facility (DWPF) at the Savannah River Site (SRS) uses a combination of reductants and oxidants while converting high level waste (HLW) to a borosilicate waste form. A reducing flowsheet is maintained to retain radionuclides in their reduced oxidation states which promotes their incorporation into borosilicate glass. For the last 20 years of processing, the DWPF has used formic acid as the main reductant and nitric acid as the main oxidant. During reaction in the Chemical Process Cell (CPC), formate and formic acid release measurably significant H_2 gas which requires monitoring of certain vessel's vapor spaces. A switch to a nitric acid-glycolic acid (NG) flowsheet from the nitric-formic (NF) flowsheet is desired as the NG flowsheet releases considerably less H_2 gas upon decomposition. This would greatly simplify DWPF processing from a safety standpoint as close monitoring of the H_2 gas concentration could become less critical. In terms of the waste glass melter vapor space flammability, the switch from the NF flowsheet to the NG flowsheet showed a reduction of H_2 gas production from the vitrification process as well. [1] [2] Due to the positive impact of the switch to glycolic acid determined on the flammability issues, evaluation of the other impacts of glycolic acid on the facility must be examined.

During processing in the CPC, the glycolic acid is not completely consumed and is carried forward to the melter, either as acid or anion. During the processing steps, entrainment or carryover could occur sending glycolate species to other HLW facilities downstream of DWPF. The impact of the acid or anion on the corrosion of the materials of construction (MOC) throughout the waste processing system has been previously evaluated. As a part of this evaluation, there was an opportunity to examine the MOC of the melter using the Cold cap Evaluation Furnace (CEF). [3] The Monofrax™ K-3 refractory was immersed in the CEF by being mounted in a cage on the argon bubbler directly above the bubbler opening. Due to the proximity of the coupon to the bubbles, cavitation on the refractory brought the corrosion measurements into question. In order to address the issues observed in the CEF testing, the current study was performed with K-3 refractory in contact with non-radioactive simulants in alumina crucibles, but without the presence of an argon bubbler to evaluate the corrosion due to the melter feed oxidants and reductants at melter temperature.

Four simulant sludges were identified that were processed with varying acid ratios and stoichiometry of oxidants and reductants. These feeds were the CEF feed as-received prepared by Harrell Industries with frit added (CEF-2 SRAT), the more oxidized remediated Harrell melter feed (CEF-2 SME), and two melter feeds prepared from the Scaling Study (GN78 and GN79). A Monofrax™ K-3 refractory (K-3) brick was cut into matchsticks for this testing so that a hot wall face (the as-fabricated face of the brick facing the DWPF melt pool) and a cut face were both exposed to the feeds during the feed-to-glass transition.

The conclusions of this study showed the following:

> The general corrosion mechanisms observed in the NG flowsheet are the same as those observed in the NF testing over the last 20+ years. Observations include Mg and Al depletion in the general corrosion region as these cations from the brick are dissolved into the molten glass and penetration of Ni from the glass into the reaction products causing spalling of Ni-Fe-Cr spinels at the refractory-glass interface.
>
> The 5 day general corrosion rates of NG glasses (all oxidant/reductant permutations studied) were less than that of the Black Frit 165 standard glass utilized for the last 20+ years. Accelerated corrosion rates exist during the early contact with glass (1/16-1 day) and this acceleration dissipates over the longer time period of the 5 day test performed when steady state corrosion is

achieved. The steady state corrosion rates of the NG glasses are equal to or less than the rate observed with the standard glass. The NG glasses are below the DWPF design basis as the design basis was determined based on 7 day ASTM testing which is after steady state corrosion rates were achieved.

Selective depletion of dense Fe^0 metallic species from within the refractory beyond the general corrosion regions at the refractory-glass interface was observed. This corresponds to the Fe^0 depletion noted in the K-3 coupon tested during the CEF-2 campaign. Exacerbating this metallic depletion was the fact that, during the CEF-2 testing, excess nitric acid was added to the melter feed to adjust the measured REDOX values. Per the revised interim REDOX model, the total molar amount of nitric acid in the CEF-2 melter feed was atypical and resulted in a fully oxidized glass product. With the implementation of the revised interim REDOX model, the remediation would likely have not been performed as the amounts of nitric and glycolic acid are dictated by the balance required to achieve a targeted REDOX ratio. [4] Even so, in typical NG flowsheet sludge, a higher fraction of nitric acid is required than in the NF flowsheet, transferring more nitric acid to the DWPF melter. The corrosive nature of nitrate in the presence of metallic species is well known. This is likely the cause of the significant Fe^0 depletion at depth in the refractory beneath the observed general corrosion front. Since bubbling was not a variable in this experiment, the cavitation was not a possible contributing factor to the corrosion/erosion/depletion observed.

Further testing in the future is recommended to bridge the gap between the non-bubbled crucible testing documented in this study and the previous bubbled testing in the CEF. This testing could provide better examination of the effects of time and chemical changes as well as increased melt pool agitation and convection on formation and removal of spinel reaction products and the overall general corrosion. Therefore, the following testing is recommended to be done in the future:

1. The original risk of excessive erosion/corrosion of the DWPF melter refractory material due to bubbler implementation was closed in revision 10 of document Y-RAR-G-00022. However, future testing of the effects of bubbling could still be important to the overall understanding of the corrosion behavior of the K-3 refractory. The following work is recommended:
    a. Perform modified ASTM C621 tests in NG feeds with bubbling to determine the extent of the impact of agitation on the general corrosion. Placement of the coupon should include testing both directly in line with the bubbles and significantly separated from the bubblers in order to examine the long range impact of the bubbles and their ability to generate erosion and cavitation at a distance.
    b. Perform various scale melter tests (i.e. QMRF, SMRF, etc.) in NG feeds with and without bubbling with careful coupon placement to examine the agitation/convection effects over a larger distance and time scale as well as to correlate the dynamics of scaling.

2. Perform additional testing at a greater variety of timeframes. The behavior of the corrosion rate between the 24 hour timeframe and the 120 hour timeframe would be important to understand given the accelerated impact of the oxidants and reductants during this time period. The behavior of the corrosion rate after 120 hours is important to determine where a steady state of corrosion exists. Examination of the corrosion rate out to extended long-term timeframes on the order of 3 to 6 months could give an even more comprehensive understanding of the effects of ion depletion from the refractory on its structural integrity.

3. If possible, take a core sample of refractory material from below the melt line of the next decommissioned melter during autopsy. Examination of the refractory from a full-scale melter after a lifetime of usage could be utilized to confirm the observations made in simulant waste and

smaller-scale melters. Comparison of these two refractories as a function of at least the following variables could expand our understanding of the corrosion mechanisms at work between the glass and refractory: the depth of the "loss of material" region, the depth of the "selective penetration" region, the depth and scale of Fe^0 depletion, the extent of spinel growth and retention at the refractory-glass interface, and the extent of Mg and Al dissolution from the refractory.

4. Perform testing with feeds containing an even wider range of anions is suggested to gain a more expansive understanding of the operational window of the refractory in terms of the effects on "loss of material" and Fe^0 depletion due to the anions alone

TABLE OF CONTENTS

LIST OF TABLES x
LIST OF FIGURES x
LIST OF ABBREVIATIONS xi
1.0 Introduction 1
1.1 Previous Corrosion Testing and the DWPF Design Basis 1
*Based on continuous powder feeding of 4.7 lb/hr-ft^2 of melt surface area and a minimum residence time of the melt in the melt pool of 12 hours. 1
1.2 Previous Crucible Testing and Determination of the Corrosion Mechanism for the Nitric-Formic DWPF Flowsheet 1
1.3 Previous Testing and Determination of the Iron Depletion for the Nitric-Glycolic DWPF Flowsheet 5
2.0 Experimental Methods 5
2.1 ASTM C621 and the Modified ASTM Method 5
2.2 Slurry Preparation and Heat Treatment 7
2.3 Coupon Preparation Corrosion Testing 8
2.4 Corrosion Layer Measurements 8
2.5 Technical Task Request and Quality Assurance 8
3.0 Results and Discussion 9
3.1 Pristine Monofrax™ K-3 Coupon 9
3.2 Corrosion Mechanisms in Black Frit 165 Standard Glass 12
3.3 Corrosion Mechanisms and Rates in Glycolic Acid Melter Feeds 15
3.3.1 Corrosion Mechanisms for Nitric-Formic and Nitric-Glycolic Flowsheet Feeds are Identical 15
3.3.2 General Corrosion Rate Measurement Difficulties 20
3.3.3 Metallic Fe^0 Depletion Observed 23
4.0 Conclusions 24
5.0 Future Work 25
6.0 References 27
Appendix A . Images of Pristine K-3 Coupons A-29
Appendix B . SEM Images of K-3 Coupons in Black Frit 165 ..... B-31
Appendix C . SEM Images of K-3 Coupons in CEF-2 SRAT Melter Feed. C-40
Appendix D . SEM Images of K-3 Coupons in CEF-2 SME Melter Feed. D-49
Appendix E . SEM Images of K-3 Coupons in GN78 Melter Feed. E-58
Appendix F . SEM Images of K-3 Coupons in GN79 Melter Feed. F-67

LIST OF TABLES

Table 1-1. DWPF Design Basis in Formic Acid Feed. 1

Table 1-2. Monofrax™ K-3 Corrosion Depths Measured in Non-Bubbled SRNL Melters and by ASTM C621 Modified and Non-Modified Crucible Measurements 4

Table 1-3. Feed Compositions Used in Monofrax K-3 Crucible and Mini-melter Tests 5

Table 2-1. Non-Bubbled K-3 Refractory Testing Matrix 7

Table 3-1. Monofrax™ K-3 Corrosion Depths Measured at the Hot Wall Face and Cut Face by Modified ASTM C621 Non-Bubbled in NG Flowsheet Melter Feeds at 1150°C 16

Table 3-2. Monofrax™ K-3 Corrosion Rates Measured at the Hot Wall Face and Cut Face by Modified ASTM C621 Non-Bubbled in NG Flowsheet Melter Feeds at 1150°C 19

Table 3-3. Reduction/Oxidation Half Reactions [3]. 23

Table 3-4. Percentage of Most Dense (Metallic) Phases from Average Atomic Number Density Area Maps. 24

LIST OF FIGURES

Figure 2-1. A) Non-Bubbled Closed (Sealed) Crucible utilized for corrosion testing and B) schematic of coupon placement. 8

Figure 3-1. SEM phase maps of unreacted K-3 coupon showing the progressive increased presence of metallic phases (dark blue, far right column) deeper into refractory interior. A) the hot wall face and B) 6mm in from the edge. 11

Figure 3-2. Elemental maps of a pristine K-3 coupon showing the A) visible image B) Mg content, C) Al content, D) Cr content, E) Fe content, and F) Si content along the hot wall face (left) and cut face (bottom). Additional images of the pristine K-3 refractory coupons can be found in Appendix A. ... 12

Figure 3-3. Elemental maps of K-3 coupon after being submerged in Black Frit 165 for 4 hours at 1150°C showing the A) visible image, B) Mg content, C) Al content, D) Cr content, E) Fe content, F) Ni content, and G) Si content. 13

Figure 3-4. Comparison of Fe elemental maps of K-3 coupons submerged in Black Frit 165 at 1150°C for A) 4 hours, B) 24 hours, and C) 120 hours. 14

Figure 3-5. Comparison of Ni elemental maps of K-3 coupons submerged in Black Frit 165 at 1150°C for A) 4 hours, B) 24 hours, and C) 120 hours. 15

Figure 3-6. Plots of A) Hot Wall Face Corrosion Rates and B) Cut Face Corrosion Rates at 120 hours versus REDOX of each feed. 19

Figure 3-7. Plot of Cut Face Corrosion Rates versus Hot Wall Corrosion Rates at 120 Hours. 20

Figure 3-8. Example SEM image displaying difficulty in elucidating the original material face and the demarcation between the "loss of material" and the "selective penetration" corrosion regions. 21

Figure 3-9. SEM elemental point mapping of corrosion region with relative elemental concentrations.... 22

LIST OF ABBREVIATIONS

AD	Analytical Development
CEF	Cold cap Evaluation Furnace
DWPF	Defense Waste Processing Facility
E&CPT	Environmental & Chemical Process Technology Research Programs
HLW	High Level Waste
K-3	Monofrax™ K-3 refractory coupons
KMA	Koopman Minimum Acid
MOC	Materials of Construction
NF	Nitric-Formic flowsheet
NG	Nitric-Glycolic flowsheet
REDOX	REDuction/OXidation
SEM	Scanning Electron Microscopy
SME	Slurry Mix Evaporator
SMRF	Slurry-Fed Melt Rate Furnace
SRAT	Sludge Receipt and Adjustment Tank
SRNL	Savannah River National Laboratory
SRS	Savannah River Site

1.0 Introduction

The Defense Waste Processing Facility (DWPF) at the Savannah River Site (SRS) uses a combination of reductants and oxidants while converting high level waste (HLW) to a borosilicate waste form. A reducing flowsheet is maintained to retain radionuclides in their reduced oxidation states which promotes their incorporation into borosilicate glass. [5] For the last 20 years of processing the DWPF has used formic acid as the main reductant and nitric acid as the main oxidant. During decomposition, formate and formic acid release H_2 gas which requires close control of the melter vapor space flammability. A switch to a nitric acid-glycolic acid (NG) flowsheet from the nitric-formic (NF) flowsheet is desired as the NG flowsheet releases considerably less H_2 gas upon decomposition. This would greatly simplify DWPF processing.

The use of glycolic acid instead of formic acid requires that the impacts of the alternate reductant on the materials of construction (MOC) of the melter must be examined. This is because the DWPF design basis was derived for the NF flowsheet and so the comparisons to the NG flowsheet must be evaluated. The experiments detailed in this report specifically address the effects of the alternate reductant, glycolic acid, in the melter feed on the corrosion of the Monofrax™ K-3 refractory (Figure A-1) used to line the melter. [6] [7]

1.1 Previous Corrosion Testing and the DWPF Design Basis

Significant study has been done on the corrosion of K-3 in the presence of NF flowsheet sludge with only minimal experimentation performed with NG flowsheet sludge. [3] [8] [9] [10] [11] [12] [13] Previous testing with the NG flowsheet was performed in the CEF in the presence of an argon bubbler. Though the presence of the argon bubbler represented conservative conditions (i.e. significant agitation beyond thermal convection), the placement of the K-3 coupon directly above the bubbling port made understanding of the corrosion/erosion mechanisms difficult to deconvolute. The experimental setup for the testing detailed in this report relied upon the non-bubbled modified ASTM crucible method to provide corrosion/erosion information related directly to the melter feed chemistry.

Table 1-1. DWPF Design Basis in Formic Acid Feed.

	Maximum Corrosion Rate (mils/day)*
DWPF Design Basis (sidewall above melt line, lid, floor) [14] [15]	3.00
DWPF Design Basis (melt line) from SCM Campaign 2 Maximum Wear 2-3 inches below melt line applied to 0-4" below melt line in DWPF [14] [15]	7.50
DWPF Design Basis (wall >4" below melt line) from SCM Campaign 2 Walls below melt line [14] [15]	5.40

*Based on continuous calcined solids feeding of 4.7 lb/hr-ft^2 of melt surface area and a minimum residence time of the melt in the melt pool of 12 hours.

1.2 Previous Crucible Testing and Determination of the Corrosion Mechanism for the Nitric-Formic DWPF Flowsheet

The K-3 refractory corrosion mechanism in the DWPF nitric-formic flowsheet was shown to be a depletion in Al_2O_3 and MgO, which leaves the corroded layer containing mostly Cr_2O_3. This is in agreement with the findings of Miller and Steggs [16]: the Al_2O_3 and MgO phases of the K-3 brick are much more vulnerable to dissolution in glass than the chrome (Cr_2O_3) phase. In addition, Fe_2O_3 and NiO

were found to be enriched in the corrosion layers of the K-3 and these components come from the DWPF waste glass when it interacts with the residual components in the outer corrosion layers of the K-3 refractory. [6] [17] Silicon appears slightly depleted in the corrosion layers but since the concentration of SiO_2 is so low in the refractory it is difficult to be quantitative. The enrichment of the corroded layer in Fe over the amount of Fe in the bulk confirms that iron oxide from the melt is absorbed by the refractory as observed by Maun and Osborn [18] in other chrome refractories and by the K-3 manufacturer. [16] The K-3 contains no NiO but was shown [6] [17] to react with NiO from the glass forming a Ni-Fe-Cr rich spinel reaction product. This confirms that the K-3 corrosion in DWPF type glasses is a strong function of the nickel oxide and iron oxide content of the glass: Ni and Fe in the glass exchange for Mg and Al in the refractory. [16] Based on elemental mapping performed with the SEM, as the Al and Mg are depleted from the corrosion region, Fe and Ni are shown to become enriched in the same region. The diffusion of cations results in the formation of Fe-Ni-Cr spinel crystalline material that expands in the corrosion region causing erosion of the refractory surface.

The reaction mechanisms were determined for DWPF oxidized and reduced feeds from the product species found on melter autopsy for various pilot scale melters at the SRNL. [6] [7] [17] These reactions indicate that the decomposition of the K-3 not only forms $NiCrFeO_4$ spinel but forms Mg rich silicates such as krinovite ($NaMg_2CrSi_3O_{10}$) at temperatures of ~1150°C which were found upon autopsy. Equation 2, which contains the impact of the oxidizing feeds, is favored over Equation 1 which is written without the O_2 from melter denitration reactions.

Equation 1

$$\underbrace{6MgAlCrO_4}_{\text{Major K-3 phase}} + \underbrace{3Fe_2O_3 + 6NiO + 8SiO_2}_{\text{melt}} \rightarrow \underbrace{6NiCrFeO_4 + 6MgO \bullet SiO_2 + Al_6Si_2O_{13}}_{\text{observed and predicted chrome refractory products}}$$

$$\Delta G_{fm}(\text{products}) - \Delta G_{fm}(\text{reactants}) = -1759 KJ / mole$$

Equation 2

$$\underbrace{6FeAlCrO_4 + 2FeCr_2O_4 + 2FeO}_{\text{K-3 phases}} + \underbrace{10NiO + 2SiO_2 + 2.5O_2}_{\text{melt}} \rightarrow \underbrace{10NiCrFeO_4 + Al_6Si_2O_{13}}_{\text{observed and predicted chrome refractory products}}$$

$$\Delta G_{fm}(\text{products}) - \Delta G_{fm}(\text{reactants}) = -3128 KJ / mole$$

Therefore, Cr-enriched $NiFe_2O_4$ spinels form as refractory corrosion products from K-3 and can fall or spall off into the HLW waste glass melt pool. These Cr-enriched spinels can agglomerate in the melt pool [17] [6] [7] [19] [20] [21] and ultimately accumulate on the floor of the DWPF melter and/or periodically become entrained in the glass and swept up the riser or pour spout, although no accumulations have been seen in pour spout samples taken from the DWPF over the last 20 years. [22]

In a melt pool with natural convection, an insoluble $NiFe_2O_4$ spinel corrosion product is formed on the K-3 that has been found to build up a protective layer along the refractory walls. Spallation and settling of the $NiFe_2O_4$ spinel corrosion product is dependent on melt pool convection/agitation. Based on the refractory corrosion study of Cooper and Nicholson, [23] glass flow can cause the outer reaction layer to spall off exposing the penetration layer as the next reaction surface. Therefore, average "loss of material" depths may underestimate refractory corrosion in highly convective, highly stirred, or bubbled melts, while "total penetration" depths may be overly conservative for non-agitated, low-flow environments. The average "loss of material" and the "total penetration" depth are defined to correspond to two different reaction mechanisms which occurred between the specimen and the molten glass: (1) a "corrosion" reaction

mechanism which results in a change in the dimensions of the specimen (corresponding to the "loss of material") and (2) "selective penetration" of a corrosion front into the material forming a new reaction layer. The "total penetration" depth is, therefore, defined as the sum of the "selective penetration" and the "loss of material". The "selective penetration" region can also be understood as the depth of ion exchange for the Mg, Al, and Ni cations.

Rankin [24] determined that the "selective penetration" is faster/greater than the "loss of material" corrosion zone in a static or quiescent melter environment. Conversely, the "loss of material" is faster/greater than the "selective penetration" in higher velocity melts as the small eddy currents that form at glass-gas-refractory interfaces, such as at the melt line, increase the "loss of material" corrosion zone. Rankin [13] also noted that higher Na_2O containing waste glass feeds caused the "total penetration" (loss of material plus selective penetration) depth of the K-3 corrosion to be greater. A similar effect was expected from any alkali in the glass. [13]

The "total penetration" depths are preferentially reported as being the most conservative measure of refractory wear. In addition the ratio of the average "loss of material" divided by the "total penetration" depths are given where determined. Average rates and the ratios are reported from various past studies in Table 1-2. When the ratios of "loss/total penetration" in Table 1-2 are coupled with the feed and glass compositions in Table 1-3 it can be seen that for corrosion studies in pre-reacted glass which is representative of formic acid feeds [6] [7] in static melt pools that the ratios are between 0.33-0.40. In oxidized feeds, the ratio is 0.63 in crucible testing and 0.65 in mini-melter testing at high nitrate concentrations, 0.69 and 0.62 molar, respectively. For agitated regions, i.e. near or at the melt line, in oxidized feeds the ratio is even higher, 0.87, at the same molar concentrations of nitrate. Note also that these feeds are simultaneously high in Na_2O content and nitrate. The significance of these ratios is that the region of average "loss of material" from the corrosion layer is much greater than the "total penetration" depth, meaning that the refractory will wear or corrode faster in oxidizing feeds and even faster in agitated oxidizing feeds.

The DWPF design basis was primarily based on the Small Cylindrical Melter (SCM-2) campaigns (see Table 1-1). Note that the design basis rates do not distinguish an average "loss of material" and a "selective penetration" depth but consider the sum of these two ("total penetration") measurements as the overall corrosion rate.

Table 1-2. Monofrax™ K-3 Corrosion Depths Measured in Non-Bubbled SRNL Melters and by ASTM C621 Modified and Non-Modified Crucible Measurements

Type of Measurement	**Temp (°C)**	**Time (Days)**	**Frit**	**Simulated Waste Type or Glass**	**Average Loss of Material (mils) normalized to test duration**	**Total Penetration (mils) normalized to test duration**	**Ratio of Loss/ Penetration**	**Na2O in Waste Glass (Wt%)**	**Ref.**
Crucible Melt Line ASTM 621	1150	7	131	TDS Average Waste Glass	0.64	1.92	0.333	12.6	[13]
Crucible Melt Line* ASTM 621	1150	7	165	Black Frit Glass	0.73	ND	ND	11.0	[24]
Crucible Melt Line* ASTM 621	1150	7	165		0.23	ND	ND	11.0	[24]
Crucible Melt Line ASTM 621**	1150	7	165		0.68	ND	ND	11.0	[24]
Crucible – ASTM C621	1150	5	165	Black Frit Glass (standard for comparison to Ref. [24])	0.79	1.97	0.40	11.0	[6]
Crucible – Sample (Modified ASTM C621	1150	5	200	Tank 51A Batch 1A High Nitrate Feed	Average of 1.57	Average of 2.49	Average of 0.63	12.7	[6]
Mini-melter Melt Line†	1150	3	200	Tank 51A Batch 1A Lower Nitrate Feed	2.29	2.62	0.87	12.2	[6]
Mini-melter Vapor Space†	1150	3	200		0.52	0.79	0.65	12.2	[6]
CEF Melt Pool Micrograph Regions of Uniform Corrosion	800-1150	25	418	SB-6 simulant	0.39	0.59	0.66	11.6	[3]

*As cast K-3 surface; **Ground K-3 surface; †Diamond cut K-3 surface, CELS = Corning Engineering Laboratory Services, Corning, NY; the comparative corrosion rates for the control standards are shaded as discussed in the table; Frit 418 is composed of 8 wt% B_2O_3, 8 wt% Li_2O, 8 wt% Na_2O, and 76 wt% SiO_2.

Table 1-3. Feed Compositions Used in Monofrax K-3 Crucible and Mini-melter Tests.

Feed Constituent	**Feed/Glass Used in Crucible Studies**	**Feed/Glass Used in Mini-melter Studies - SME Product 2-11** [25]	**Feed/Glass Used in CEF melter Studies** [26]	**Units**
	Tank 51 sludge simulant with Frit 200		SB6 Simulant with Frit 418	
Waste Loading	24.8	25.6	36.0	wt% dry oxide basis
Frit Loading	75.2	74.4	64.0	
Nitrate	0.694	0.616	1.0-1.5	Molar
Nitrite	0.0086	<0.002	<0.0028-0.0030	
Formate	0.40	0.853	0.045-0.072	
Glycolate	N/A	N/A	0.48-0.86	
Sulfate	1.69×10^{-3}	1.28×10^{-3}	$1.2\text{-}2.0 \times 10^{-2}$	
Chloride	$<2.82 \times 10^{-3}$	$<2.82 \times 10^{-3}$	$1.0\text{-}1.2 \times 10^{-2}$	
Fluoride	$<5.26 \times 10^{-3}$	$<5.26 \times 10^{-3}$	$<6.9\text{-}7.2 \times 10^{-3}$	
Na	1.3-1.6		1.7	
Fe	1.7-1.8		0.64	
Melter feed solids	41	45.61	42-49	Wt %
Na_2O in Glass	12.7	12.2	11.6	
Fe_2O_3 in Glass	12.5	-----	10.8	
Al_2O_3 in Glass	4.3	-----	9.21	
NiO in Glass	0.07	-----	1.35	
MnO in Glass	1.2	-----	3.19	

1.3 Previous Testing and Determination of the Iron Depletion for the Nitric-Glycolic DWPF Flowsheet

Previous testing of the K-3 refractory in glycolic acid feeds [3] was examined when a corrosion coupon of the K-3 was submerged in the Cold cap Evaluation Furnace (CEF). However, the corrosion coupon was mounted in a cage attached to the inlet pipe of an argon bubbler. Therefore, the corrosion coupon was directly in line with the argon bubbles as they traversed from the bottom to the top of the melt pool. During examination of the corrosion coupon, it was difficult to measure a general corrosion rate as cavitation had occurred in many places from the flow of bubbles produced by the argon. In addition, the CEF feeds were overly oxidized, $Fe^{2+}/\Sigma Fe << 0$, and there was selective attack of one of the K-3 refractory components, metallic Fe^0, by the nitric acid in the melter feeds. This report details the observed corrosion rates of various NG flowsheet feeds in static crucibles as a function of their REDuction/OXidation (REDOX) or $Fe^{2+}/\Sigma Fe$ ratio at 1150°C for various lengths of time.

2.0 Experimental Methods

2.1 ASTM C621 and the Modified ASTM Method

ASTM C621 [27] is a standard procedure used in the commercial glass industry for measuring isothermal corrosion resistance of refractories in molten glass. The procedure calls for the transfer of a preheated (1000°C) refractory specimen into pre-melted hot glass. After a predetermined length of time in the melt, the refractory specimen is removed from the glass melt pool and allowed to cool separate from the glass. The refractory specimen is sectioned length-wise so that the diameter at the melt line and halfway between the melt line and the bottom may be measured.

In 1998, modified ASTM C621 corrosion testing in crucibles was initiated at SRNL using melter feed instead of pre-reacted glass in order to determine the refractory corrosion rate and mechanisms operable during the feed-to-glass conversion. [6] [7] [17] Testing the refractory coupon during the feed-to-glass conversion exposes the refractory to the oxidizing and reducing species of the feed and those being released during the vitrification process, e.g. NO_3^-, NO_2^-, CO_2, CO, O_2. This modification was made to evaluate the impact of the oxidizing feed species on the very reduced ($Fe^{2+}/\Sigma Fe$ = 0.91-0.94) K-3 refractory because thermodynamic calculations performed by Degterov and Pelton [19] indicated that the solubility limit of Cr_2O_3 from Cr_2O_3-Al_2O_3 refractories such as K-3 is strongly dependent on the oxygen partial pressure of a melt. Although the example given by these authors is for oxygen partial pressures that are more reduced than the DWPF melts, i.e. at the Cr^{+2}/Cr^{+3} equilibria, similar[1] oxygen partial pressure dependency governs the Cr^{+3}/Cr^{+6} equilibria under the more oxidizing conditions of the DWPF melter. [28]

Comparisons were performed with the modified ASTM C621 procedure to compare the corrosion rates in reducing formic acid flowsheets and in more oxidizing nitric acid flowsheets. Confirmatory corrosion rates were measured on K-3 refractory coupons immersed in oxidizing feed in a 1/100th scale HLW pilot-scale melter. [6] [17] Corrosion rates measured in highly oxidizing (high nitrate) feeds were ~1.8-2.8 times higher than those determined using pre-reacted glass or reduced feeds. [6] [17] Corrosion rates measured using the modified ASTM C621 in reduced feeds were found to be comparable to those measured in ASTM C621 in pre-reacted glass.

The ASTM C621 procedure calls for the coupons to be inserted into molten glass and removed while still at temperature. In the modified ASTM C621 procedure, the K-3 coupons were submerged in samples of dried sludge in sealed alumina crucibles. Both the hot wall face of the refractory, the manufactured outer faces of the refractory brick that contacts the melt pool first, and a freshly cut face of the refractory were submerged in the feed during the feed-to-glass conversion. The modified ASTM C621 tests were heated to and held at 1150°C for 4 hours, 24 hours, and 120 hours, in duplicate. Table 2-1 details the test matrix: the feeds utilized, the percent reducing acid in the feed, the total acid stoichiometry and the durations of the experiments.

[1] Free limited access to the F*A*C*T (Facility for the Analysis of Chemical Thermodynamics) thermodynamic software used by these authors is available on the World Wide Web and model calculations involving Cr^{+3}/Cr^{+6} equilibria and its oxygen dependency were performed by C.M. Jantzen and A.D. Cozzi of SRNL.

Table 2-1. Non-Bubbled K-3 Refractory Testing Matrix

Feed	Percent Reducing Acid	Acid Stoichiometry (KMA)	Time (h)
Black Frit 165 Standard†	----------	----------	4
			24
			120
CEF-2 SME*	~43.4[2]	~114[2]	4
			24
			120
CEF-2 SRAT	49.4	100	4
			24
			120
GN-78	52.21	110	4
			24
			120
GN-79	54.54	100	4
			24
			120

†Pre-formed reference glass material. * Remediated SRAT product with additional nitric acid and dry frit added

2.2 Slurry Preparation and Heat Treatment

The preparation and heat treatment of each K-3 refractory coupon was identical to the non-bubbled REDOX testing, following procedure ITS-0052, rev. 5. [29] Each sludge sample is dried to a "thick peanut butter" consistency and stirred to homogeneity. Once a satisfactory consistency is reached, the refractory coupon is inserted in such a way as to maximize coverage of both the hot wall face and a cut face by the surrounding glass when vitrification is complete but still allows space between the hot wall face and the bottom surface of the crucible. Coupons, cut into "matchsticks" (approx. 2 in. long by ½ in. wide by ¼ in. thick; hot wall face ½ in. by ¼ in. square), were then inserted at an angle, leaving a gap between most of the hot wall face and the bottom surface of the crucible so that a maximum amount of the hot wall face may be in contact with the melt during the testing.(Figure 2-1B) In most cases, the coupons retained this alignment throughout testing; in a minority of cases the coupons shifted, approaching horizontal, changing the amount of refractory-glass interface.

Per ITS-0052, to maintain the atmosphere, the crucibles were sealed with a nepheline gel to allow outgassing of reaction products but prevent in-gassing of atmospheric gases. The nepheline gel sets between 400 and 600°C while the major off-gassing events occur before 400°C. This allows the crucibles to maintain positive pressure without over pressurizing or allowing oxygen from the atmosphere into the crucible to oxidize the glass.

Sealed crucibles are preheated to prevent thermal shock and then transferred directly to a preheated 1150°C oven; a method referred to as "hot insertion." Once the oven temperature recovers, the crucibles are held at temperature for the prescribed time based on the experimental test matrix given in Figure 2-1. After the dwell time, the crucibles are removed to a pan of sand to air cool. Cooled crucibles are sectioned with a diamond saw to expose both the hot face refractory-glass interface and the cut face refractory-glass interface for polishing and imaging via Scanning Electron Microscopy (SEM).

[2] Nitric acid was added to the melter feed after the SRAT process had been completed. Determination of the acid ratio is then an estimation at best based on the fact that the additional nitric acid did not participate in the reactions of glycolate or nitrite destruction, among others. The estimation of percent reducing acid may be made by assuming the additional nitric acid passed through the SRAT as inert and simply adding the additional amount to the original amount and dividing the original glycolic acid by the new total acid.

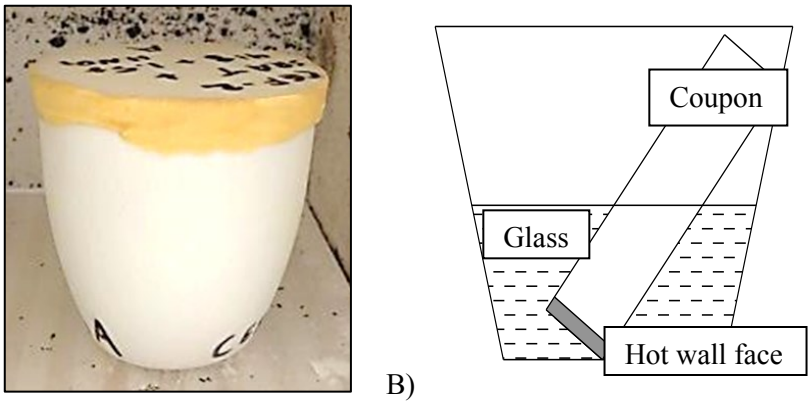

Figure 2-1. A) Non-Bubbled Closed (Sealed) Crucible utilized for corrosion testing and B) schematic of coupon placement.

2.3 Coupon Preparation Corrosion Testing

To be examined with the SEM, the coupon must be sectioned and polished. A diamond saw is utilized to cut each sample across the refractory-glass interface and reveal an internal surface of the refractory. Once sectioned, the cut internal surface revealing the interfaces between the hot wall face and the cut face are ground using silicon carbide sandpaper (grits ranging from 240 down to 800) followed by polishing with diamond paste (ranging from 9 down to 3 microns). Each sample is then washed with deionized H_2O and dried with air. Previous testing had the coupons mounted in epoxy to perform these tasks. However, due to the porosity of the K-3 refractory it is possible that uncured epoxy could have remained in the samples and caused bubbles when exposed to the vacuum in the SEM instrument. Therefore, these grinding/polishing steps were performed by hand in this series of tests without epoxy mounts. [30]

2.4 Corrosion Layer Measurements

Measurement of each coupon hot wall face-glass and cut face-glass interface were performed digitally using the public domain imaging software ImageJ, version 1.49 [31] versus previous studies which used rulers and printed images. The software uses individual pixels to measure distances allowing for very precise placement of endpoints of measurement bars and eliminating much of the subjective bias in setting the scale. The start and end of various corrosion regions are determined by the researcher.

To quantify the subjective measurement bias between researchers, duplicate samples were divided into Set A and Set B and the interfaces were measured at multiple points by two researchers. Each researchers' measurements were averaged independently and together to generate single corrosion values as well as a range of values and standard deviations demonstrating the variation in the corrosion regions and measurement precision. The "total penetration" corrosion region is reported as opposed to the separate "loss of material" and "selective penetration" regions due to the lack of distinct delineation as seen in previous studies. [3] The alterations to the polishing method made distinction of the various intermediate corrosion regions less determinable and more variable.

Precision in the ASTM method is determined related to the number of replicates performed per sample. Since only duplicates were made for each melter feed, the percent of average critical difference is 42.7%. To achieve a percent within 15.1%, sixteen samples must be measured. [27].

2.5 Technical Task Request and Quality Assurance

This document and findings are related to the Technical Task Request (TTR) HLW-DWPF-TTR-2013-0004 ("Impact of Nitric-Glycolic Acid Flowsheet – Materials Evaluation for DWPF and Downstream Tank Farm Processes") and the associated Task Technical/Quality Assurance Plan (TTQAP) SRNL-RP-

2012-00834, rev 2 ("Task Technical and Quality Assurance Plan for Material Evaluation for DWPF Nitric-Glycolic Acid Flowsheet").

Requirements for performing reviews of technical reports and the extent of review are established in manual E7 2.60. SRNL documents the extent and type of review using the SRNL Technical Report Design Checklist contained in WSRC-IM-2002-00011, Rev. 2.

3.0 Results and Discussion

3.1 Pristine Monofrax™ K-3 Coupon

High Cr_2O_3-containing Monofrax™ K-3 is the refractory that lines the DWPF melter and has been chosen to line other HLW and Low Activity Waste (LAW) melters worldwide. K-3 is tolerant of transition metal oxides in the HLW glass and is composed of highly reduced solid solutions of spinels, i.e. $(Mg,Fe^{2+})(Al,Cr)_2O_3$, FeO, and small amounts of Fe^0. [6] [17] Casting of the K-3 brick produces a dense region around the surface known as the hot wall face. This dense region is depleted in the reduced iron metal (Fe^0) used throughout the brick to control REDOX. This gradient of Fe^0 is a noticeable visible feature as shiny metallic flakes are observed with depth into the brick. Figure A-1 shows that there is a visible gradient in the K-3 refractory material. This gradient is also visible in phase maps taken using SEM (Figure 3-1) where the various colors represent void spaces (red, first column) and phases of increasing average atomic number density (yellow [2nd column] less dense than green [3rd column] less dense than dark blue [last column]). The highest atomic number density phases are typically metallic phases, in this case either Fe^0 or Fe^0-Cr^0. The medium density phases relate to one of the spinel solid solution series with the lower density having a higher percentage of Mg and/or Al spinels and the higher density having a higher percentage of Fe and/or Cr.

A)

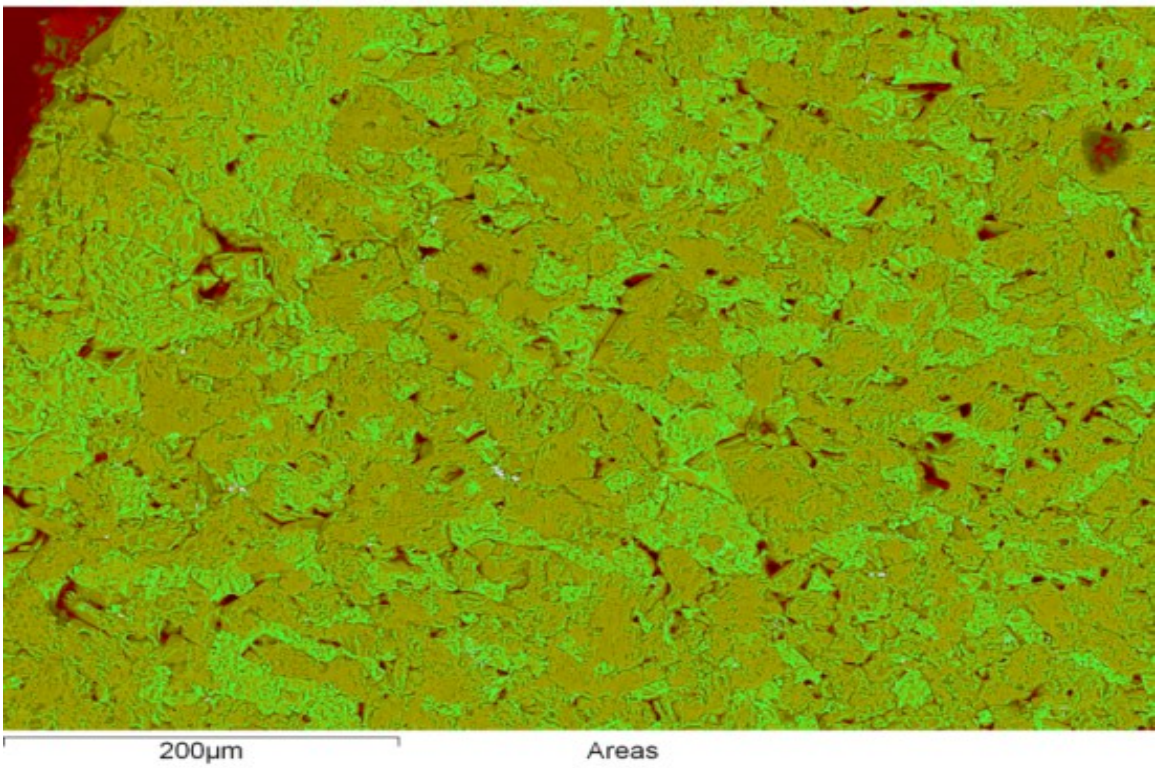
200µm
Areas

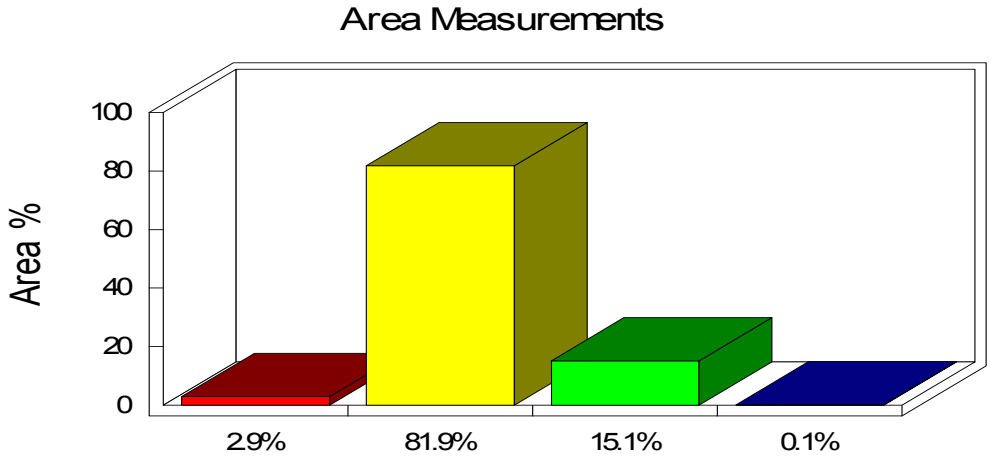
Area Measurements
Area %
100
80
60
40
20
0
2.9%
81.9%
15.1%
0.1%

B)

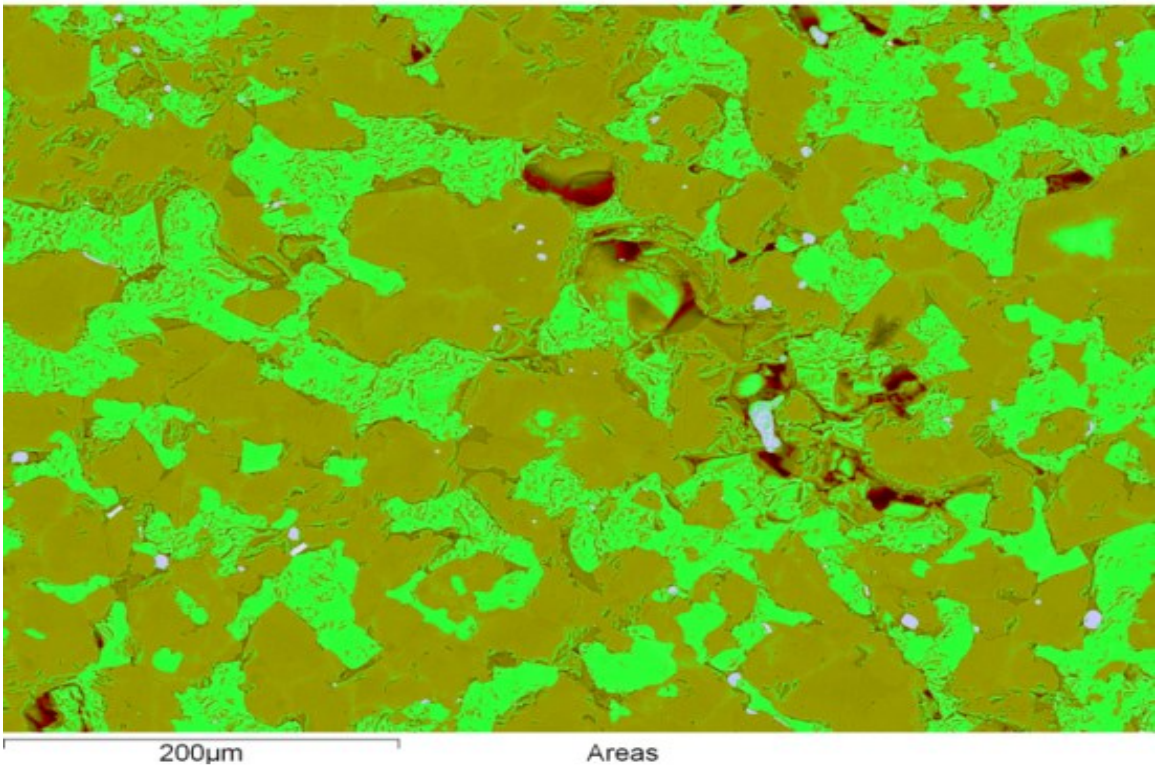

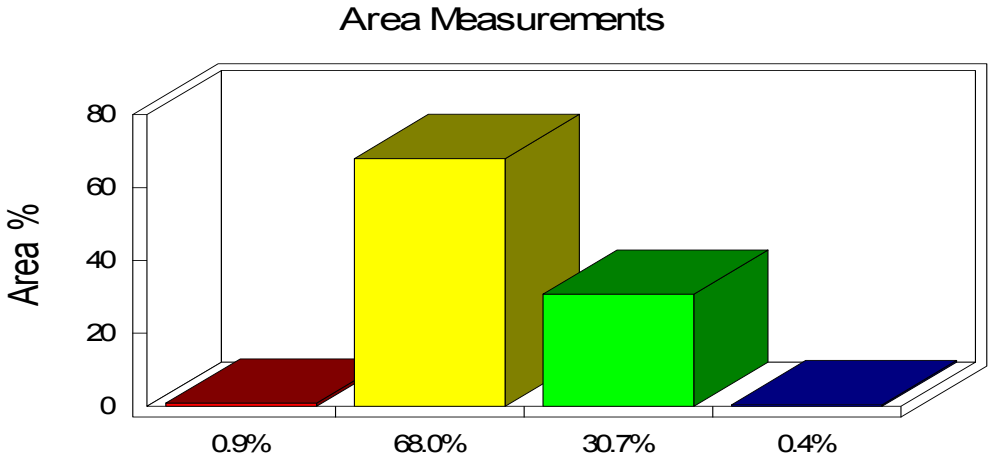

Figure 3-1. SEM phase maps of unreacted K-3 coupon showing the progressive increased presence of metallic phases (dark blue, far right column) deeper into refractory interior. A) The hot wall face and B) 6mm in from the edge.

Figure 3-2 shows that the bulk of the K-3 is homogeneous with respect to the solid solution series, but the hot wall face is rich in Mg. This compositional gradient means that corrosion behavior may change as feeds of various chemical natures come in contact with various portions of the brick.

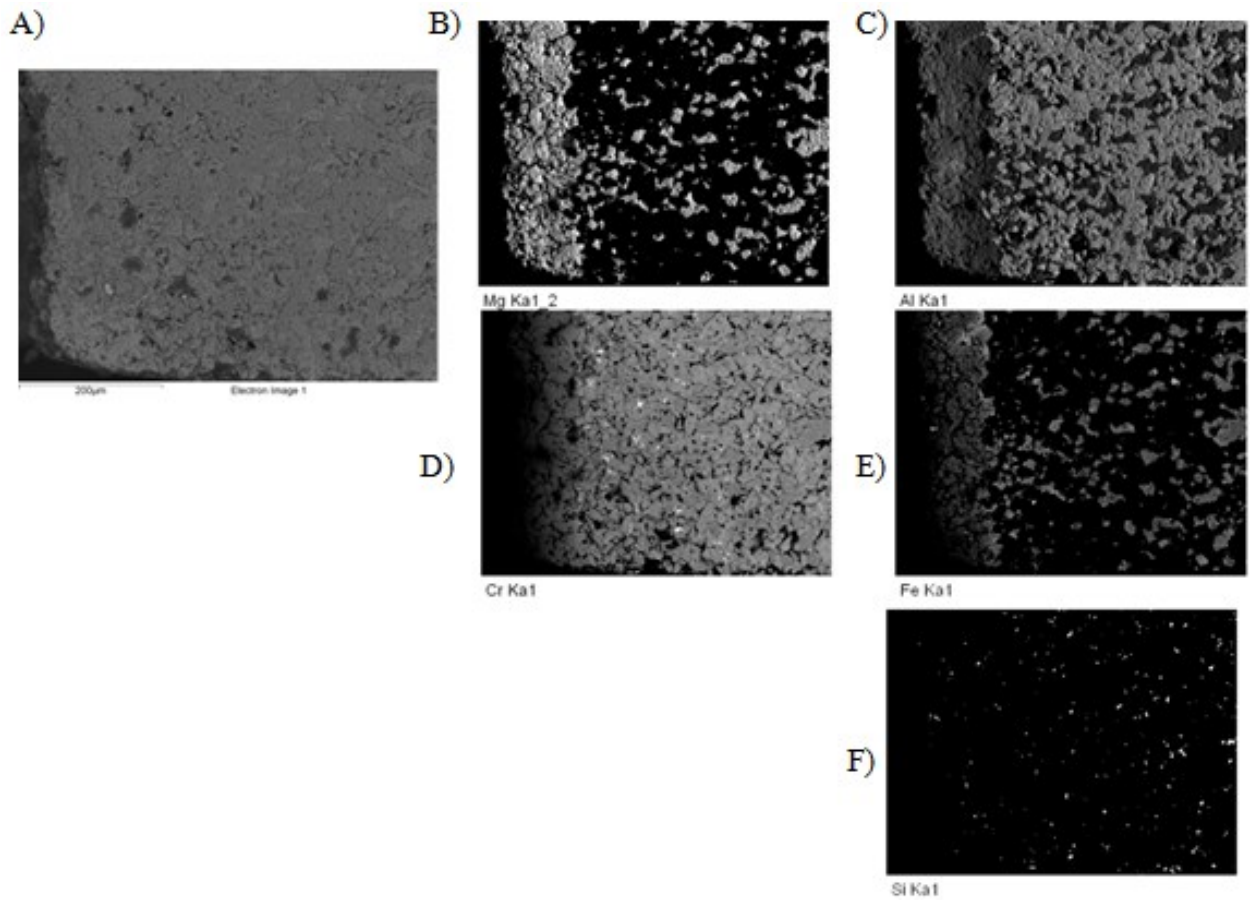

Figure 3-2. Elemental maps of a pristine K-3 coupon showing the A) visible image B) Mg content, C) Al content, D) Cr content, E) Fe content, and F) Si content along the hot wall face (left) and cut face (bottom). Additional images of the pristine K-3 refractory coupons can be found in Appendix A.

3.2 Corrosion Mechanisms in Black Frit 165 Standard Glass

The diffusion of cations out of the K-3 brick into the glass and into the K-3 brick from the glass results in the formation of Fe-Ni-Cr spinel crystalline material that expands in the corrosion region causing erosion of the refractory surface. These diffusion-related mechanisms were observed here, agreeing with previously established corrosion/erosion mechanisms detailed in Section 1.2.

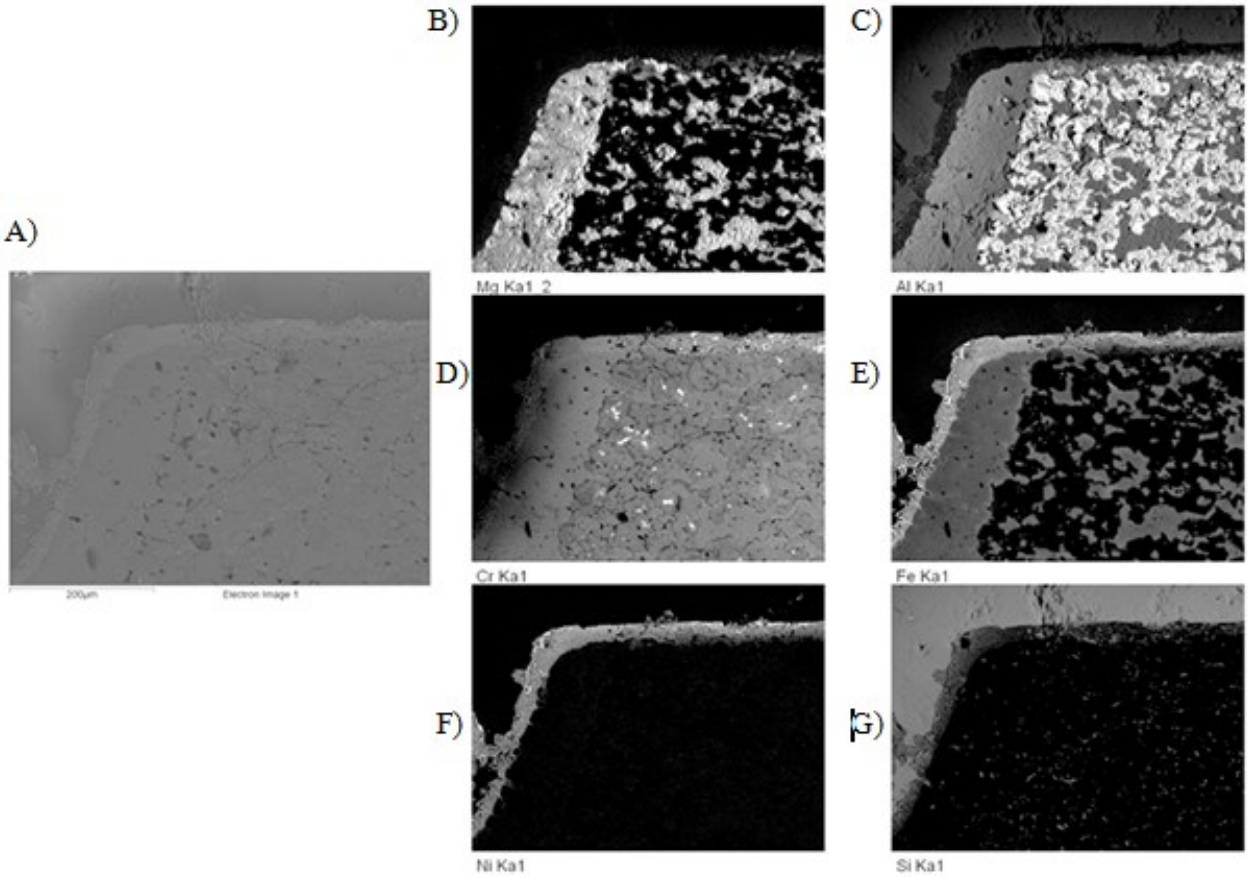

Figure 3-3. Elemental maps of K-3 coupon after being submerged in Black Frit 165 for 4 hours at 1150°C showing the A) visible image, B) Mg content, C) Al content, D) Cr content, E) Fe content, F) Ni content, and G) Si content.

Figure 3-3 shows that the dense hot wall face on the left and cut face on the top of the refractory have begun to corrode, losing Mg and Al from the outer most edges and becoming enriched with Ni and Fe. Crystalline material, Ni-Fe-Cr spinel-rich, is already beginning to spall off even at only 4 hours in the molten glass. A majority of the original dense hot wall phase remains after 4 hours of contact time in the glass. Ni and Fe penetration, spalling crystalline material, and loss of the dense hot wall phase increase as time in the molten glass increases (Figure 3-4 and Figure 3-5). The dense hot wall face is completely consumed by the 24-hour mark and the hot wall face and cut face begin to corrode similarly by the 120-hour mark.

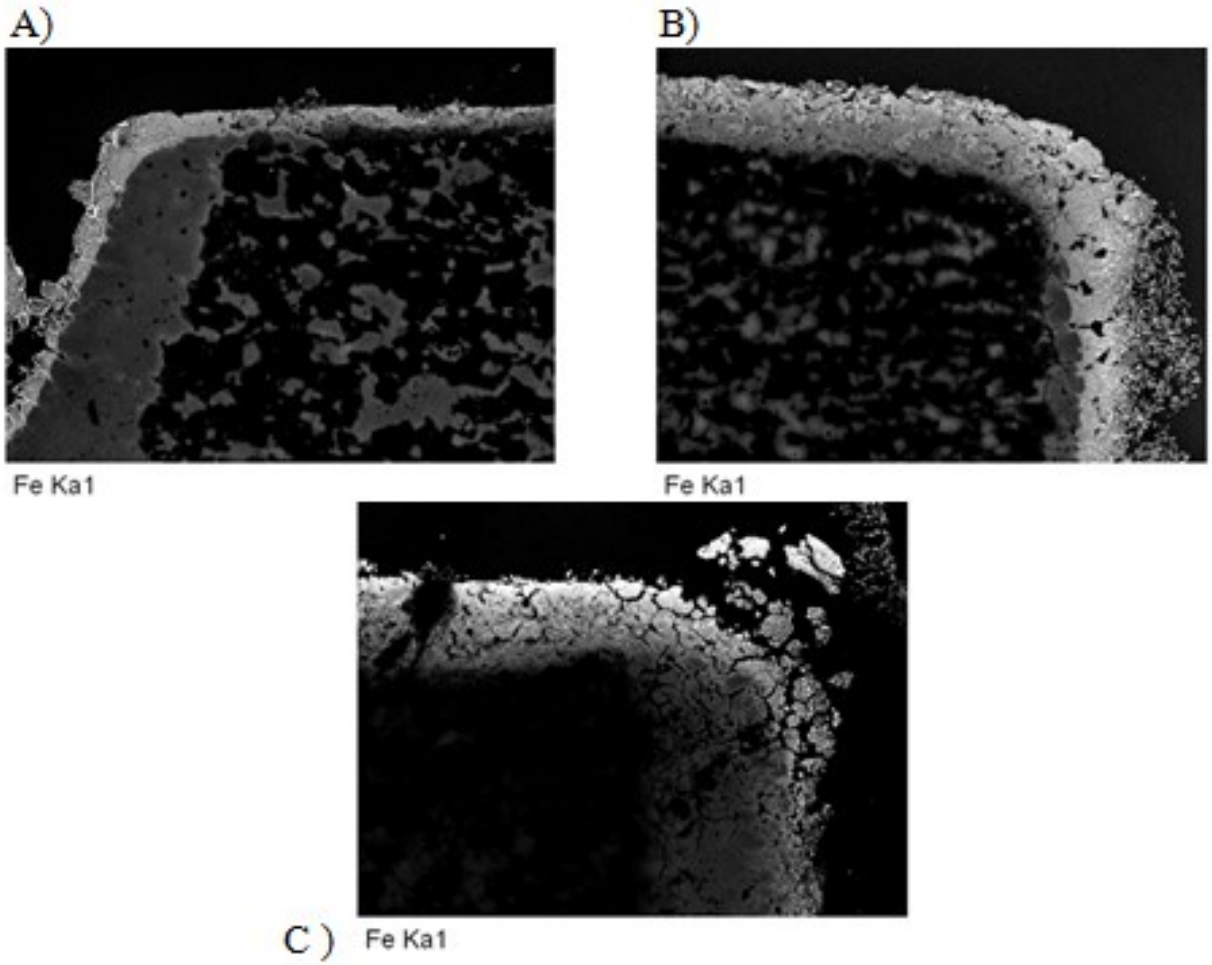

Figure 3-4. Comparison of Fe elemental maps of K-3 coupons submerged in Black Frit 165 at 1150°C for A) 4 hours, B) 24 hours, and C) 120 hours.

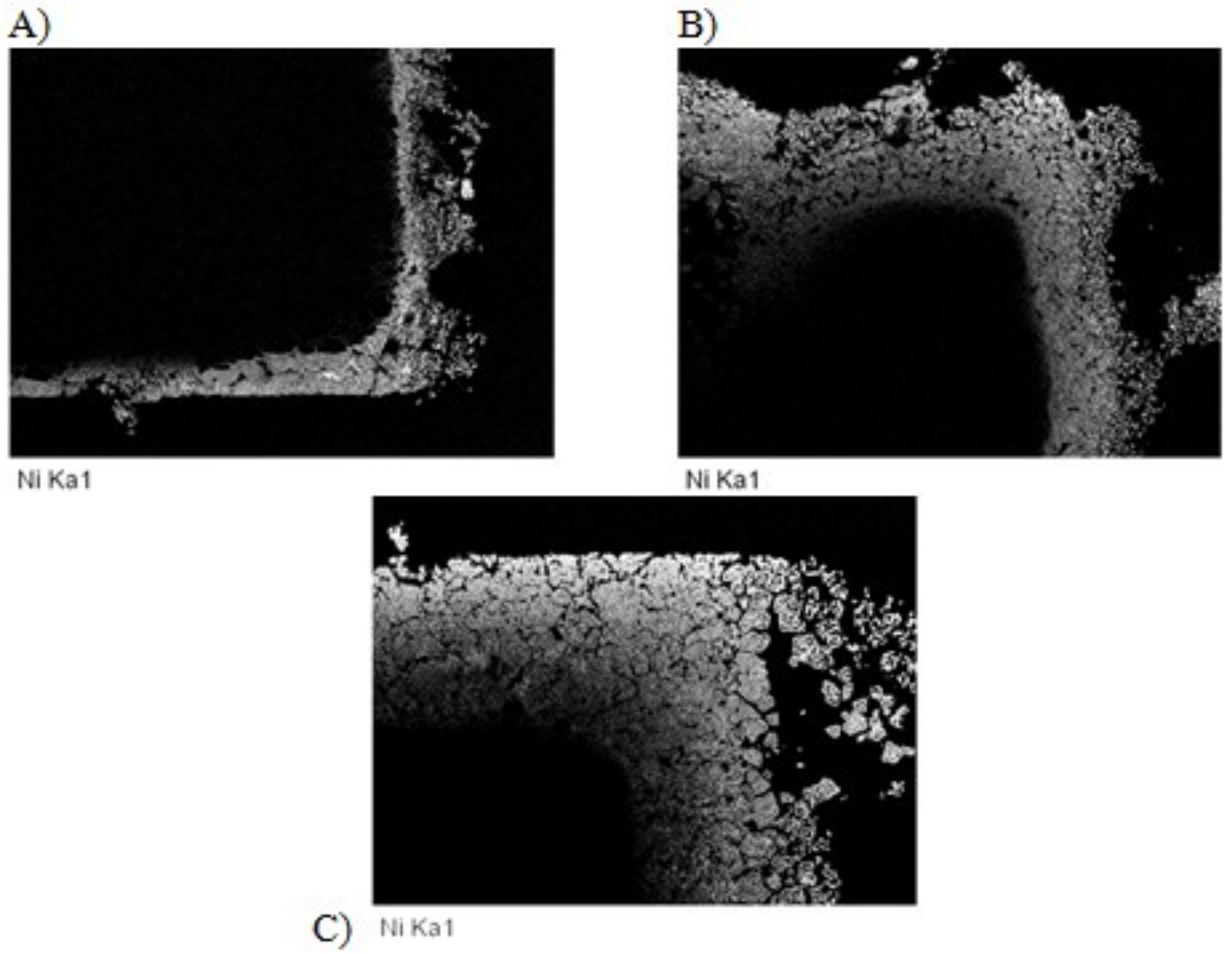

Figure 3-5. Comparison of Ni elemental maps of K-3 coupons submerged in Black Frit 165 at 1150°C for A) 4 hours, B) 24 hours, and C) 120 hours.

3.3 Corrosion Mechanisms and Rates in Glycolic Acid Melter Feeds

3.3.1 Corrosion Mechanisms for Nitric-Formic and Nitric-Glycolic Flowsheet Feeds are Identical

In the glycolic flowsheet the corrosion mechanisms involving Mg and Al depletion accompanied by Ni and Fe enrichment and spinel growth are also observed. In all cases, the corrosion region becomes depleted in Mg and Al and becomes enriched by Ni and Fe. As the Ni and Fe increase, Ni-Fe-Cr spinels crystallize and spall off in to the glass melt. Table 3-2 details the comparison of the "total penetration" corrosion depth between the melter feeds tested in the NG series of experiments. All of the SEM images that were used to derive the data in Table 3-4 are given in Appendix B (165 Black Frit), Appendix C (CEF-2 SRAT), Appendix D (CEF-2 SME), Appendix E (GN78), and Appendix F (GN79). Since these feeds were not agitated by bubbling, the corrosion mechanisms are driven by natural convection and the feed chemistry, i.e. composition and REDOX of the glass. Table 3-1 details all measurements made of the "total penetration" corrosion depths as a function of the researcher responsible for the measurement and whether the measurement was taken at the hot wall face or at the cut face. Averages and percent relative standard deviations are calculated for each set of measurements from individual samples and replicates.

Table 3-1. Monofrax™ K-3 Corrosion Depths Measured at the Hot Wall Face and Cut Face by Modified ASTM C621 Non-Bubbled in NG Flowsheet Melter Feeds at 1150°C.

Sample ID	Sample A/Researcher#1		Sample B/Researcher#2		Pooled	Pooled
	Measurements (mils/day)	Average (mils/day)	Measurements (mils/day)	Average (mils/day)	Average (mils/day)	Percent Relative Standard Deviation
Hot Wall Face						
BF165_4hr_HF	6.82	5.91	5.50	6.04	5.98	24.0
BF165_4hr_HF	5.75		4.27			
BF165_4hr_HF	5.15		8.36			
BF165_24hr_HF	1.45	1.39	1.54	1.55	1.47	7.5
BF165_24hr_HF	1.46		1.56			
BF165_24hr_HF	1.27		1.55			
BF165_120hr_HF	n/m	n/m	1.84	1.61	1.61	18.0
BF165_120hr_HF	n/m		1.70			
BF165_120hr_HF	n/m		1.28			
CEF_SME_4hr_HF	8.16	8.91	5.93	5.48	7.20	27.6
CEF_SME_4hr_HF	9.48		5.89			
CEF_SME_4hr_HF	9.10		4.63			
CEF_SME_24hr_HF	2.10	1.98	2.74	3.57	2.77	35.5
CEF_SME_24hr_HF	1.93		3.91			
CEF_SME_24hr_HF	1.90		4.05			
CEF_SME_120hr_HF	0.80	0.96	1.02	0.98	0.97	14.0
CEF_SME_120hr_HF	0.90		1.03			
CEF_SME_120hr_HF	1.19		0.89			
CEF_SRAT_4hr_HF	13.26	13.82	6.44	6.11	9.97	44.5
CEF_SRAT_4hr_HF	13.44		7.88			
CEF_SRAT_4hr_HF	14.78		3.99			
CEF_SRAT_24hr_HF	7.29	6.14	3.07	2.90	4.52	52.4
CEF_SRAT_24hr_HF	3.36		2.30			
CEF_SRAT_24hr_HF	7.76		3.33			
CEF_SRAT_120hr_HF	2.34	2.30	1.53	1.83	2.06	18.3
CEF_SRAT_120hr_HF	2.35		2.31			
CEF_SRAT_120hr_HF	2.22		1.64			
GB78_4hr_HF	11.97	10.53	7.37	7.05	8.79	25.6
GB78_4hr_HF	11.08		7.52			
GB78_4hr_HF	8.55		6.27			
GB78_24hr_HF	1.52	2.12	2.19	2.51	2.31	21.1
GB78_24hr_HF	2.10		2.47			
GB78_24hr_HF	2.73		2.87			
GB78_120hr_HF	1.17	1.03	0.87	0.84	0.94	14.4

Sample ID	Sample A/Researcher#1		Sample B/Researcher#2		Pooled	Pooled
	Measurements (mils/day)	Average (mils/day)	Measurements (mils/day)	Average (mils/day)	Average (mils/day)	Percent Relative Standard Deviation
GB78_120hr_HF	0.98		0.78			
GB78_120hr_HF	0.95		0.88			
GB79_4hr_HF	9.74		11.12			
GB79_4hr_HF	10.62	9.71	10.02	10.29	10.00	8.1
GB79_4hr_HF	8.78		9.73			
GB79_24hr_HF	2.04		1.58			
GB79_24hr_HF	1.76	1.89	2.02	1.74	1.82	10.8
GB79_24hr_HF	1.87		1.62			
GB79_120hr_HF	1.18		1.10			
GB79_120hr_HF	1.03	1.09	1.18	1.13	1.11	5.9
GB79_120hr_HF	1.05		1.12			
Cut Face						
BF165_4hr_CF	8.23		6.77			
BF165_4hr_CF	7.96	8.02	5.37	6.65	7.33	14.8
BF165_4hr_CF	7.87		7.81			
BF165_24hr_CF	2.52		3.36			
BF165_24hr_CF	2.58	2.54	2.72	3.08	2.81	13.0
BF165_24hr_CF	2.51		3.17			
BF165_120hr_CF	n/m		1.60			
BF165_120hr_CF	n/m	n/m	1.56	1.58	1.58	1.7
BF165_120hr_CF	n/m		n/m			
CEF_SME_4hr_CF	8.70		5.80			
CEF_SME_4hr_CF	6.59	7.45	5.55	5.66	6.55	18.5
CEF_SME_4hr_CF	7.06		5.61			
CEF_SME_24hr_CF	3.07		2.44			
CEF_SME_24hr_CF	3.21	3.15	2.31	2.66	2.91	14.4
CEF_SME_24hr_CF	3.18		3.24			
CEF_SME_120hr_CF	0.85		0.82			
CEF_SME_120hr_CF	0.80	0.89	0.77	0.81	0.85	9.9
CEF_SME_120hr_CF	1.01		0.83			
CEF_SRAT_4hr_CF	12.26		10.74			
CEF_SRAT_4hr_CF	10.81	11.25	11.17	10.63	10.94	6.9
CEF_SRAT_4hr_CF	10.68		9.99			
CEF_SRAT_24hr_CF	7.46		4.25			
CEF_SRAT_24hr_CF	5.18	6.00	4.89	4.57	5.28	22.9
CEF_SRAT_24hr_CF	5.37		n/m			

Sample ID	Sample A/Researcher#1		Sample B/Researcher#2		Pooled	Pooled
	Measurements (mils/day)	Average (mils/day)	Measurements (mils/day)	Average (mils/day)	Average (mils/day)	Percent Relative Standard Deviation
CEF_SRAT_120hr_CF	2.07	2.06	2.02	2.01	2.03	2.7
CEF_SRAT_120hr_CF	2.06		2.08			
CEF_SRAT_120hr_CF	2.04		1.93			
GB78_4hr_CF	8.06	8.55	8.49	8.96	8.76	7.3
GB78_4hr_CF	8.08		9.09			
GB78_4hr_CF	9.53		9.30			
GB78_24hr_CF	2.10	2.09	2.44	2.62	2.35	14.5
GB78_24hr_CF	2.32		2.72			
GB78_24hr_CF	1.85		2.69			
GB78_120hr_CF	1.03	1.07	1.43	1.30	1.19	13.0
GB78_120hr_CF	1.12		1.19			
GB78_120hr_CF	n/m		1.27			
GB79_4hr_CF	6.40	6.14	6.08	7.28	6.71	15.7
GB79_4hr_CF	5.28		8.23			
GB79_4hr_CF	6.74		7.52			
GB79_24hr_CF	2.94	2.42	2.74	2.50	2.46	12.9
GB79_24hr_CF	2.14		2.42			
GB79_24hr_CF	2.18		2.33			
GB79_120hr_CF	0.71	0.78	0.96	0.97	0.88	14.7
GB79_120hr_CF	0.73		0.95			
GB79_120hr_CF	0.90		1.01			

HF = hot wall face; CF = cut face; n/m = not measured.

The percent relative standard deviations of the average measurements between the two researchers are calculated for each sample and can be compared to the percent critical difference given by the ASTM C621. ASTM C621 provides data that demonstrates that the typical percent critical difference for any series of measurements performed on duplicate samples should be on the order of 40%. Table 3-1 shows the majority of the standard deviation values fall well below this value.

The measured general corrosion rate for the standard Black Frit 165 prepared glass was 1.61 ±0.29 mils/day, based on the 120h average "total penetration" depth. This is comparable to previous data where the measured "total penetration" depth was 1.97 mils/day (see Table 1-3). [6]

Table 3-2. Monofrax™ K-3 Corrosion Rates Measured at the Hot Wall Face and Cut Face by Modified ASTM C621 Non-Bubbled in NG Flowsheet Melter Feeds at 1150°C.

Melter Feed	Time	CC_{hot} REDOX	Avg. Total Penetration		Avg. Corrosion Rate	
	(h)	$Fe^{2+}/\Sigma Fe$	Hot Wall Face (mils)	Cut Face (mils)	Hot Wall Face (mils/day)	Cut Face (mils/day)
Black Frit 165	4	-----	0.98	1.22	5.98	7.33
	24		1.58	2.25	1.47	2.81
	120		8.27	8.47	1.61	1.58
CEF-2 SRAT	4	0.267	1.55	2.08	9.97	10.94
	24		4.52	5.29	4.52	5.28
	120		10.32	10.17	2.06	2.03
CEF-2 SME	4	0.136	1.2	1.09	7.20	6.55
	24		2.77	2.91	2.77	2.91
	120		4.86	4.24	0.97	0.85
GN78	4	0.097	1.33	1.46	8.79	8.76
	24		2.31	2.35	2.31	2.35
	120		4.74	5.93	0.94	1.19
GN79	4	0.158	1.40	1.42	10.00	6.71
	24		1.82	2.46	1.82	2.46
	120		5.55	4.36	1.11	0.88

The impact of having reducing and oxidizing chemicals present, as in the dried sludge, is seen as the corrosion rates for the sludge samples are significantly greater than the rates for the already melted Black Frit 165 glass at 4 hours and 24 hours. The rates at 4 hours and 24 hours for NG feeds are between 1.2x and 2.9x greater than the rates of Black Frit 165. At the 120-hour mark, the corrosion rates drop to levels more consistent with prepared glass. By 120 hours, the reductants and oxidants have been consumed and the corrosion is based on the natural convection and remnant REDOX nature of the transition metal oxides dissolved in the glass. Figure 3-6 shows that feeds that are more reducing (higher REDOX value) have lower corrosion rates after 120 hours.

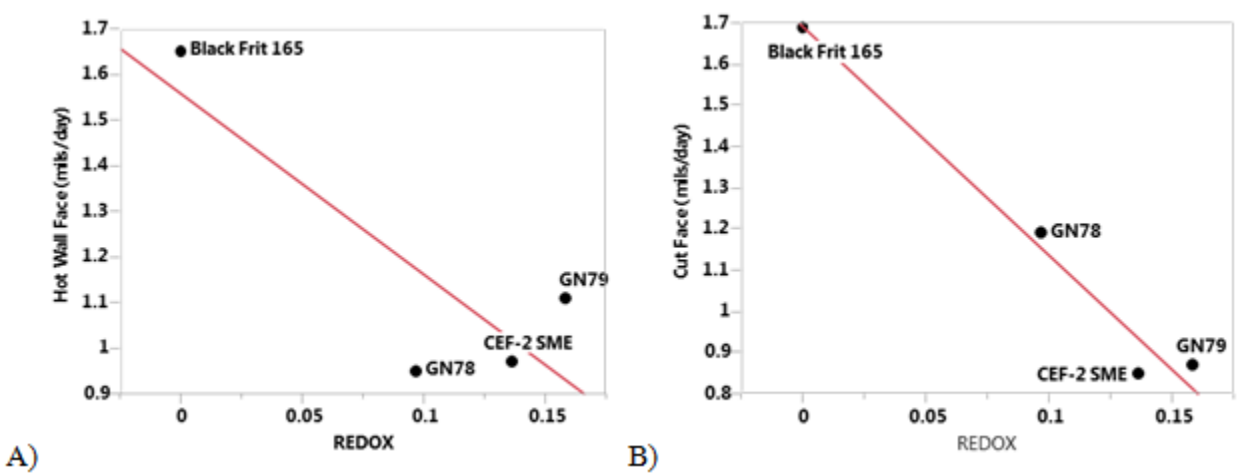

Figure 3-6. Plots of A) Hot Wall Face Corrosion Rates and B) Cut Face Corrosion Rates at 120 hours versus REDOX of each feed.

This reduction in corrosion rate is likely due to the reduced attack on the metallic species in the refractory and the buildup of a concentration gradient of exchanging cations at the refractory-glass interface. Ni and Fe dissolve from the glass into the refractory to form spinels that do not dissolve easily in to the glass.

This new layer of spinel crystals may form a protective secondary refractory layer at the corrosion interface, as long as agitation and convection are mild, reducing further corrosion of the refractory. Al and Mg are dissolved from the refractory into the glass raising their local concentrations near the refractory-glass interface. Similar to the dissolution of salt in water, as more solute is dissolved by the solvent, the rate of dissolution slows as saturation is approached. In the case of the refractory and the glass, the Mg and Al components are the solute being dissolved by the glass acting as a solvent. As the concentration of Mg and Al increase near the refractory-glass interface, the dissolution of the two species slows, reducing the corrosion rate with time.

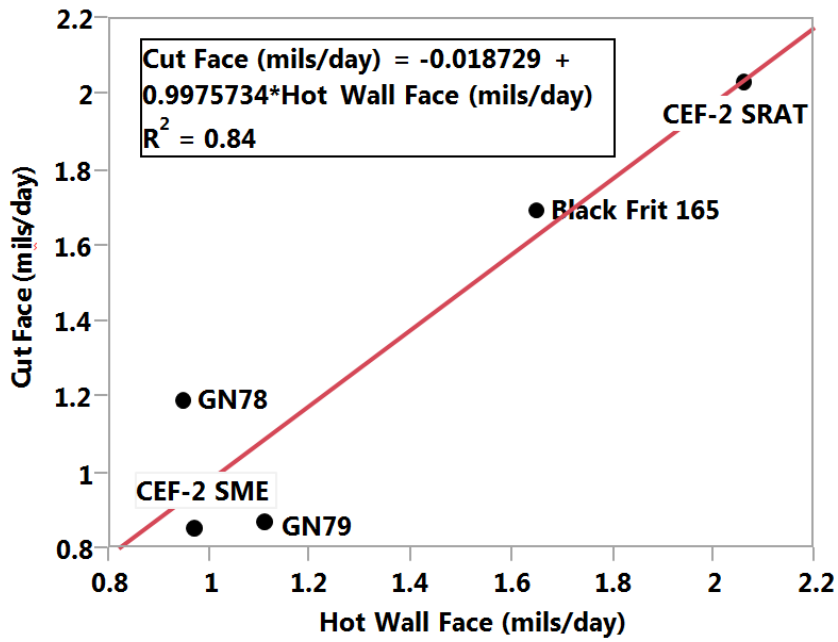

Figure 3-7. Plot of Cut Face Corrosion Rates versus Hot Wall Corrosion Rates at 120 Hours.

Comparing the corrosion at the hot wall face to the cut face, the slope of the line of comparison in Figure 3-7 shows that after five days in the melt pool, the two faces corrode at the same rate.

3.3.2 General Corrosion Rate Measurement Difficulties

Quantitative determination of the corrosion rate is difficult due to the dual reaction layers of "loss of material" and "selective penetration" appearing varied and somewhat subjective in the delineation of these two layers; therefore, the individual values are not represented except where their demarcation is explicitly obvious and the "total penetration" is reported instead. Determination of the original surface was also difficult to pinpoint due to significant spalling of spinel crystalline material into the glass. These demarcations are noted, where applicable. In the ASTM C621 procedure section on precision and bias, the precision of the corrosion measurements is 42.7% for duplicate samples. Therefore, it is best to observe the quantitative results as qualitative trends due to the high variability of the measurements without significant replicates; for example, sixteen replicates are required to get a precision of 15.1%.

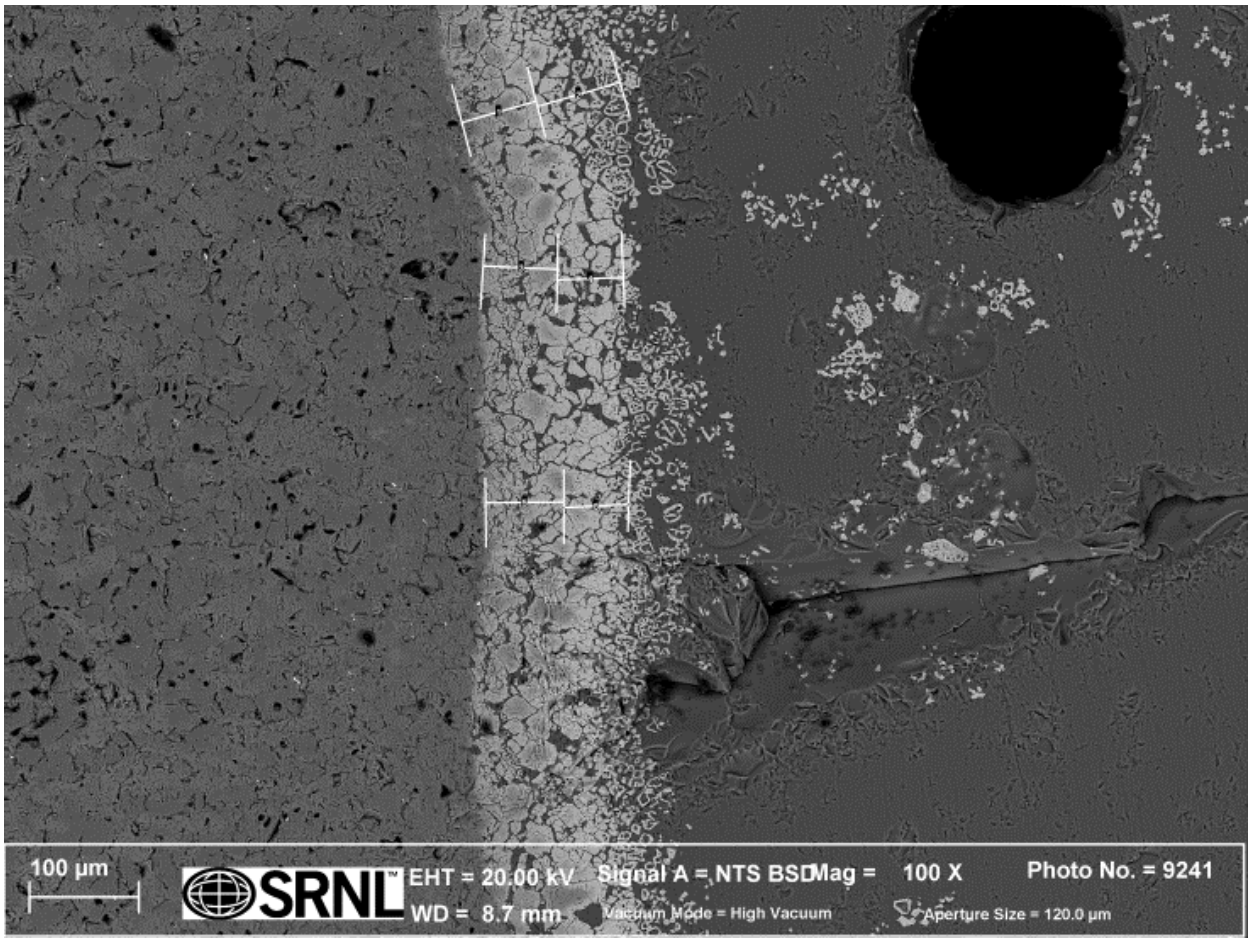

Figure 3-8. Example SEM image displaying difficulty in elucidating the original material face and the demarcation between the "loss of material" and the "selective penetration" corrosion regions.

Some aid in elucidating the depth of corrosion regions comes from elemental point maps. Utilizing SEM, point areas throughout the glass can be compositionally examined. Tracking the changes in Fe, Ni, Al, Mg and Si follow spinel formation, Al and Mg dissolution and glass inclusion.

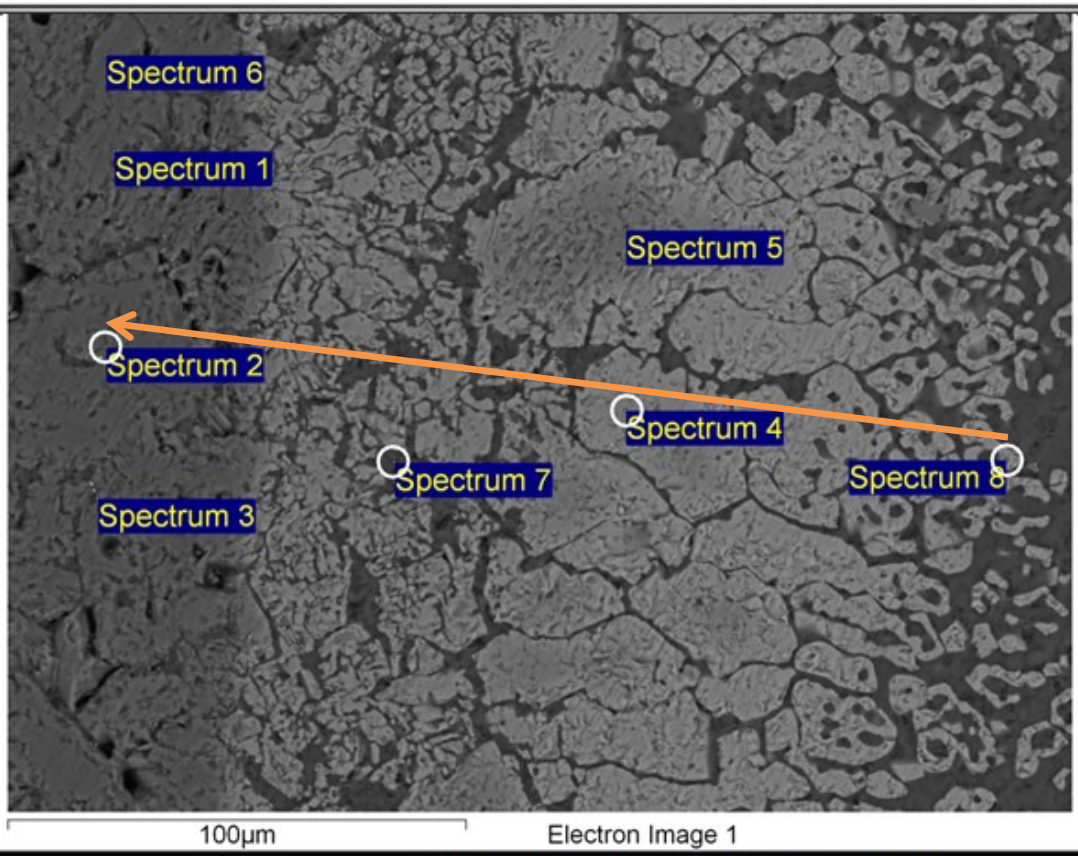

	Elemental weight percent				
Spectrum	Mg	Al	Si	Cr	Fe
Spectrum 1	1.21	30.97	0.60	17.03	2.33
Spectrum 2	3.59	30.84	0.34	20.06	4.47
Spectrum 3	0.18	35.90	4.03	13.86	1.86
Spectrum 4	1.81	11.16	0.21	18.43	37.73
Spectrum 5	3.31	24.00	0.00	18.83	16.83
Spectrum 6	0.00	35.47	0.18	21.03	1.45
Spectrum 7	0.66	17.57	27.49	1.23	3.08
Spectrum 8	1.17	4.01	0.86	13.91	53.09

Figure 3-9. SEM elemental point mapping of corrosion region with relative elemental concentrations.

For example, compare the analyses labelled "Spectrum 2", "Spectrum 4" and "Spectrum 8" from the SEM data for the sample from GN79 held for 120 hours (Figure 3-9). Point spectra are taken at various locations in the refractory-glass interface region. The incident electron beam is located relative to a corner of the spectrum label (indicated by a white circle ○ in Figure 3-9). The diameter of the analyzed area is approximately 6.6 µm. As you follow the line from right to left across the image, you are moving from the corroded edge with spinels spalling into the glass toward the minimally corroded reaction front of the "selective penetration" region within the K-3 coupon. Analyzing the relative compositions at each point,

Fe from the glass is shown to be penetrating the corrosion front, highest where it has formed the separating spinel crystals, while Mg and Al are being dissolved from the K-3 into the glass, their relative concentrations low but present. This gradient analysis corroborates the corrosion mechanisms occurring at the refractory-glass interface. Analyses of locations such as that indicated by "Spectrum 7" represent regions where glass has flowed through cracks and voids formed in the "loss of material" region to begin encroaching on the corrosion front inside the refractory corrosion region, hence, the higher Si concentration at this location further away from the initial refractory-glass interface.

3.3.3 Metallic Fe^0 Depletion Observed

Below the region of general corrosion, deeper into the K-3 coupon, further chemical reaction is observed. The CEF glycolic campaign, which was targeted to have a reducing REDOX, had nitrate concentrations in the 1.0-1.5 molar range after it was remediated. This is twice as much nitrate used in any typical nitric-formic flowsheet. Iron metal, Fe^0, is especially susceptible to attack by nitric acid forming iron nitrate species and NO by the following reaction [3]:

$$2Fe^0 + 8HNO_3 \rightarrow 2Fe(NO_3)_3 + 2NO + 4H_2O$$

A similar reaction could be written with $NaNO_3$ as the Fe^0 is unstable under oxidizing conditions in the feed or the melt (excess O_2 in the melt). According to the table of reduction/oxidation half reactions from Reference 3, reproduced here as Table 3-3, nitrate is a stronger oxidizing agent than iron is a reductant but nitrate is not as strong an oxidizer as Cr is a reductant, so Fe^0 would get preferentially oxidized/dissolved compared to Cr^0.

Table 3-3. Reduction/Oxidation Half Reactions [3].

Pertinent "Half" Reactions	E° Potential, (Volts)
REDUCTIONS	
$N_2O + 2H^+ + 2e^- \rightarrow N_2 + H_2O$	+1.77
$NO_3^- + 6H^+ + 5e^- \rightarrow 0.5N_2 + 3H_2O$	+1.24
OXIDATIONS	
$2Cr^{+3} + 7H_2O \rightarrow Cr^{+6}{}_2O_7^{-2} + 14\,H^+ + 6e^-$	-1.33
$Mn^{+2} + 2H_2O \rightarrow Mn^{+4}O_2 + 4H^+ + 2e^-$	-1.21
$Mn^{+4}O_2 + 2H_2O \rightarrow Mn^{+7}O_4^- + 4H^+ + 3e^-$	-1.68
$Ni^{+2} + 2H_2O \rightarrow Ni^{+4}O_2 + 4H^+ + 2e^-$	-1.93
$Fe^{+2} \rightarrow Fe^{+3} + e^-$	-0.77

To help substantiate the selective attack of nitrates on the metallic species in the K-3, average atomic number density maps tracking phases up to 7mm from the edge of the coupon, reveal depletion similar to that observed in the previous CEF-2 testing with the NG feeds.

Table 3-4 details the percentage of the highest density phase (metallic phase) as a function of the feed and experiment comparing to the density map from the previous study using the CEF melter. The data from the previous tests in the CEF melter [3] showed aggressive attack on the Fe^0 deeper in the coupon due to the combination of cavitation and a high percentage of nitric acid in the feed. Preferential attack of the metallic phase by the nitric acid along cracks or within voids created by cavitation moved the corrosion effects beyond the typical corrosion reaction front observed as the "selective penetration" region.

By comparison, all feeds in this experiment showed some depletion of the metallic phase with longer experimental durations. This could still be an effect of the higher nitric acid concentrations in the NG melter feeds as compared to NF melter feeds. With the REDOX target tied to the acid ratio and stoichiometry, the Fe^0 depletion could also be a function of REDOX nature of the glass melt pool. Since bubbling was not a variable in this experiment, the cavitation was not a possible contributing factor.

Table 3-4. Percentage of Most Dense (Metallic) Phases from Average Atomic Number Density Area Maps.

Melter Feed	Time of Experiment (h)	Area Percent at Depth							
		Edge	1mm	2mm	3mm	4mm	5mm	6mm	7mm
Unreacted K-3	----------	0.10	0.00	0.10	0.10	0.10	0.20	0.40	0.60
Black Frit 165	4	0.05	0.10	0.15	0.20	0.20	0.35	0.50	0.45
	24	0.05	0.05	0.05	0.05	0.15	0.10	0.10	0.15
	120	0.10	0.10	0.05	0.00	0.10	0.10	0.10	0.20
CEF-2 SRAT	4	0.05	0.00	0.00	0.00	0.10	0.25	0.30	0.45
	24	0.00	0.10	0.10	0.10	0.10	0.10	0.15	0.10
	120	0.00	0.05	0.05	0.10	0.10	0.05	0.10	0.10
CEF-2 SME	4	0.10	0.00	0.10	0.05	0.10	0.20	0.25	0.50
	24	0.00	0.05	0.05	0.05	0.10	0.10	0.10	0.00
	120	0.00	0.05	0.10	0.10	0.10	0.20	0.10	0.10
GN78	4	0.10	0.10	0.15	0.10	0.05	0.10	0.30	0.35
	24	0.00	0.00	0.00	0.10	0.00	0.00	0.00	0.10
	120	0.15	0.05	0.05	0.10	0.15	0.15	0.05	0.15
GN79	4	0.00	0.05	0.00	0.05	0.05	0.15	0.35	0.55
	24	0.10	0.00	0.10	0.10	0.10	0.30	0.10	0.10
	120	0.10	0.10	0.05	0.10	0.20	0.15	0.10	0.05

The cracks and voids seen in the CEF-2 campaign due to the cavitation from the argon bubbler were not present in this series of crucible experiments; therefore, the extended penetration of the corrosion fronts was not observed. Regions that show void-space corrosion were due to the porosity of the K-3 refractory. If the full effects of the cavitation are to be studied, bubbled crucible experiments and larger scale melter (i.e. CEF and SMRF) experiments where the bubbler and coupon placement can be adjusted must be performed.

4.0 Conclusions

Static crucible corrosion testing utilizing nitric-glycolic flowsheet melter feeds was performed to further examine the effect of the alternate reductant on the refractory MOC of the DWPF HLW melter. The results were compared to previous large-scale CEF melter testing and a pre-formed glass standard representing nitric-formic flowsheet glass.

The corrosion mechanisms, “loss of material” and “selective penetration” as well as selective Fe^0 attack, were observed as in previous nitric-glycolic flowsheet testing [3] with some variation. The “loss of material” and “selective penetration” had also been observed in the nitric-formic flowsheet [11] [12] [13] but the selective Fe^0 attack had not been observed in the nitric-formic flowsheet. While the same mechanisms were determined, it is possible that the change in the polishing procedure for the current study

versus the previous studies made the delineation between the "loss of material" and "selective penetration" corrosion regions less obvious and a larger variable in this series of experiments. This difficulty in defining these two sub-regions of corrosion led to the data presentation of only the "total penetration". From the "total penetration" the corrosion rates were determined and compared to those determined from the CEF testing and those determined from the Black Frit 165 standard glass which represents the nitric-formic flowsheet corrosion rates. The general corrosion rates for the NG flowsheet were observed to be on the order of 1.2 – 1.6x higher during the first 4 hours and 1.2 – 2.9x higher during the first 24 hours of testing as compared to the Black Frit 165 standard glass. However, the general corrosion rates reached similar values at the 120-hour mark. This is likely due to the formation of a protective layer of spinels and saturation of Mg and Al cations at the refractory-glass interface in all the glasses. These corrosion rates at the extended run times are the most important to extrapolating melter lifetime information due to the fact that the past and current melters have operated on the order of 8-10 years each. Since these values are similar for NG melter feed and Black Frit 165 (the NF-comparative standard), there should be little difference in melter life when agitation and convection within the melt pool are low. Accelerated corrosion in the short run time experiments is possibly due to the higher fraction of nitric acid in the NG feeds as compared to the NF feeds. Until this extra portion of nitric acid has reacted or the protective spinel layer has built up, the corrosion could be accelerated.

Corrosion rates at the time of flowsheet changeover or new melter startup will depend on the starting conditions. During flowsheet changeover, the corrosion of the refractory will be dictated primarily by the material already in the melter. The additional impact of the feed on top of the melt pool will be minimized due to the separation from the refractory by the present material until it has significantly reacted and reached the molten melt pool. Corrosion may become temporarily accelerated if drying feed reaches the refractory as it moves across the cold cap, but the impact could be decreased as a function of the time spent at temperature on top of the cold cap. During startup of a new melter, if startup frit, similar to Black Frit 165, is utilized, the initial corrosion rates before feeding begins will be reflected by the corrosion rates observed in preformed glass. The corrosion rates will change as feeding begins, similar to during flowsheet changeover, but will not be as aggressive as starting with dried NG flowsheet feed. There was no difference observed in the corrosion of the hot face versus the cut faces of the K-3 refractory telling us the difference in density between the two faces has little to no impact on the corrosion response.

Variation in the measured corrosion values stems from the use of only two samples per melter feed and having those measurements performed by two different researchers. Though the use of the ImageJ software made the scale more reproducible and the selection of measurement points more precise, the bias raised by multiple investigators and limited number of samples increased the percent critical difference from average of each measurement taken. Per ASTM C621, the typical percent difference for only two samples is on the order of 40%. Based on the observed percent relative standard deviations for the averages of the measurements between investigators, the measured values in this study typically remained within this precision.

Suggestions for future work are presented to further our understanding of the impacts of the alternate reductant, with and without argon bubblers, on the service life of the Monofrax™ K-3 refractory material used in HLW glass melters.

5.0 Future Work

Further testing in the future is recommended to bridge the gap between the non-bubbled crucible testing documented in this study and the previous bubbled testing in the CEF. This testing could provide better examination of the effects of time and chemical changes as well as increased melt pool agitation and convection on formation and removal of spinel reaction products and the overall general corrosion. Therefore, the following testing is recommended to be done in the future:

With the addition of agitation, i.e. argon bubblers, the "loss of material" region is likely to grow significantly. The corrosion rates are shown to slow as the region of glass near the refractory becomes saturated by the dissolution of Mg and Al from the refractory into the glass and as a layer of passivating spinel crystalline material builds up at the interface. Agitation will increase the convection of material in this region, spreading out the higher concentration of dissolved and spalled materials acting as a corrosion barrier. As these materials are moved, fresh surfaces of the refractory become exposed and susceptible to unabated corrosion. The original risk of excessive erosion/corrosion of the DWPF melter refractory material due to bubbler implementation was closed in revision 10 of document Y-RAR-G-00022. However, future testing of the effects of bubbling could still be important to the overall understanding of the corrosion behavior of the K-3 refractory. The following work is recommended:

1. Perform modified ASTM C621 tests in NG feeds with bubbling to determine the extent of the impact of agitation on the general corrosion. Placement of the coupon should include testing both directly in line with the bubbles and significantly separated from the bubblers in order to examine the long range impact of the bubbles and their ability to generate erosion and cavitation at a distance.
    a. Perform various scale melter tests (i.e. QMRF, SMRF, etc.) in NG feeds with and without bubbling with careful coupon placement to examine the agitation/convection effects over a larger distance and time scale as well as to correlate the dynamics of scaling.

The time frame of the accelerated corrosion rate is possibly as long as 2.5 days. [32] To get a complete understanding of corrosion rates over time, multiple points of data should be acquired in a region of time where the changing rates have a linear correlation.

2. Perform additional testing at a greater variety of timeframes. The behavior of the corrosion rate between the 24 hour timeframe and the 120 hour timeframe would be important to understand given the accelerated impact of the oxidants and reductants during this time period. The behavior of the corrosion rate after 120 hours is important to determine where a steady state of corrosion exists. Examination of the corrosion rate out to extended long-term timeframes on the order of 3 to 6 months could give an even more comprehensive understanding of the effects of ion depletion from the refractory on its structural integrity.

3. If possible, take a core sample of refractory material from below the melt line of the next decommissioned melter during autopsy. Examination of the refractory from a full-scale melter after a lifetime of usage could be utilized to confirm the observations made in simulant waste and smaller-scale melters. Comparison of these two refractories as a function of at least the following variables could expand our understanding of the corrosion mechanisms at work between the glass and refractory: the depth of the "loss of material" region, the depth of the "selective penetration" region, the depth and scale of Fe^0 depletion, the extent of spinel growth and retention at the refractory-glass interface, and the extent of Mg and Al dissolution from the refractory

The increased "loss of material" corrosion regions observed in NG feeds with higher nitric acid/nitrate anion concentrations than previous NF feeds presents concerns with the spalling of additional spinel crystalline material into the glass melt pool or to the bottom of the melter. Also, the loss of metallic Fe^0 from the interior of the refractory raises concerns over maintaining the internal integrity of the refractory brick for the types of lifetimes exhibited for the NF flowsheet with DWPF Melter #1 (8 years) and Melter #2 (10+years).

4. Testing with feeds containing an even wider range of anions is suggested to gain a more expansive understanding of the operational window of the refractory in terms of the effects on "loss of material" and Fe^0 depletion due to the anions alone.

6.0 References

[1] J. W. Amoroso and J. R. Zamecnik, "Measurement of Offgas Species from Thermal Decomposition of Simulated DWPF Melter Feed," U.S. Dept. of Energy, Savannah River National Laboratory, Aiken, SC, 2014.

[2] A. S. Choi, "DWPF Melter Off-Gas Flammability Model for the Nitric-Glycolic Acid Flowsheet," U.S. Dept. of Energy, Savannah River National Laboratory, Aiken, SC, 2014.

[3] J. L. Mickalonis, K. J. Imrich, C. M. Jantzen, T. H. Murphy and J. E. Wilderman, "Corrosion Impact of Alternate Reductant of DWPF and Downstream Facilities," U.S. Dept. of Energy, Savannah River National Laboratory, SRNL-STI-2014-00281, 2014.

[4] C. M. Jantzen, M. S. Williams, J. R. Zamecnik and D. M. Missimer, "Interim Glycol Flowsheet REDuction/OXidation (REDOX) Model for the Defense Waste Processing Facility (DWPF)," U.S. Dept. of Energy, Savannah River National Laboratory, Aiken, SC, 2015.

[5] C. M. Jantzen, F. C. Johnson, M. E. Stone, D. C. Koopman, J. R. Zamecnik, K. G. Brown, J. B. Pickett and C. C. Herman, "Melter REDuction/OXidation (REDOX) Control to Optimize Melting and Retain Radiomuclides: Part I. High Level Waste Melter REDOX Requirements and Measurement," *draft for the International Journal of Applied Glass Science. ,* 2014.

[6] C. M. Jantzen, K. J. Imrich and J. B. Pickett, "High Chrome Refractory Characterization: Part I Impact of Melt Reduction/Oxidation on the Corrosion Mechanism," *International Journal of Applied Glass Science,* pp. 1-21, 2015.

[7] C. M. Jantzen, K. J. Imrich and J. B. Pickett, "High Chrome Refractory Characterization: Part II Accumulation of Spinel Corrosion Deposits in Radioactive Waste Glass Melters," *International Journal of Applied Glass Sciences,* vol. 6, no. 2, pp. 158-171, 2015.

[8] G. G. Wicks, "Melter Materias Compatibility Program, Part I: Static and Dynamic Finger Tests-Simulated Glass Waste," U.S. Dept. of Energy, E. I. duPont deNemours & Co., Savannah River Laboratory, Aiken, SC, 1978.

[9] G. G. Wicks, "Melter Materials Compatibility Program, Part II: Static and Dynamic Finger Tests, Radioactive Waste Glass and Long-Term Simulated Tests," U.S. Dept. of Energy, duPont deNemours & Co., Savannah River Laboratory, Aiken, SC, 1979.

[10] G. G. Wicks, "Compatibility Tests of Materials for a Prototype Ceramic Melter for Defense Waste Products," U.S. Dept. of Energy, Natil. Tech. Info. Serv., Springfield, VA, 1979.

[11] G. G. Wicks, "Corrosion of Melter Materials," U.S. Dept. of Energy, E. I. duPont deNemours & Co., Savannah River Laboratory, Aiken, SC, 1980.

[12] W. N. Rankin, "Evaluation of Glass-contact Materials for Waste Glass Melters," *Nuclear Waste Management, Advances in Ceramics,* vol. 8, pp. 559-566, 1984.

[13] W. N. Rankin, "Corrosion of Melter Materials: Part III. Effect of Na2O," U.S. Dept. of Energy, E. I. duPont deNemours & Co., Savannah River Laboratory, Aiken, SC, 1982.

[14] "Basic Data Report Defense Waste Processing Facility Sludge Plant Savannah River Site 200-S Area," U.S. Dept. of Energy, Westinghouse Savannah River Company, Aiken, SC, 1992.

[15] "Technical Data Summary for the Defense Waste Processing Facility Sludge Plant," U.S. Dept. of Energy, E. I. duPont deNemours & Co., Savannah River Laboratory, Aiken, SC, 1982.

[16] W. A. Miller and W. C. Steggs, "Evolution and Application of Chrome Bearing Fused Cast Refractories," Carborundum Co, Falconer, NY, 1975 as cited in reference 9.

[17] C. M. Jantzen, K. G. Brown, K. J. Imrich and J. B. Pickett, "High Cr2O3 refractory Corrosion in Oxidizing Melter Feeds: Relevance to Nuclear and Hazardous Waste Vitrification," *Ceramic Transactions,* vol. 93, pp. 203-212, 1999.

[18] A. Muan and E. F. Osborn, "Phase Equilibria Among Oxides in Steelmaking," Addison-Wesley Publishing Company, Inc., Reading, MA, 1965.

[19] S. A. Degterov and A. D. Pelton, "Thermodynamic Calculation of Glass/Slag/Refractory Equilibria in Coal Gassification," *Ceram. Trans,* vol. 78, pp. 91-103, 1996.

[20] M. J. LaMont and P. Hrma, "A Crucible Study of Spinel Settling in a High-Level Waste Glass," *Ceramic Trans,* vol. 87, pp. 343-348, 1998.

[21] J. Klouzek, J. Alton, P. Hrma and T. Plaisted, "Crucible Study of Spinel Settling in Molten High-Level Waste Glass," *Ceramic Trans,* vol. 119, pp. 301-308, 2001.

[22] J. W. Amoroso, D. K. Peeler and T. B. Edwards, "Elimination of the Characterization of DWPF Pour Stream Sample and the Glass Fabrication and Testing of the DWPF Sludge Batch Qualification Sample," U.S. Dept. of Energy, Savannah River National Laboratory, Aiken, SC, 2012.

[23] S. A. Cooper and P. S. Nicholson, "Influence of Glass Redox Conditions on the Corrosion of Fusion-Cast Chrome-Alumina Refractories," *Ceramic Bulletin,* vol. 59, no. 7, pp. 715-717, 1980.

[24] Corning Engineering Laboratory Services Report for W. N. Rankin #11988-008, (July 31, 1985).

[25] N. E. Bibler, O. B. Hodoh and T. F. Fellinger, "Analysis and Water Leaching of a Radioactive Sample from the Pour Spout of DWPF Melter," U.S. Dept. of Energy, Westinghouse Savannah River Company, Aiken, SC, 1996.

[26] F. C. Johnson, M. E. Stone and D. H. Miller, "Alternate Reductant Cold Cap Evaluation Furnace Phase II Testing," U.S. Dept. of Energy, Savannah River National Laboratory, Aiken, SC, 2014.

[27] ASTM C621-09(2014), "Standard Test Method for Isothermal Corrosion Resistance of Refractories to Molten Glass," ASTM International, West Conshohocken, PA, 2014.

[28] H. D. Schreiber and A. L. Hockman, "Redox Chemistry in Candidate Glasses for Nuclear Waste immobilization," *J. Am. Ceram. Soc.,* vol. 70, no. 8, pp. 591-594, 1987.

[29] "Heat Treatment of Waste Slurries for REDOX and Corrosion Analysis," Technical Reference Procedure, Manual L29 Procedure ITS-0052, current revision, 2016.

[30] *Personal communication with C. Brown. (2016)..*

[31] W. Rasband, "ImageJ," National Institutes of Health, USA, [Online]. Available: http://imagej.nih.gov/ij. [Accessed 2016].

[32] H. Gan, X. Lu, A. C. Buechele, M. C. Paul and I. L. Pegg, "Corrosion of Chromium-Rich Oxide Refractories in Molten Waste Glasses," U.S. Dept. of Energy, Vitreous State Laboratory, Washington, DC, 2002.

Appendix A. Images of Pristine K-3 Coupons

Figure A-1. Images of a pristine K-3 coupon A) in a holder using an optical microscope B) showing density and metallic fleck gradient, and C) of the hot wall face under SEM.

a)

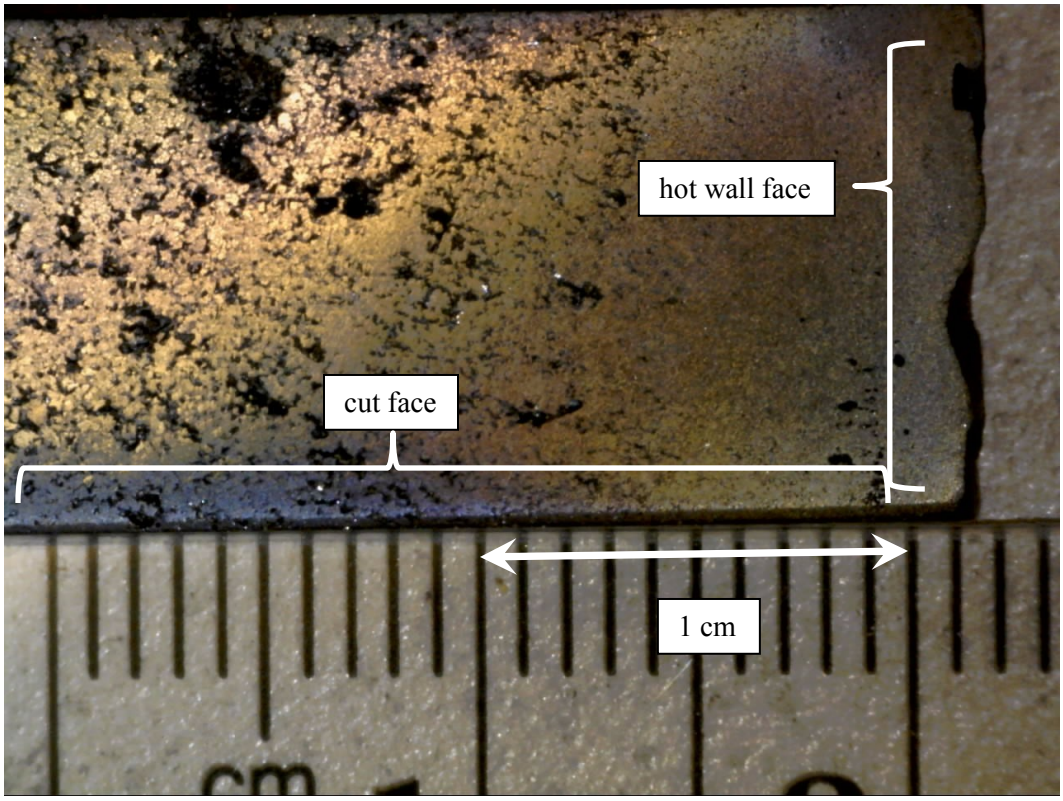

b)

c) 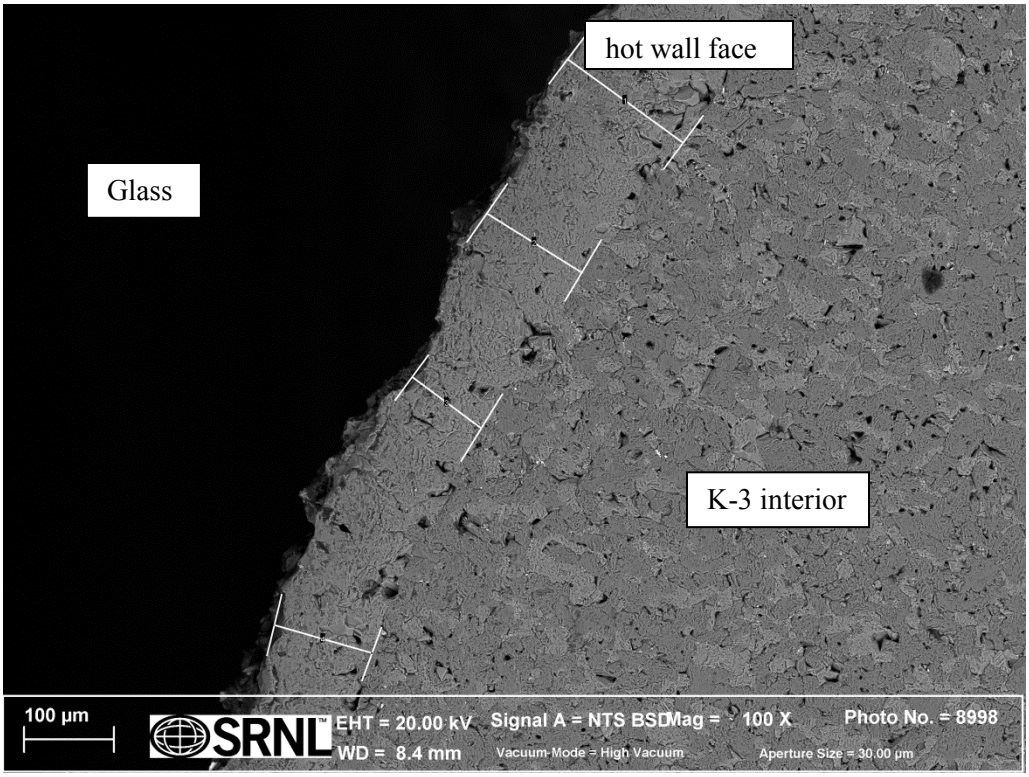
hot wall face
Glass
K-3 interior
100 µm
SRNL
EHT = 20.00 kV
WD = 8.4 mm
Signal A = NTS BSD
Vacuum Mode = High Vacuum
Mag = 100 X
Photo No. = 8998
Aperture Size = 30.00 µm

Appendix B. SEM Images of K-3 Coupons in Black Frit 165.

Figure B-1. Images of the a) and b) hot wall face and c) and d) cut face of a K-3 coupon immersed in Black Frit 165 after heat treatment for 4 hours. The regions measured for this study are shown as numbered lines.

a)

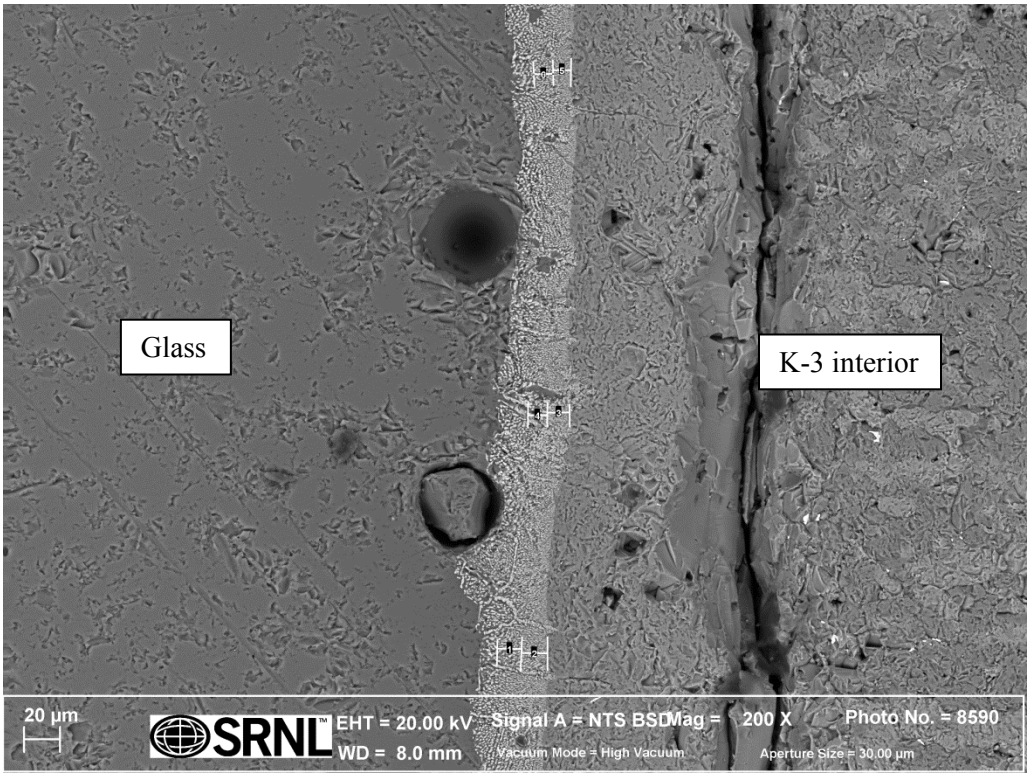

b)

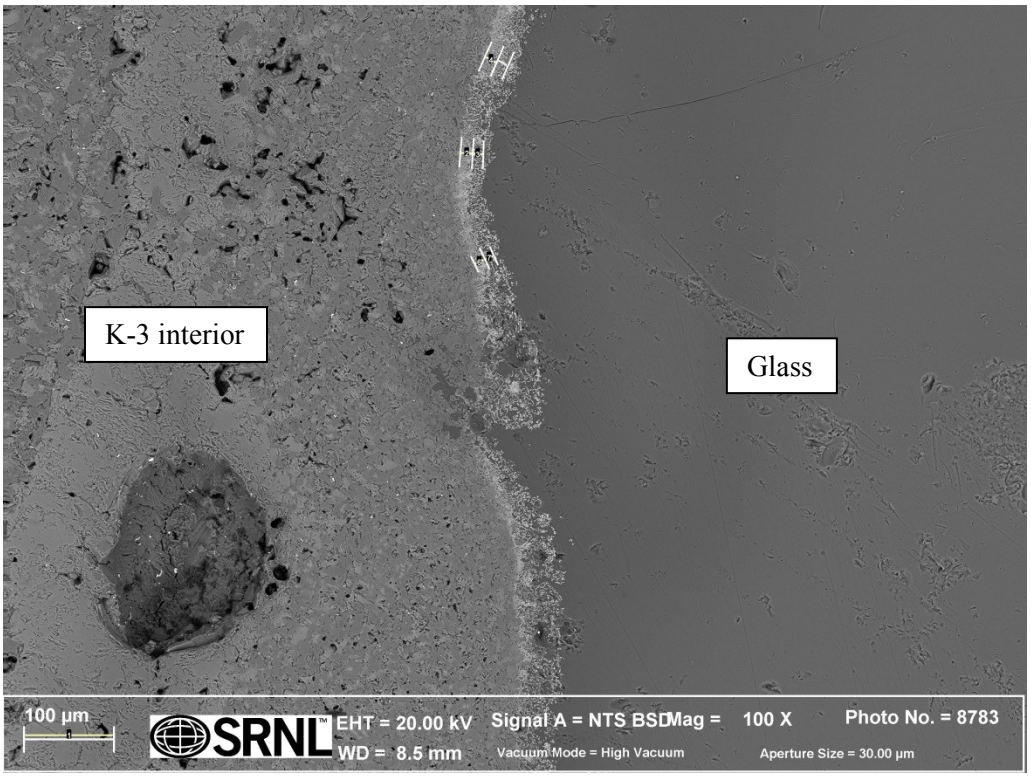
K-3 interior
Glass
100 µm
SRNL
EHT = 20.00 kV
WD = 8.5 mm
Signal A = NTS BSD
Vacuum Mode = High Vacuum
Mag = 100 X
Aperture Size = 30.00 µm
Photo No. = 8783

c)

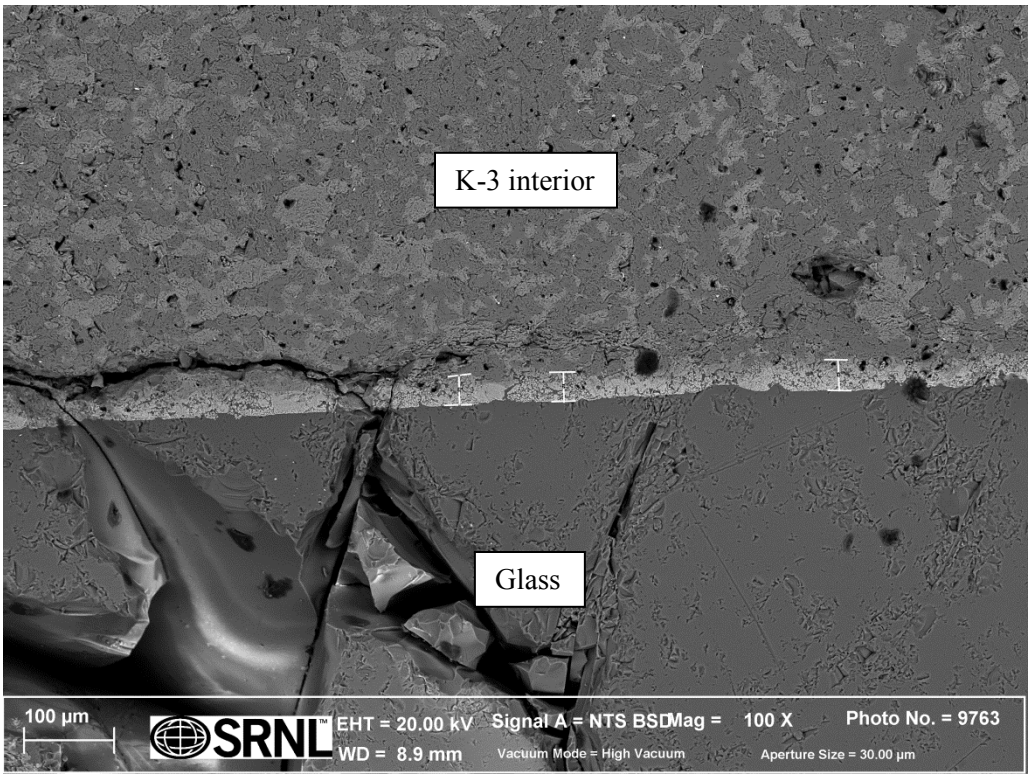
K-3 interior
Glass
100 µm
SRNL
EHT = 20.00 kV
WD = 8.9 mm
Signal A = NTS BSD
Vacuum Mode = High Vacuum
Mag = 100 X
Aperture Size = 30.00 µm
Photo No. = 9763

d)

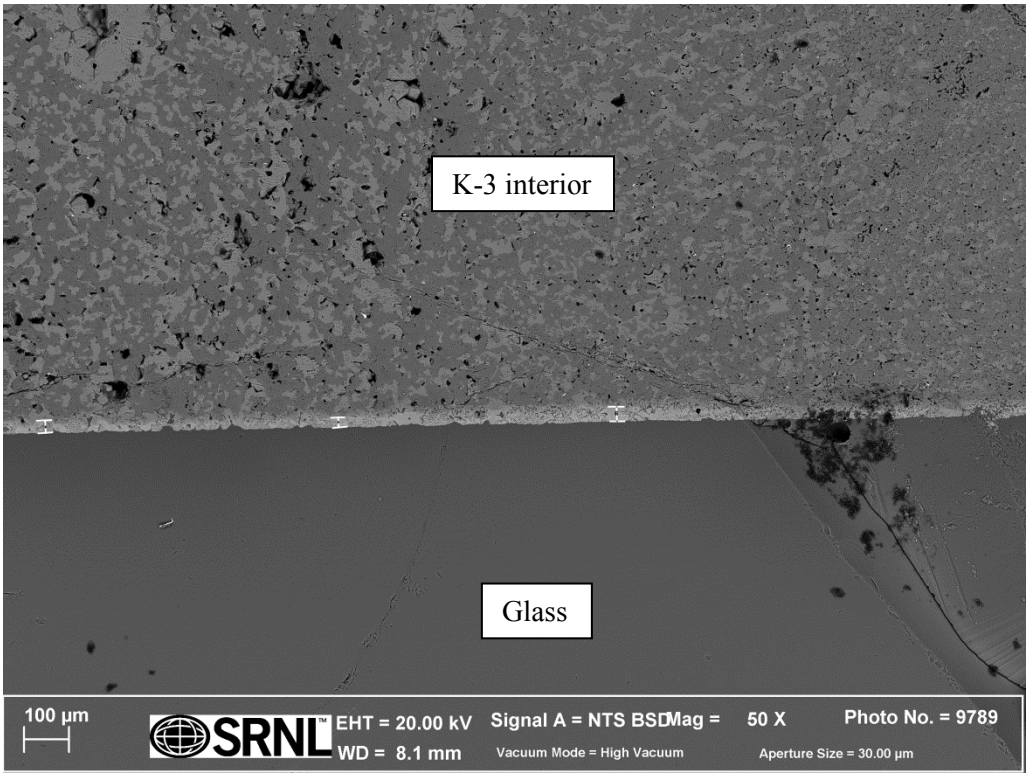

Figure B-2. SEM Elemental Maps of K-3 Coupon Embedded Black Frit 165 for 4 Hours.

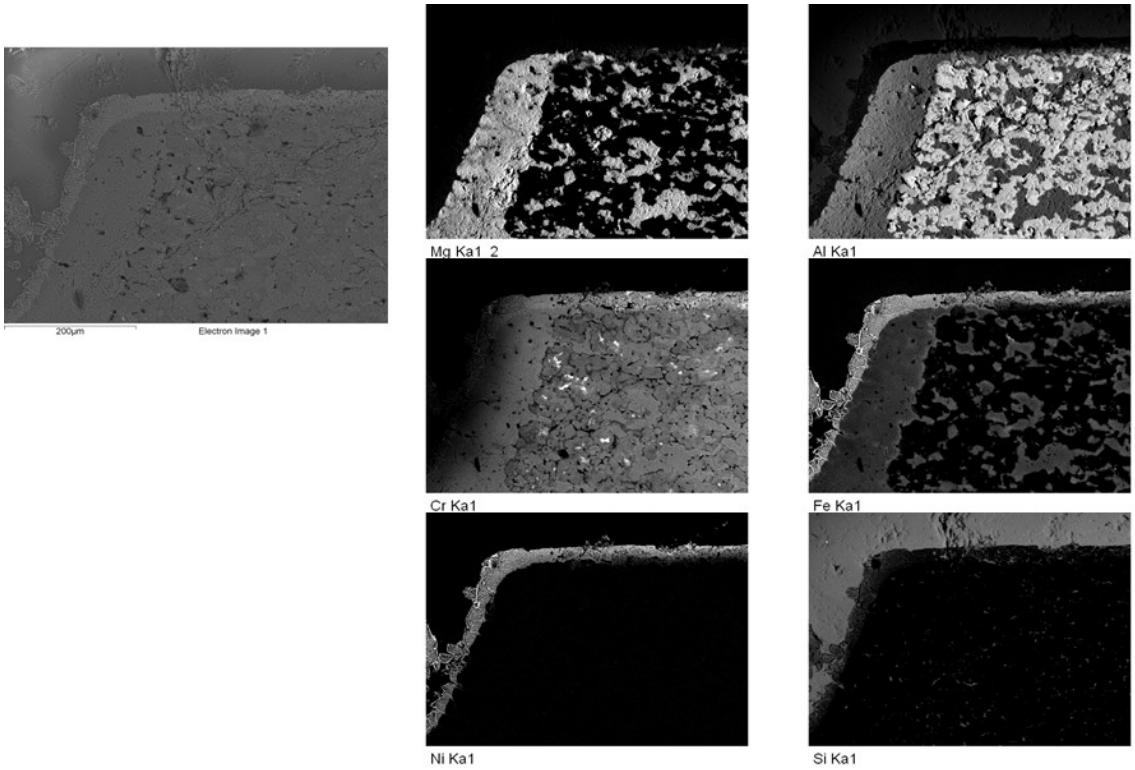

Figure B-3. Images of the a) and b) hot wall face and c) and d) cut face of a K-3 coupon immersed in Black Frit 165 after heat treatment for 24 hours. The regions measured for this study are shown as numbered lines.

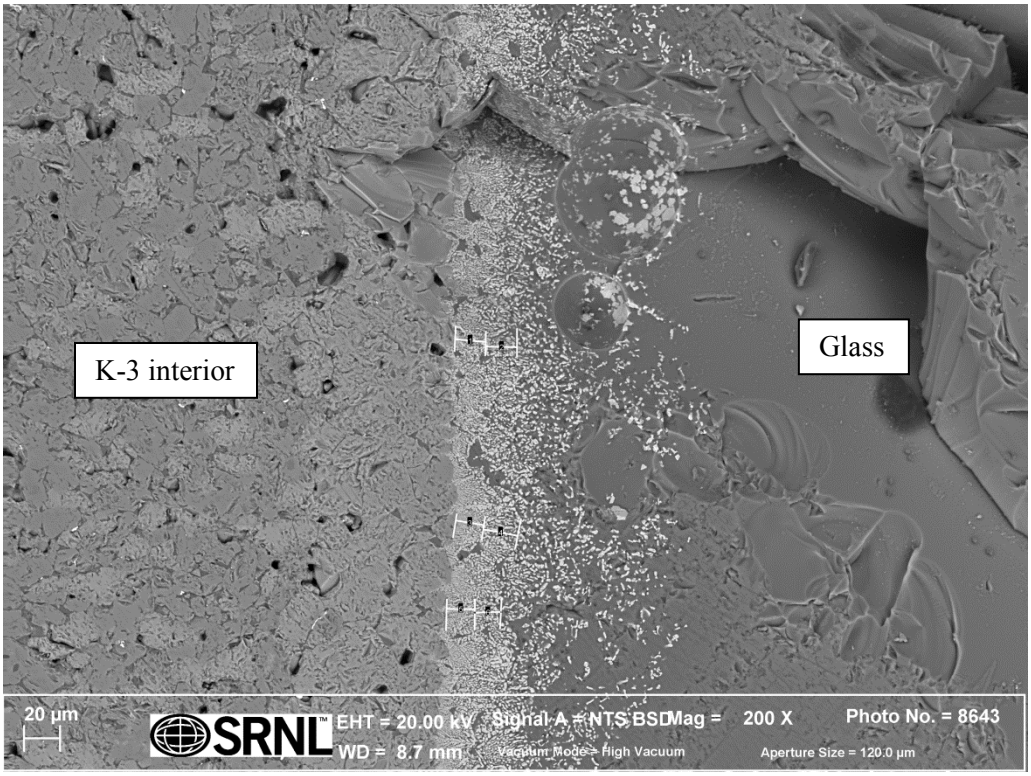

a)

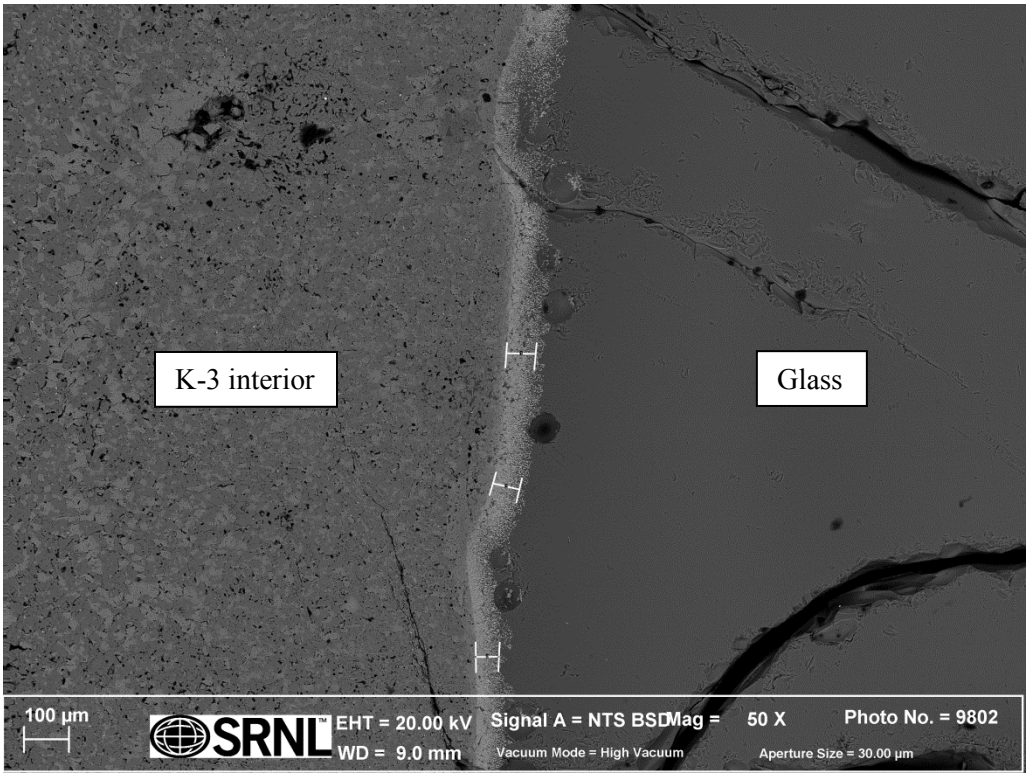

b)

c)

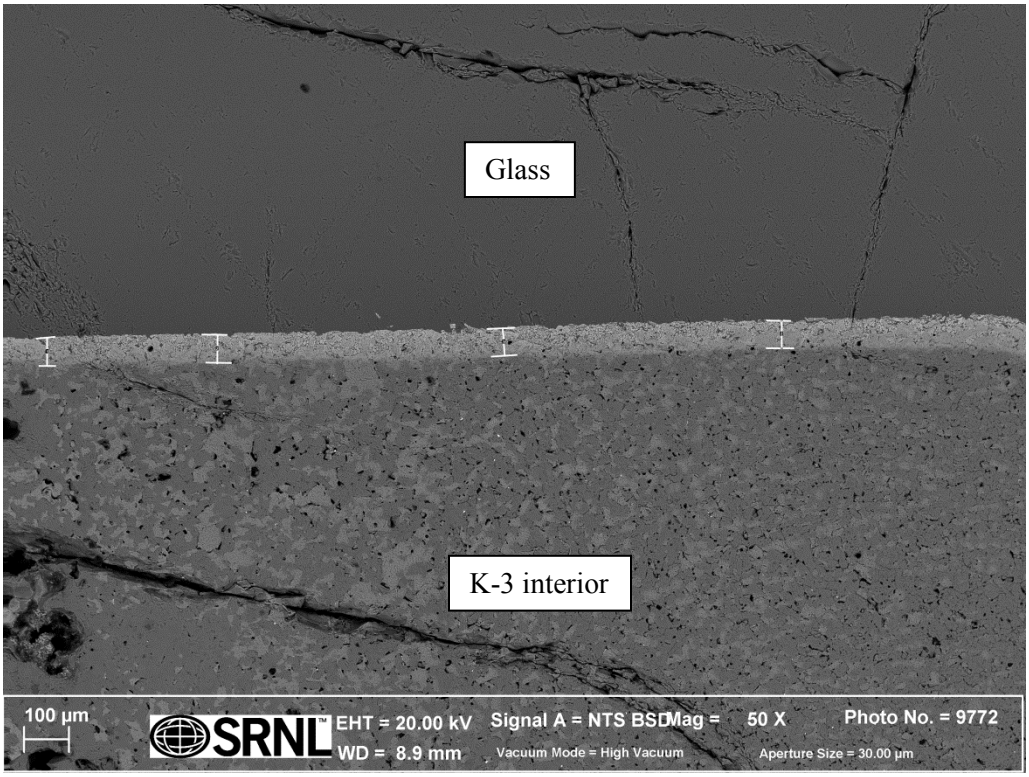
Glass
K-3 interior
100 µm
SRNL
EHT = 20.00 kV
WD = 8.9 mm
Signal A = NTS BSD
Mag = 50 X
Vacuum Mode = High Vacuum
Photo No. = 9772
Aperture Size = 30.00 µm

d)

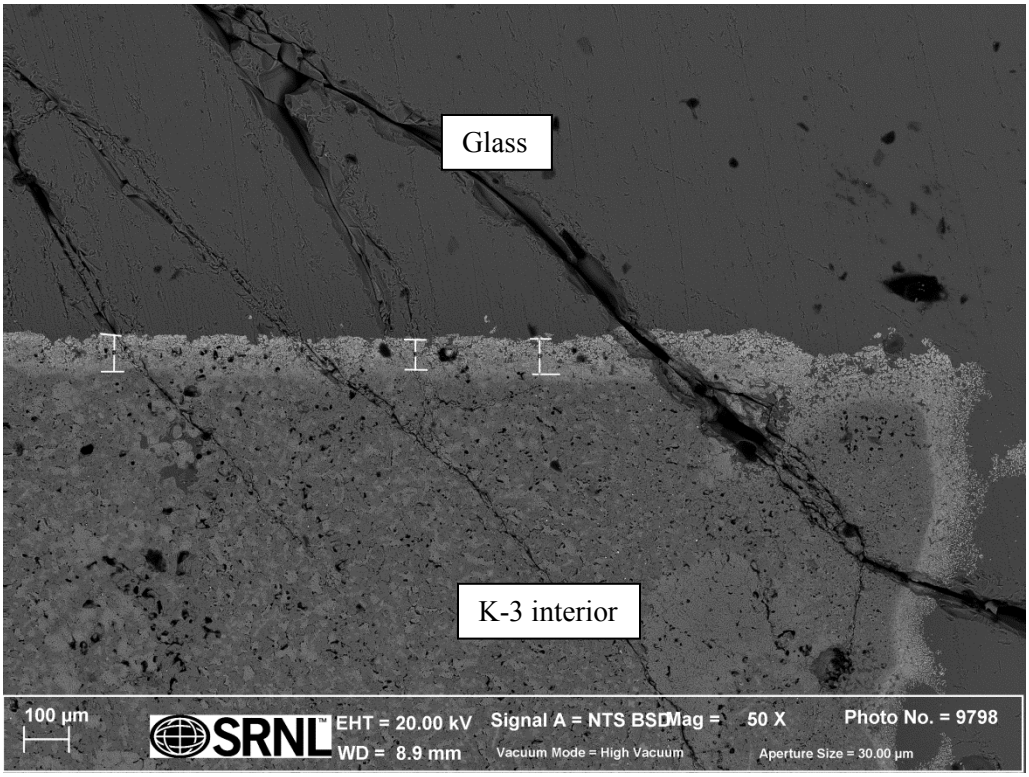
Glass
K-3 interior
100 µm
SRNL
EHT = 20.00 kV
WD = 8.9 mm
Signal A = NTS BSD
Mag = 50 X
Vacuum Mode = High Vacuum
Photo No. = 9798
Aperture Size = 30.00 µm

Figure B-4. SEM Elemental Maps of K-3 Coupon Embedded Black Frit 165 for 24 Hours.

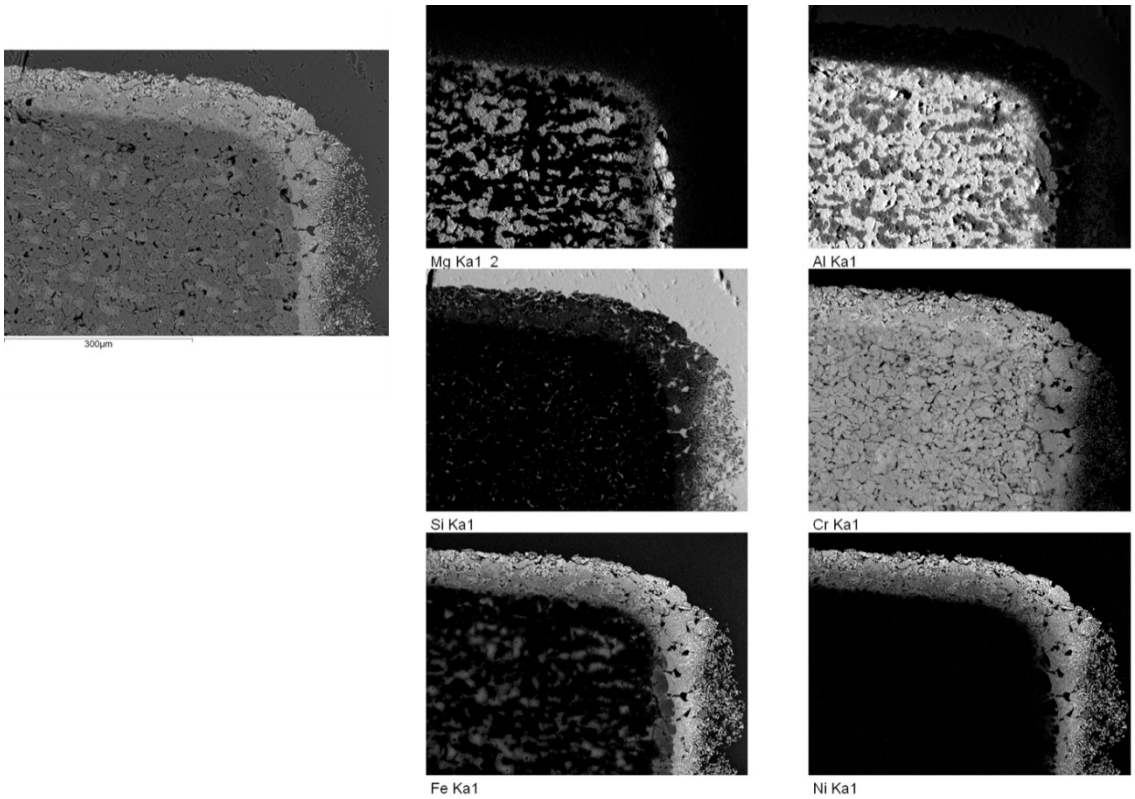

Figure B-5. Images of the a) and b) hot wall face and c) and d) cut face of a K-3 coupon immersed in Black Frit 165 after heat treatment for 120 hours. The regions measured for this study are shown as numbered lines.

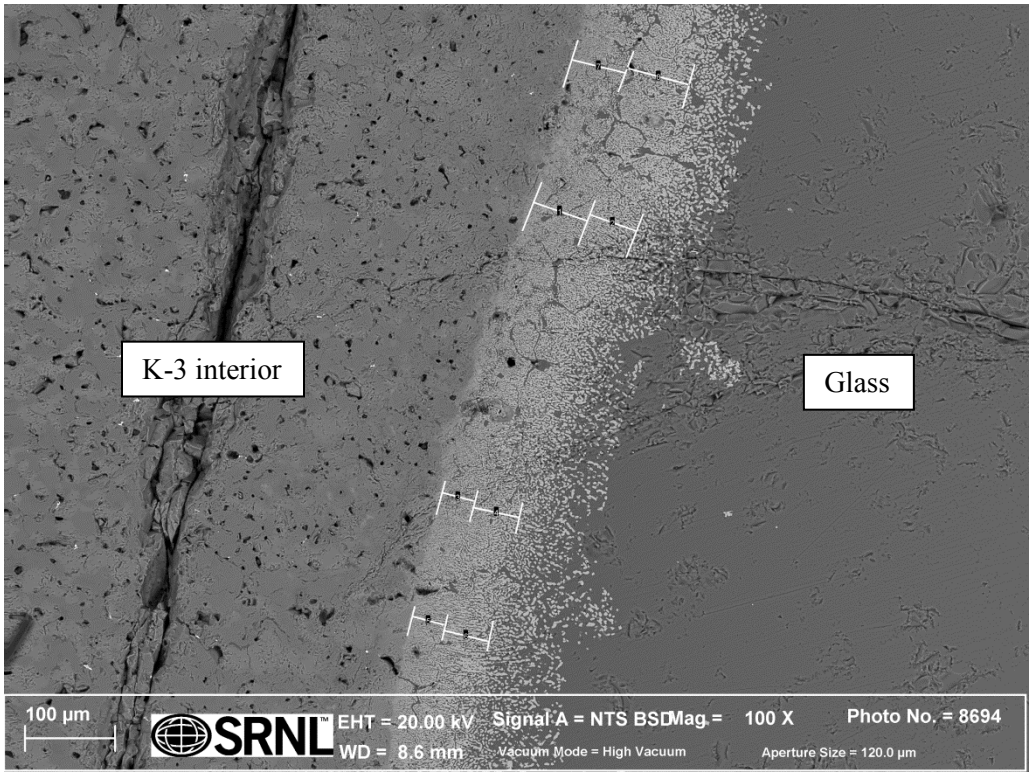

a)

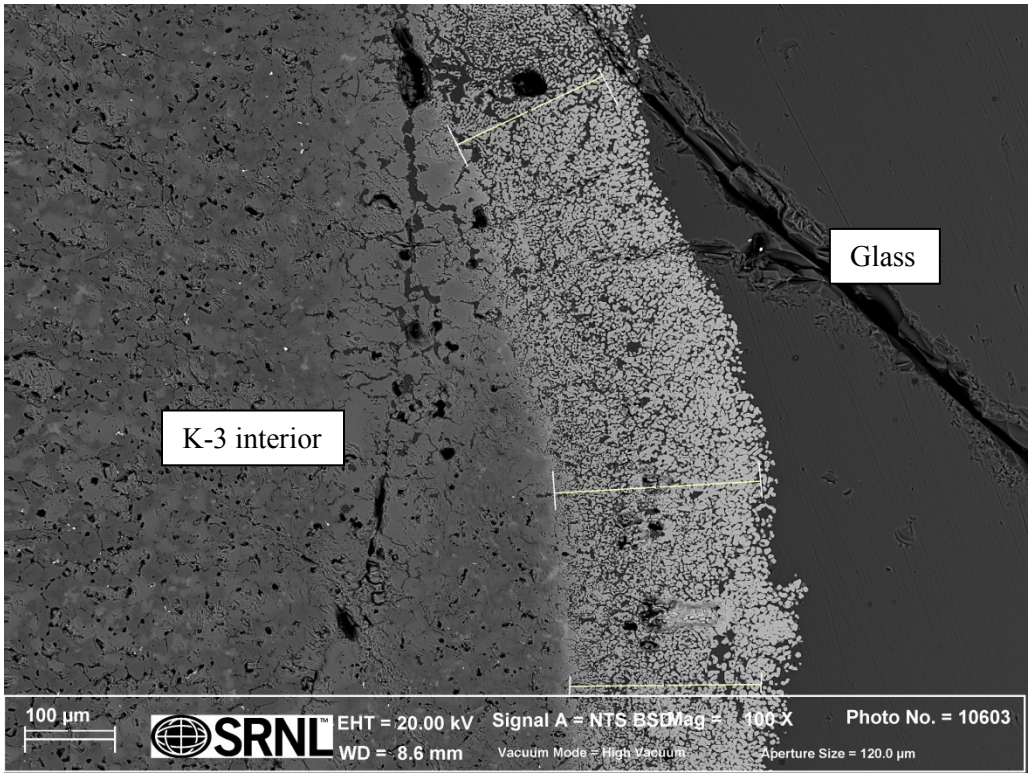

b)

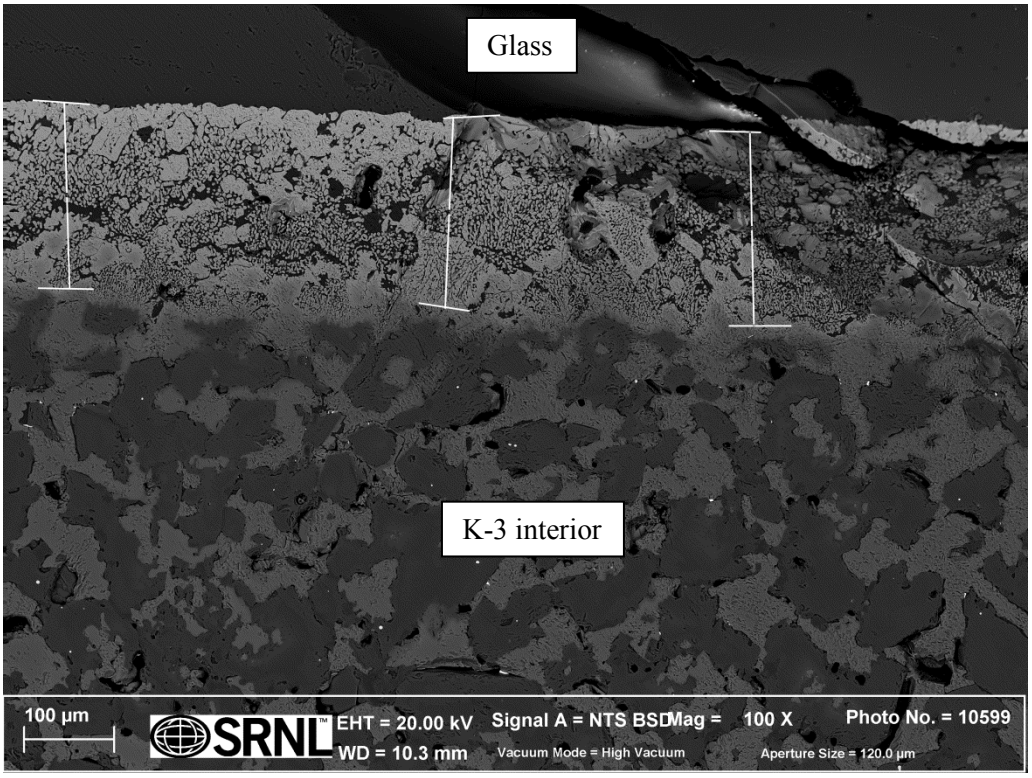
Glass
K-3 interior
100 µm
SRNL
EHT = 20.00 kV
WD = 10.3 mm
Signal A = NTS BSD
Vacuum Mode = High Vacuum
Mag = 100 X
Aperture Size = 120.0 µm
Photo No. = 10599

c)

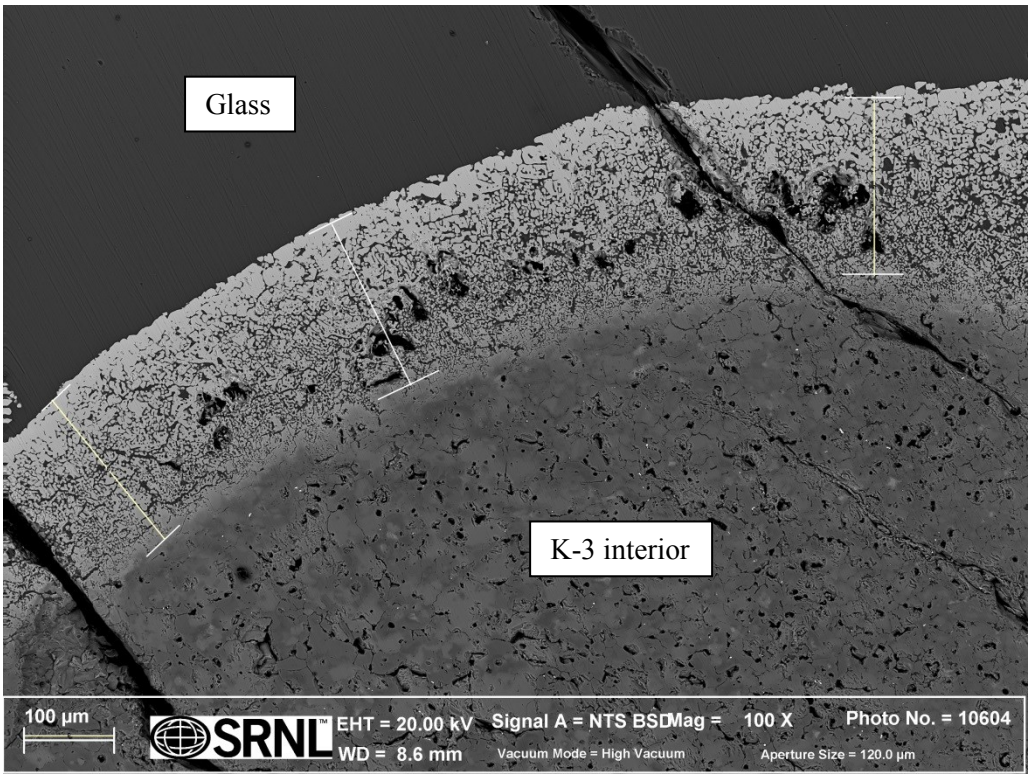
Glass
K-3 interior
100 µm
SRNL
EHT = 20.00 kV
WD = 8.6 mm
Signal A = NTS BSD
Vacuum Mode = High Vacuum
Mag = 100 X
Aperture Size = 120.0 µm
Photo No. = 10604

d)

Figure B-6. SEM Elemental Maps of K-3 Coupon Embedded Black Frit 165 for 120 Hours.

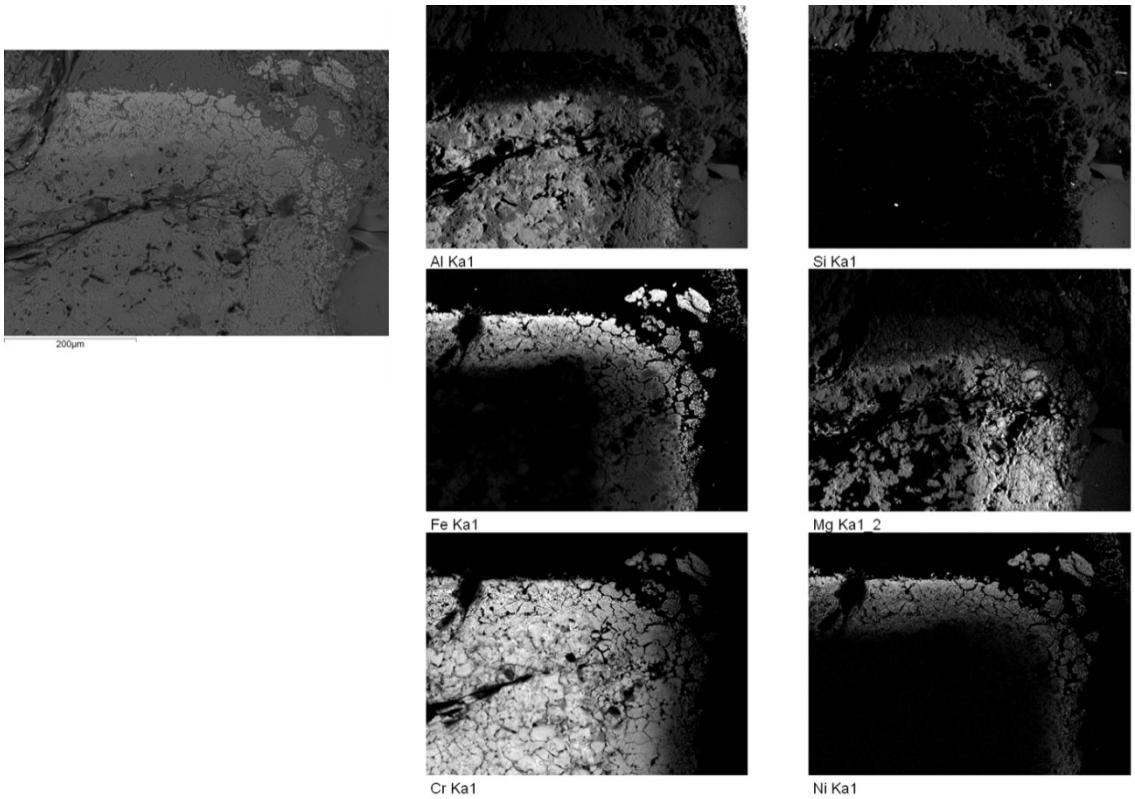

Appendix C. SEM Images of K-3 Coupons in CEF-2 SRAT Melter Feed.

Figure C-1. Images of the a) and b) hot wall face and c) and d) cut face of a K-3 coupon immersed in CEF-2 SRAT after heat treatment for 4 hours. The regions measured for this study are shown as numbered lines.

a)

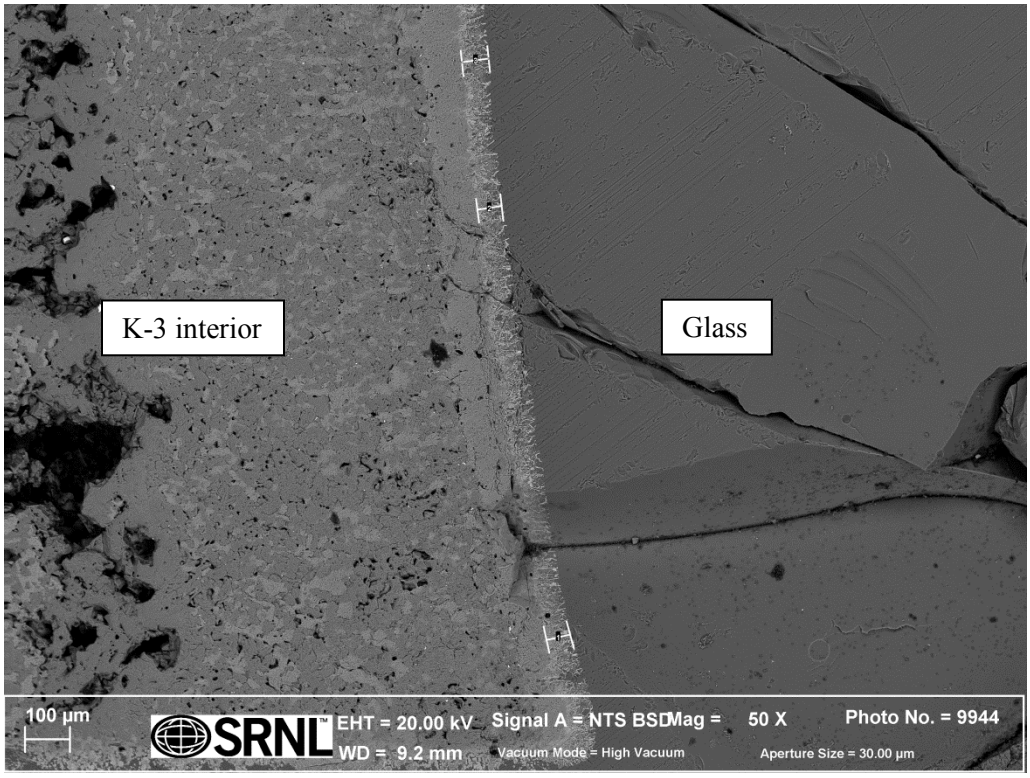

b)

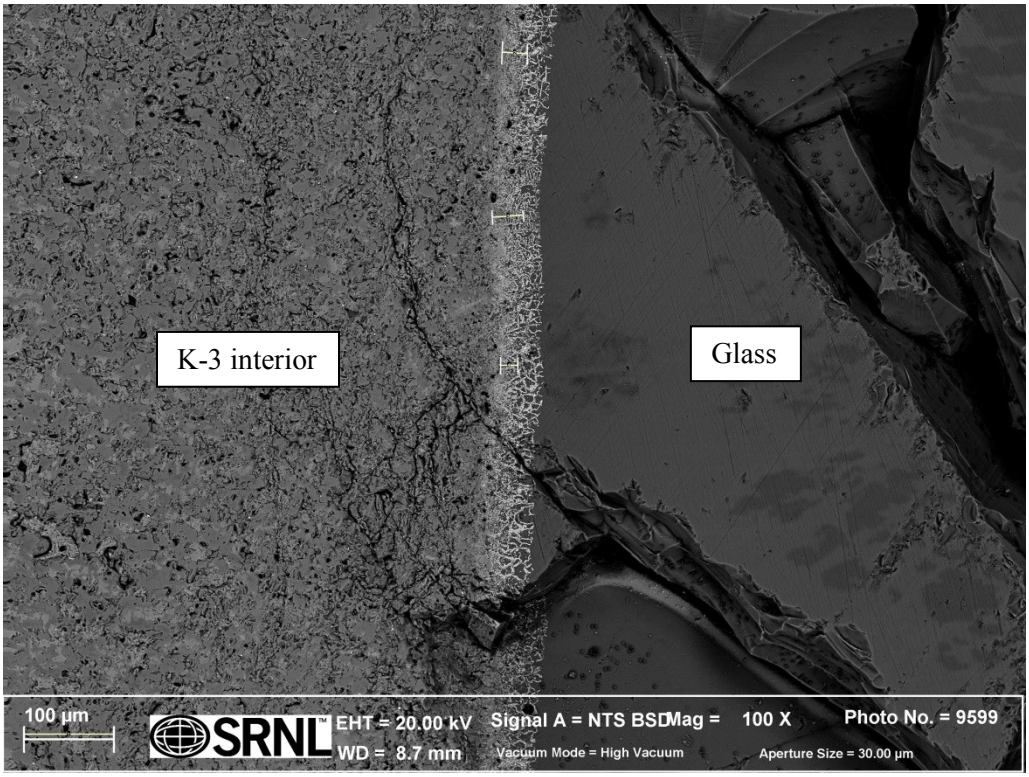
K-3 interior
Glass
100 µm
SRNL
EHT = 20.00 kV
WD = 8.7 mm
Signal A = NTS BSD
Vacuum Mode = High Vacuum
Mag = 100 X
Aperture Size = 30.00 µm
Photo No. = 9599

c)

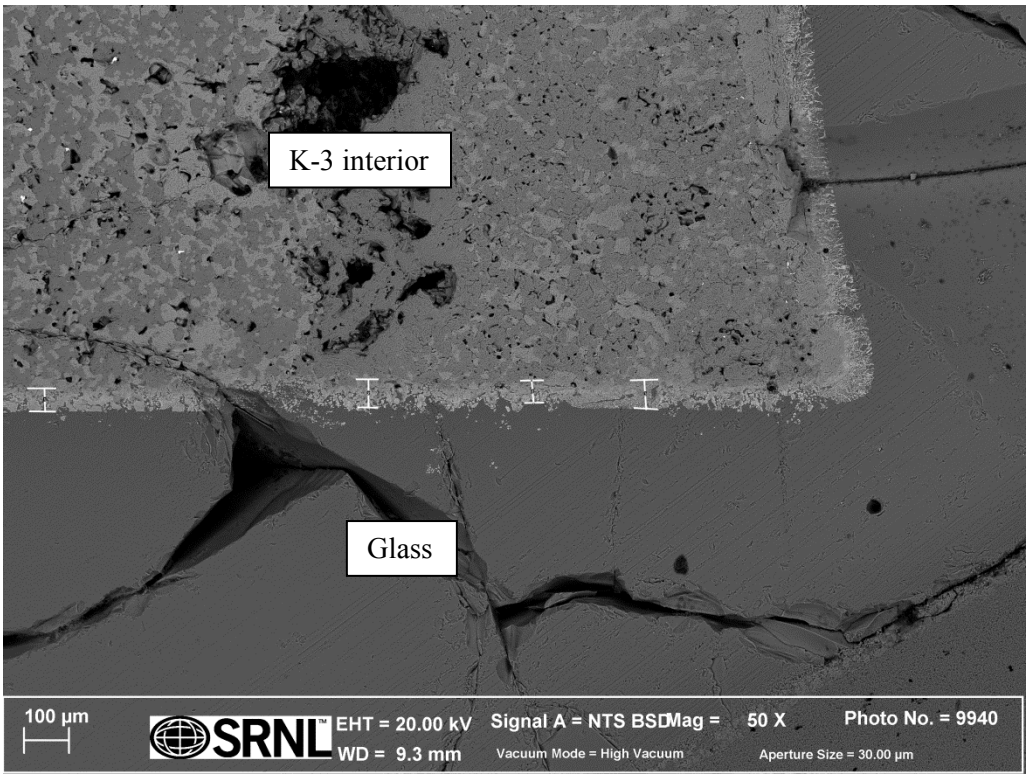
K-3 interior
Glass
100 µm
SRNL
EHT = 20.00 kV
WD = 9.3 mm
Signal A = NTS BSD
Vacuum Mode = High Vacuum
Mag = 50 X
Aperture Size = 30.00 µm
Photo No. = 9940

d)

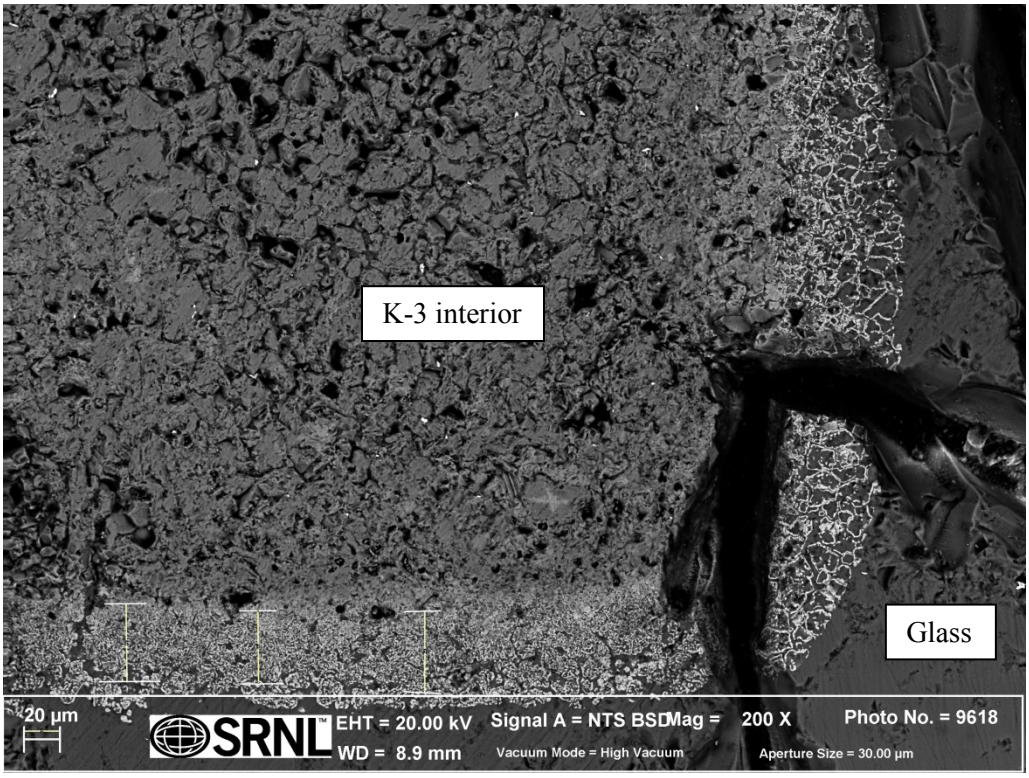

Figure C-2. SEM Elemental Maps of K-3 Coupon Embedded CEF-2 SRAT Melter Feed for 4 Hours.

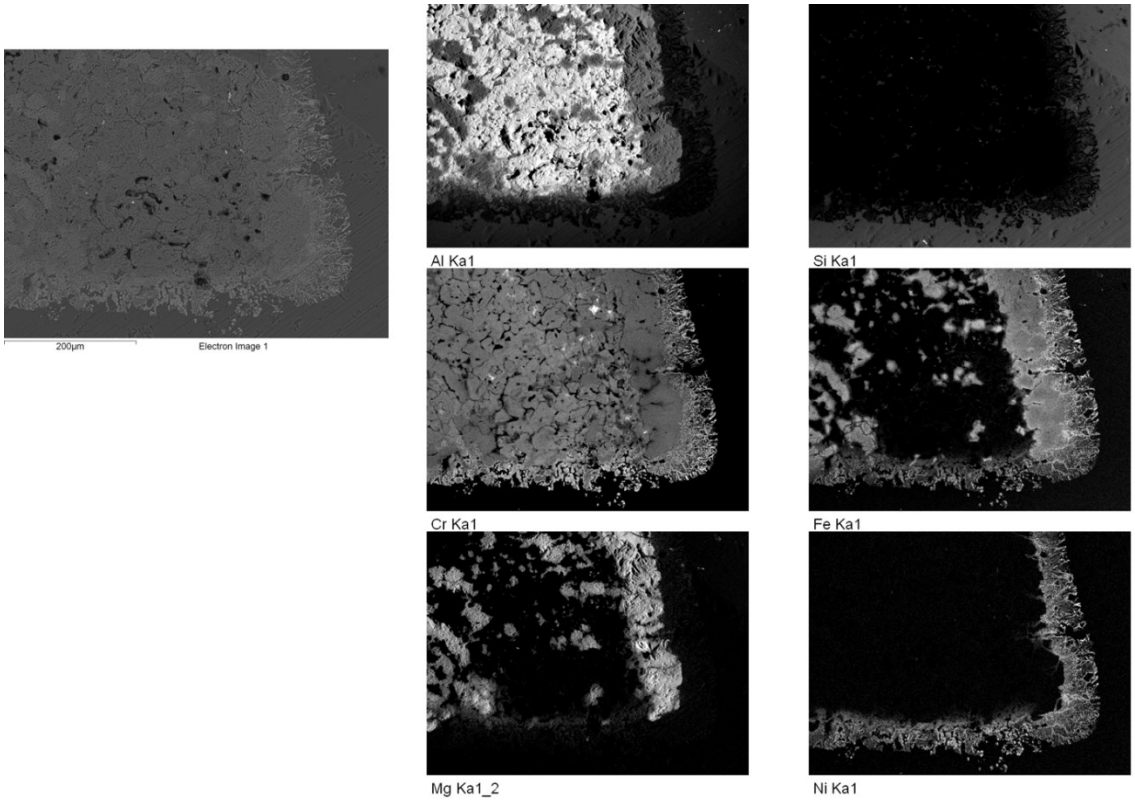

Figure C-3. Images of the a) and b) hot wall face and c) and d) cut face of a K-3 coupon immersed in CEF-2 SRAT after heat treatment for 24 hours. The regions measured for this study are shown as numbered lines.

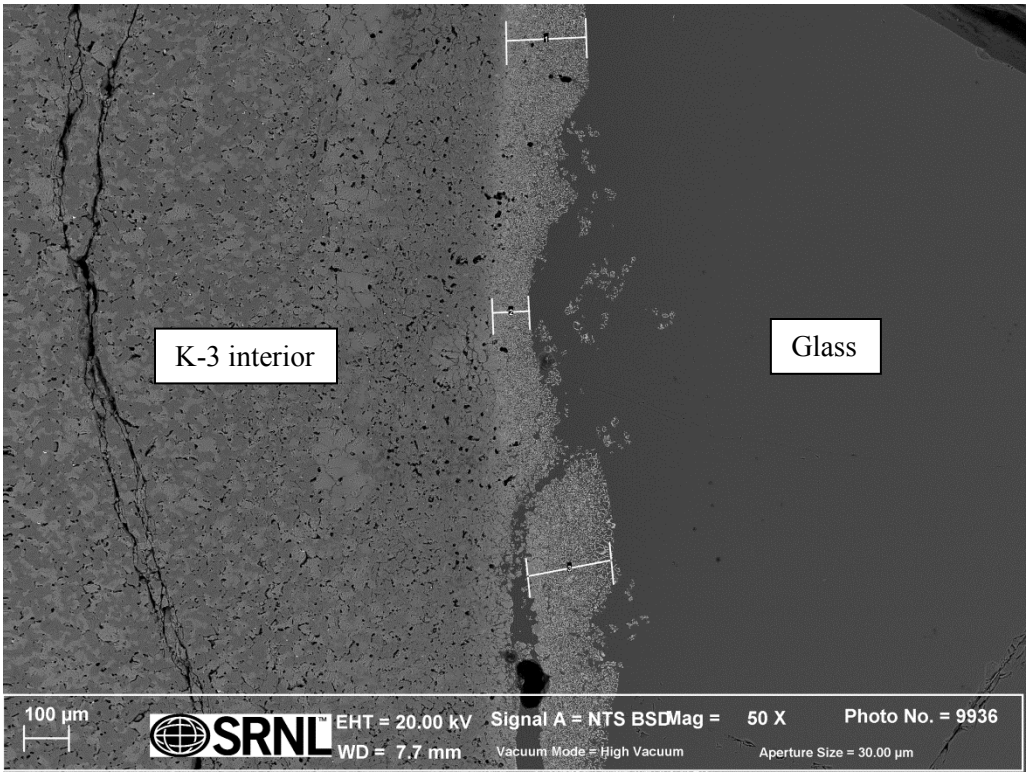

a)

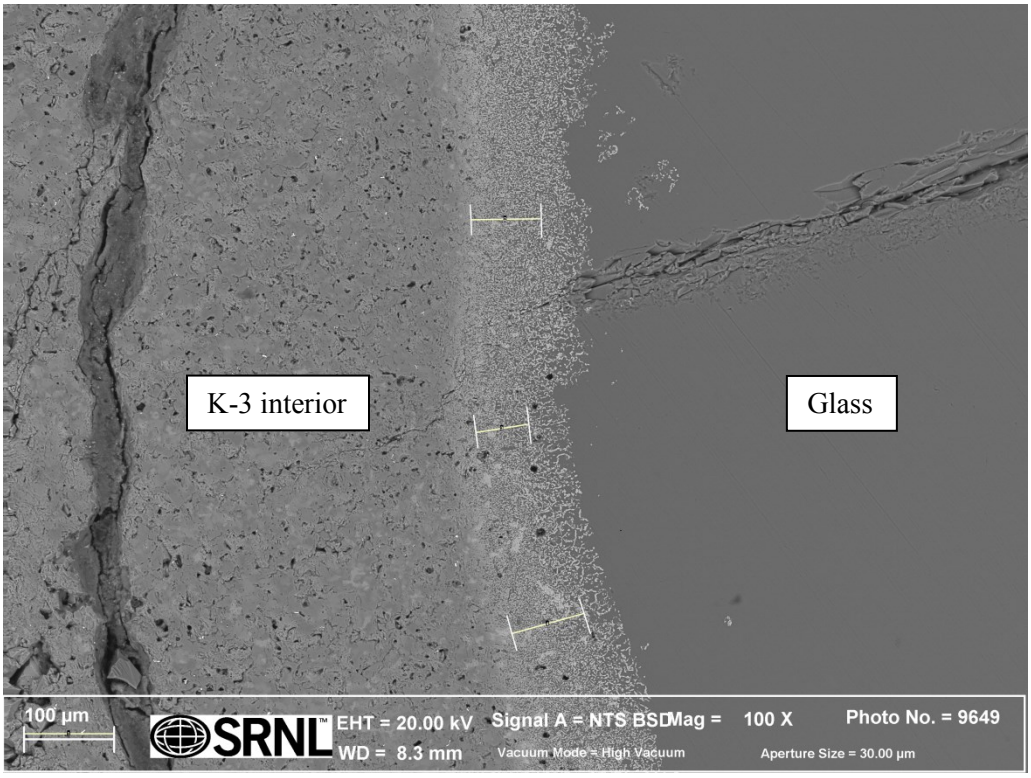

b)

c)

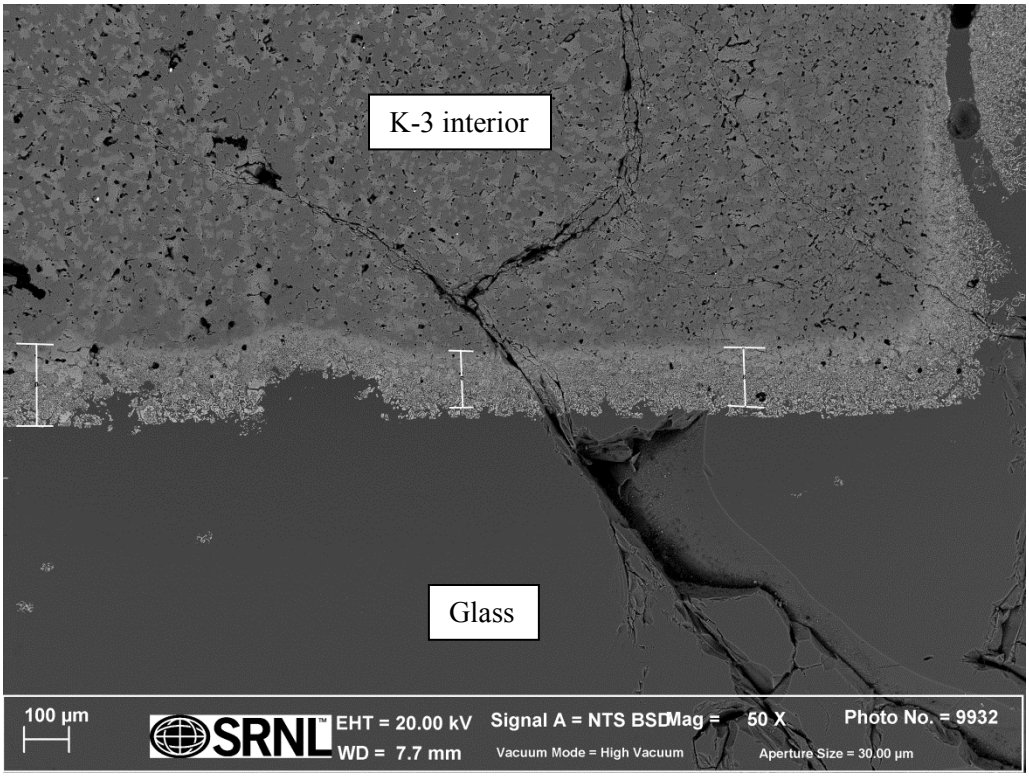
K-3 interior
Glass
100 µm
SRNL
EHT = 20.00 kV
WD = 7.7 mm
Signal A = NTS BSD
Vacuum Mode = High Vacuum
Mag = 50 X
Aperture Size = 30.00 µm
Photo No. = 9932

d)

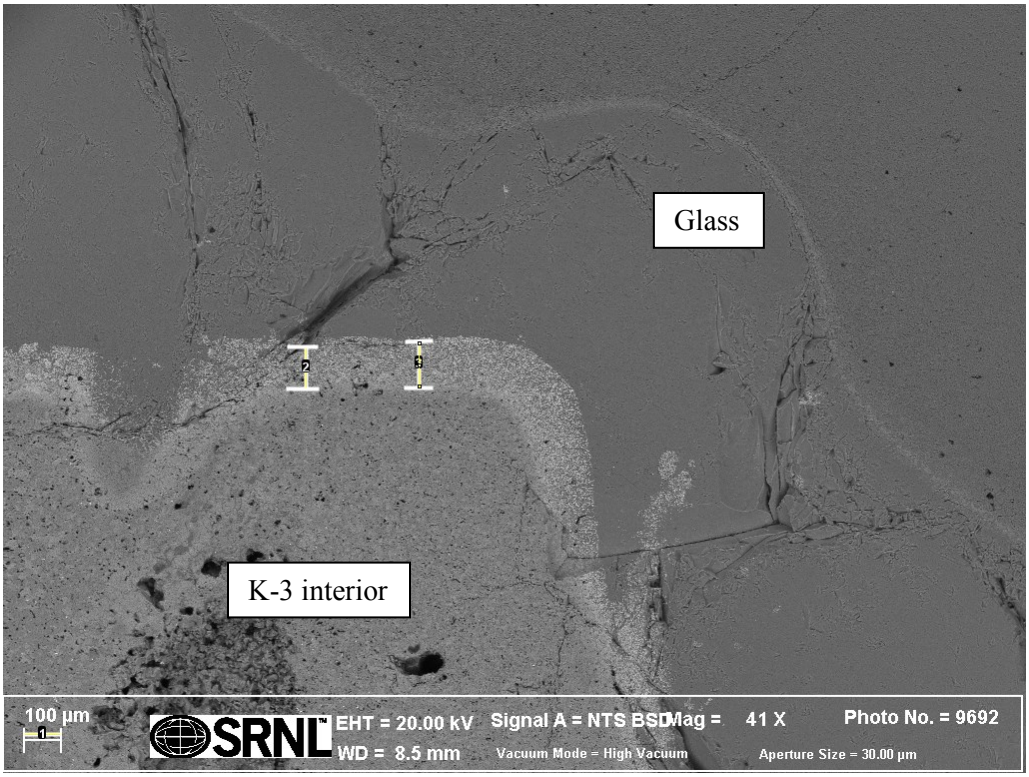
Glass
K-3 interior
100 µm
SRNL
EHT = 20.00 kV
WD = 8.5 mm
Signal A = NTS BSD
Vacuum Mode = High Vacuum
Mag = 41 X
Aperture Size = 30.00 µm
Photo No. = 9692

Figure C-4. SEM Elemental Maps of K-3 Coupon Embedded CEF-2 SRAT Melter Feed for 24 Hours.

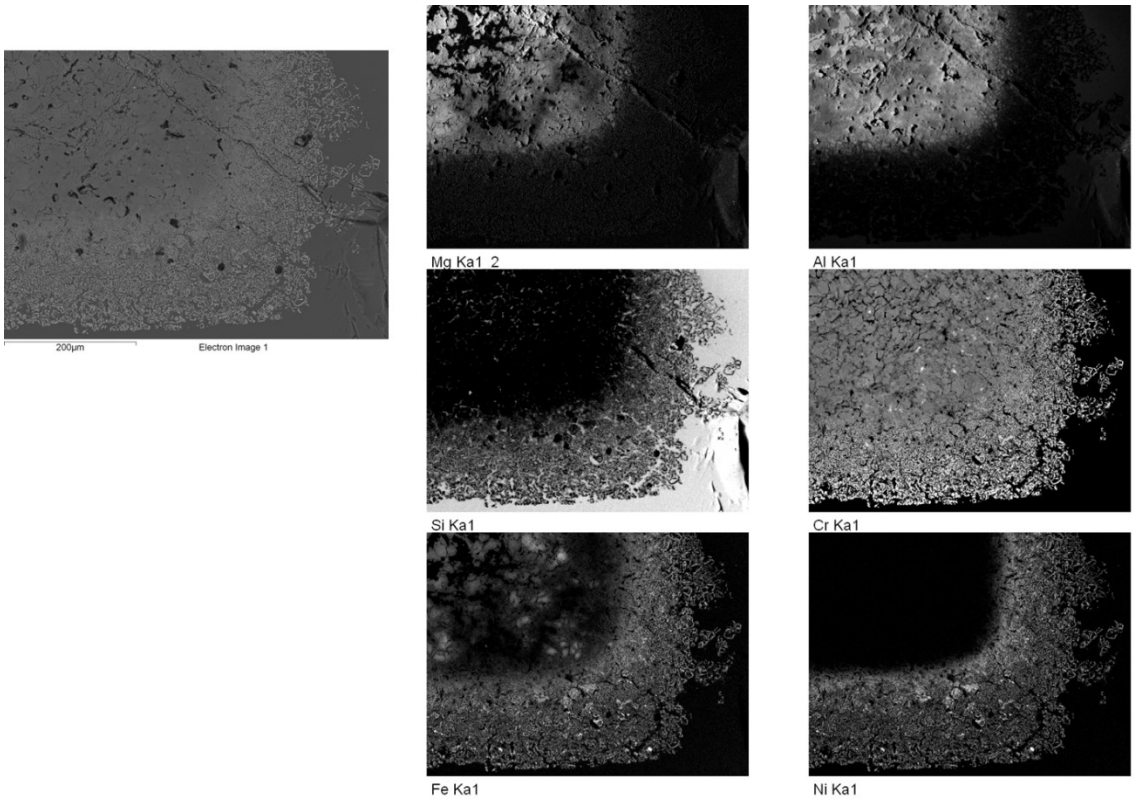

Figure C-5. Images of the a) and b) hot wall face and c) and d) cut face of a K-3 coupon immersed in CEF-2 SRAT after heat treatment for 120 hours. The regions measured for this study are shown as numbered lines.

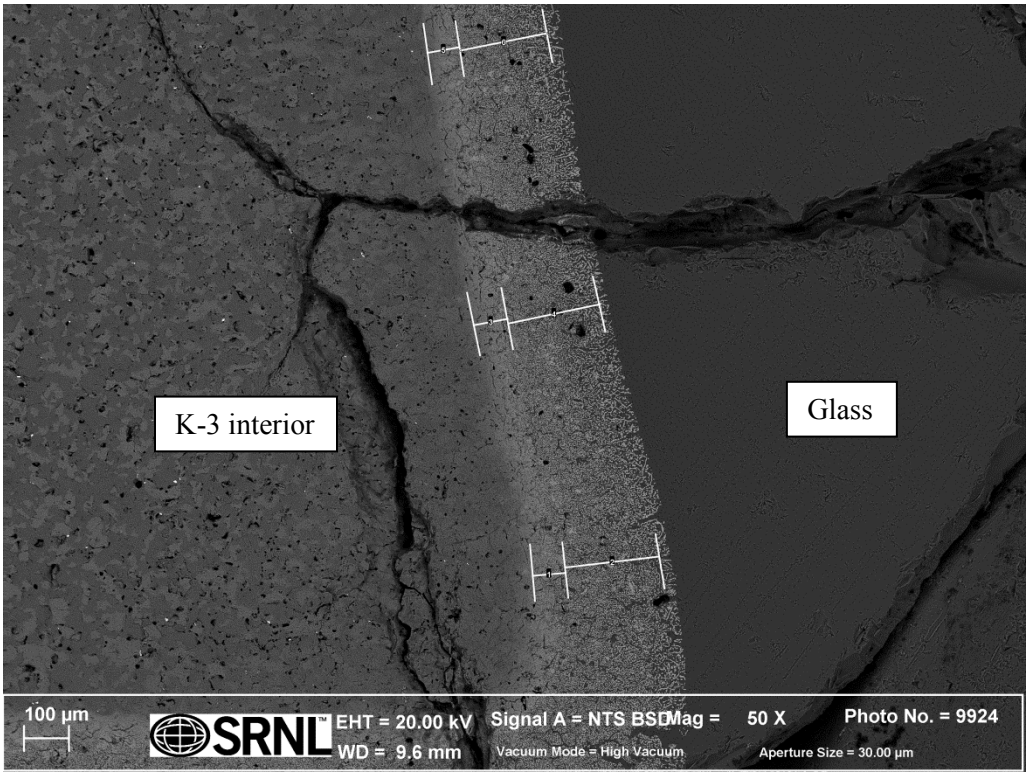

a)

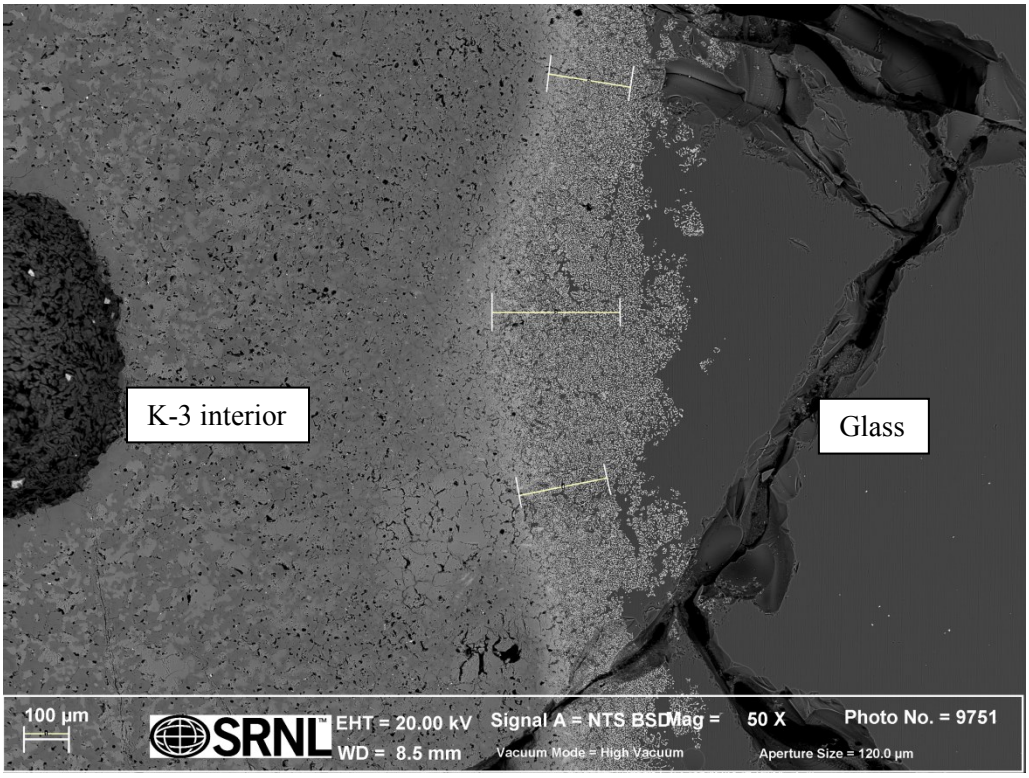

b)

c)

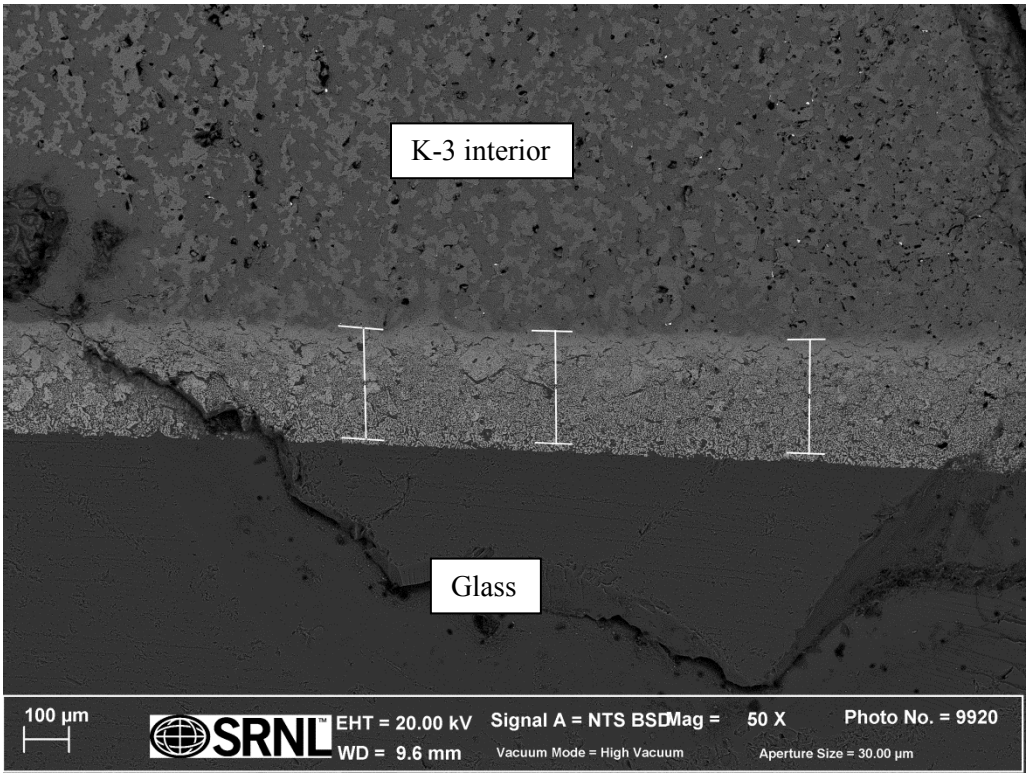
K-3 interior
Glass
100 µm
SRNL
EHT = 20.00 kV
WD = 9.6 mm
Signal A = NTS BSD
Mag = 50 X
Vacuum Mode = High Vacuum
Photo No. = 9920
Aperture Size = 30.00 µm

d)

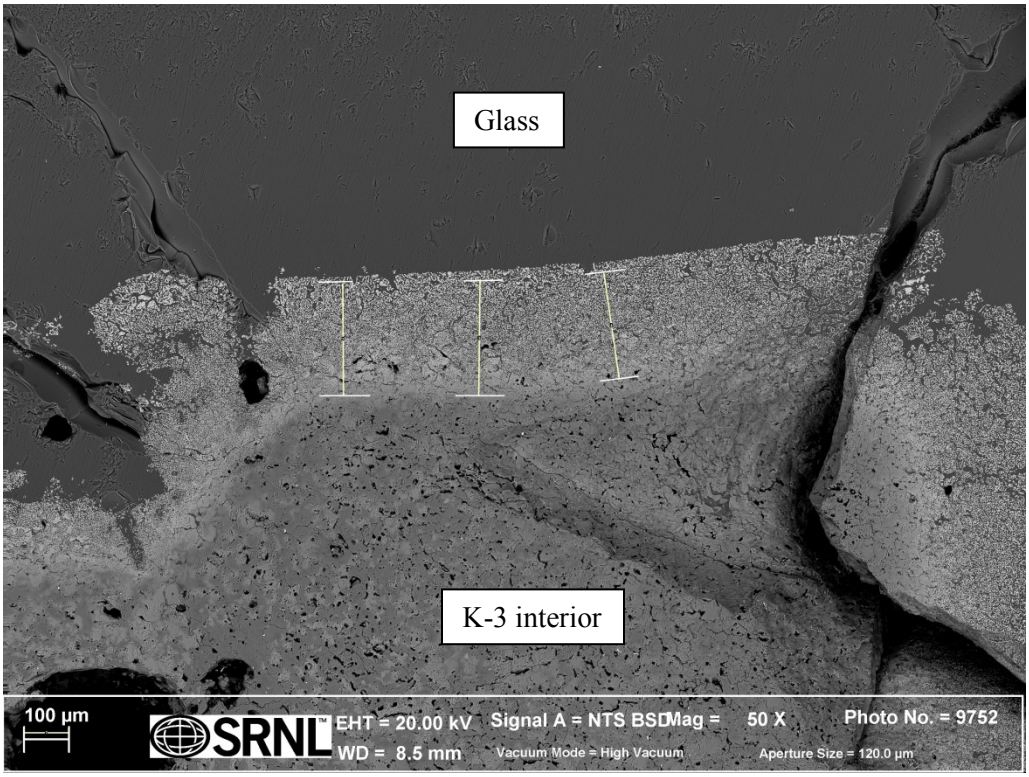
Glass
K-3 interior
100 µm
SRNL
EHT = 20.00 kV
WD = 8.5 mm
Signal A = NTS BSD
Mag = 50 X
Vacuum Mode = High Vacuum
Photo No. = 9752
Aperture Size = 120.0 µm

Figure C-6. SEM Elemental Maps of K-3 Coupon Embedded CEF-2 SRAT Melter Feed for 120 Hours.

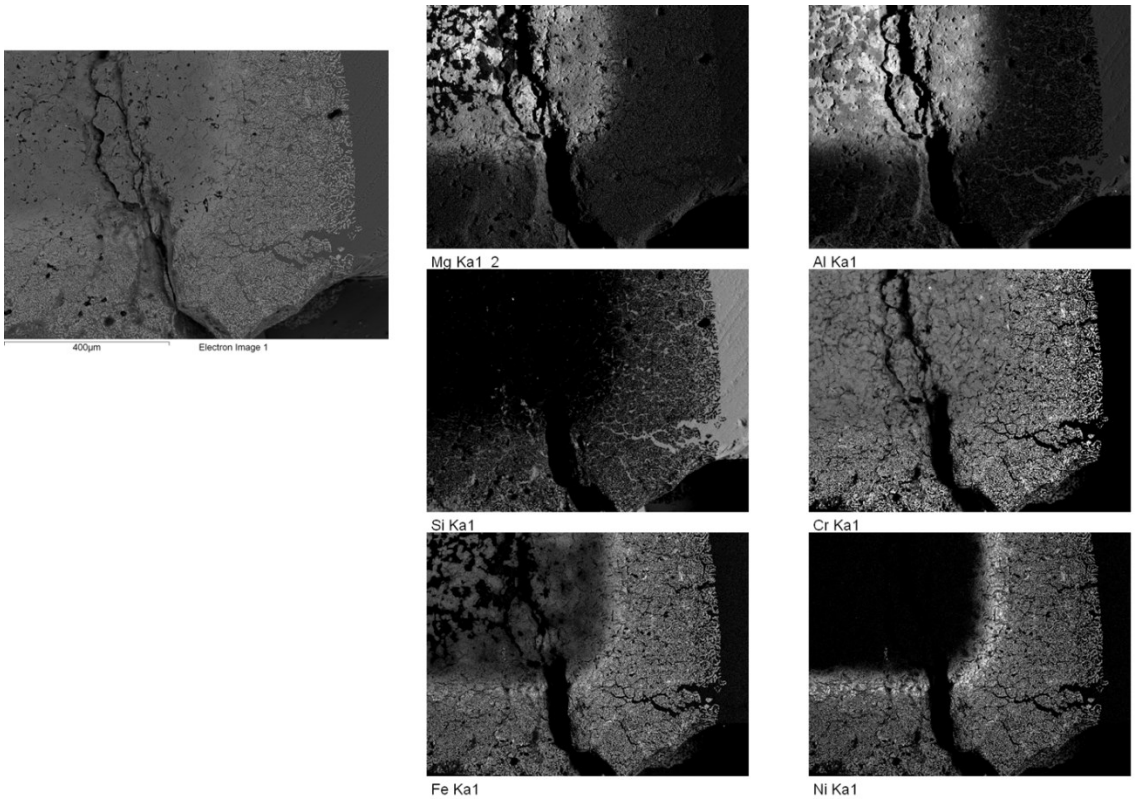

Appendix D. SEM Images of K-3 Coupons in CEF-2 SME Melter Feed.

Figure D-1. Images of the a) and b) hot wall face and c) and d) cut face of a K-3 coupon immersed in CEF-2 SME after heat treatment for 4 hours. The regions measured for this study are shown as numbered lines.

a)

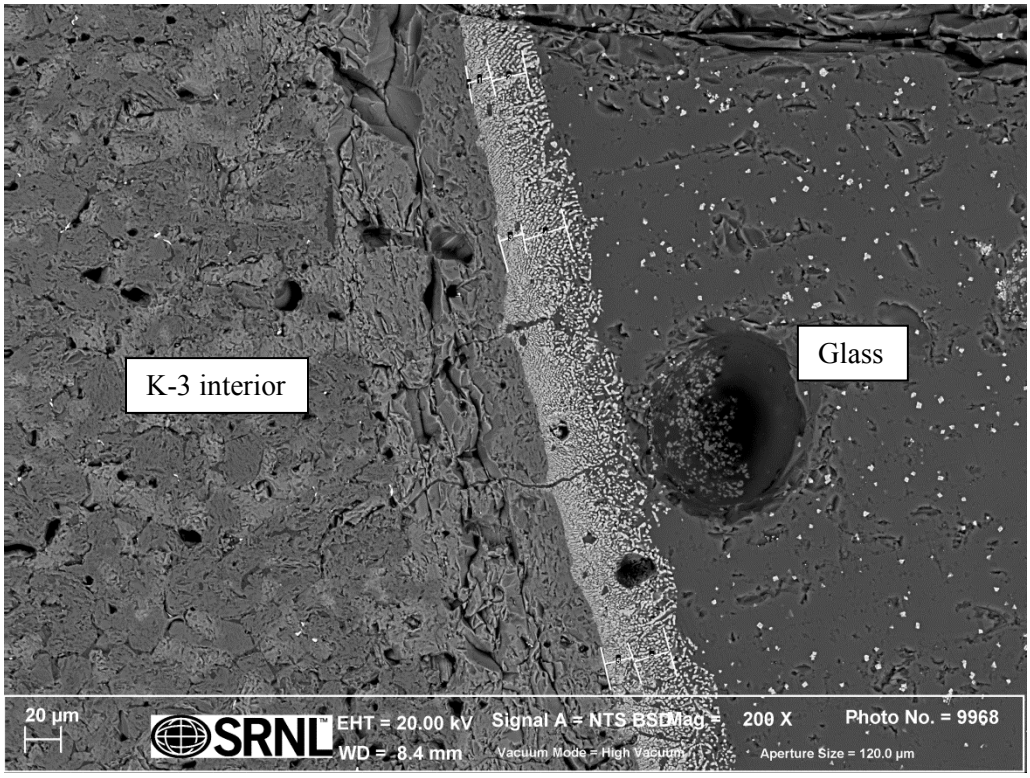

b)

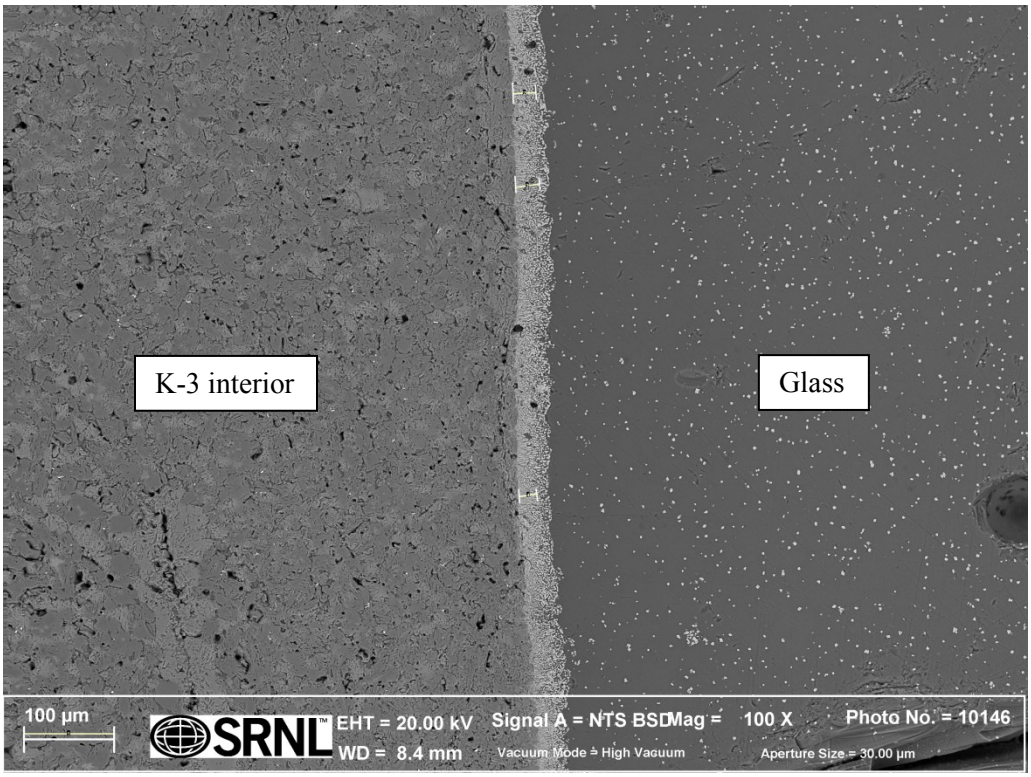
K-3 interior
Glass
100 µm
SRNL
EHT = 20.00 kV
WD = 8.4 mm
Signal A = NTS BSD
Vacuum Mode = High Vacuum
Mag = 100 X
Aperture Size = 30.00 µm
Photo No. = 10146

c)

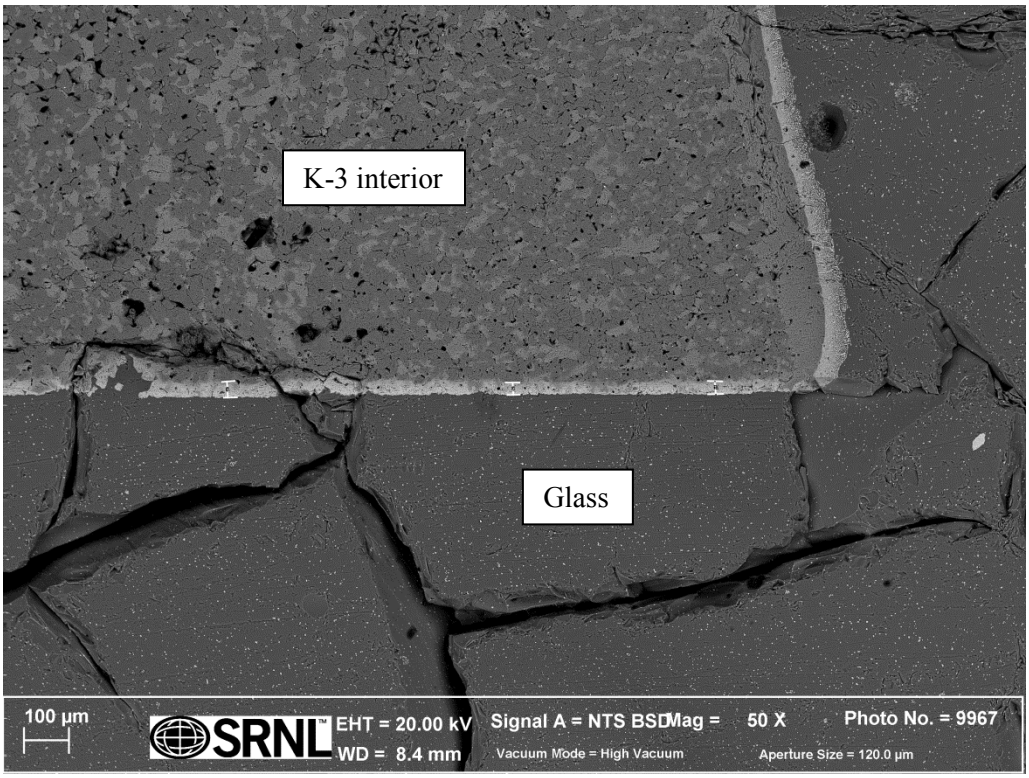
K-3 interior
Glass
100 µm
SRNL
EHT = 20.00 kV
WD = 8.4 mm
Signal A = NTS BSD
Vacuum Mode = High Vacuum
Mag = 50 X
Aperture Size = 120.0 µm
Photo No. = 9967

d)

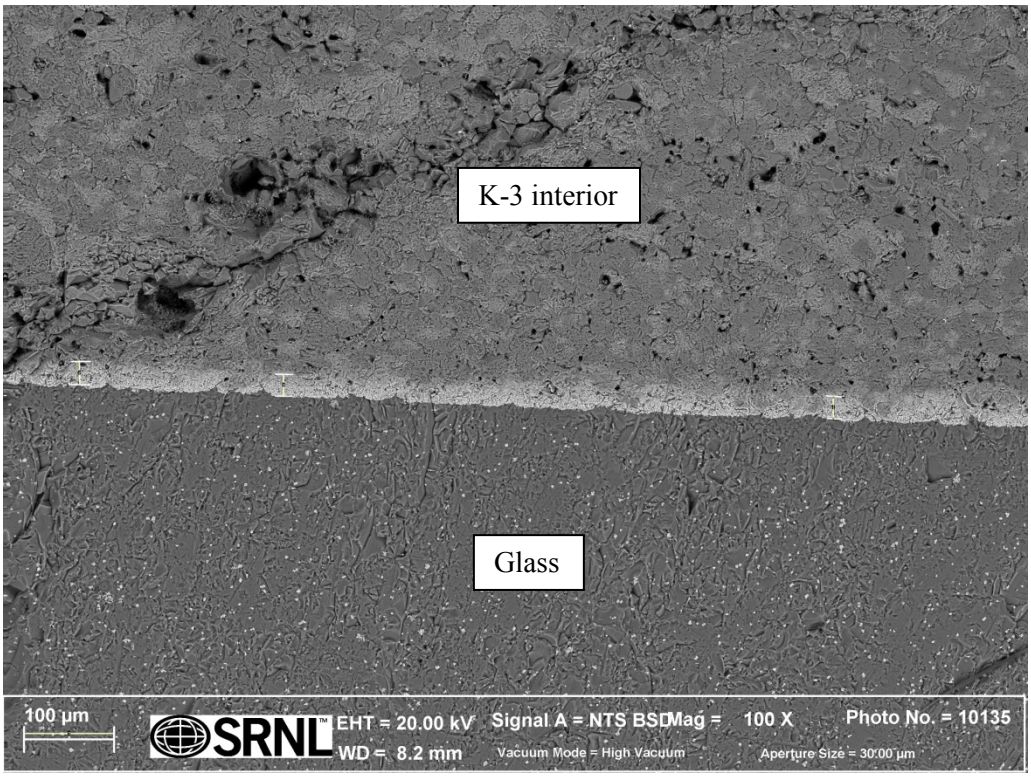

Figure D-2. SEM Elemental Maps of K-3 Coupon Embedded CEF-2 SME Melter Feed for 4 Hours.

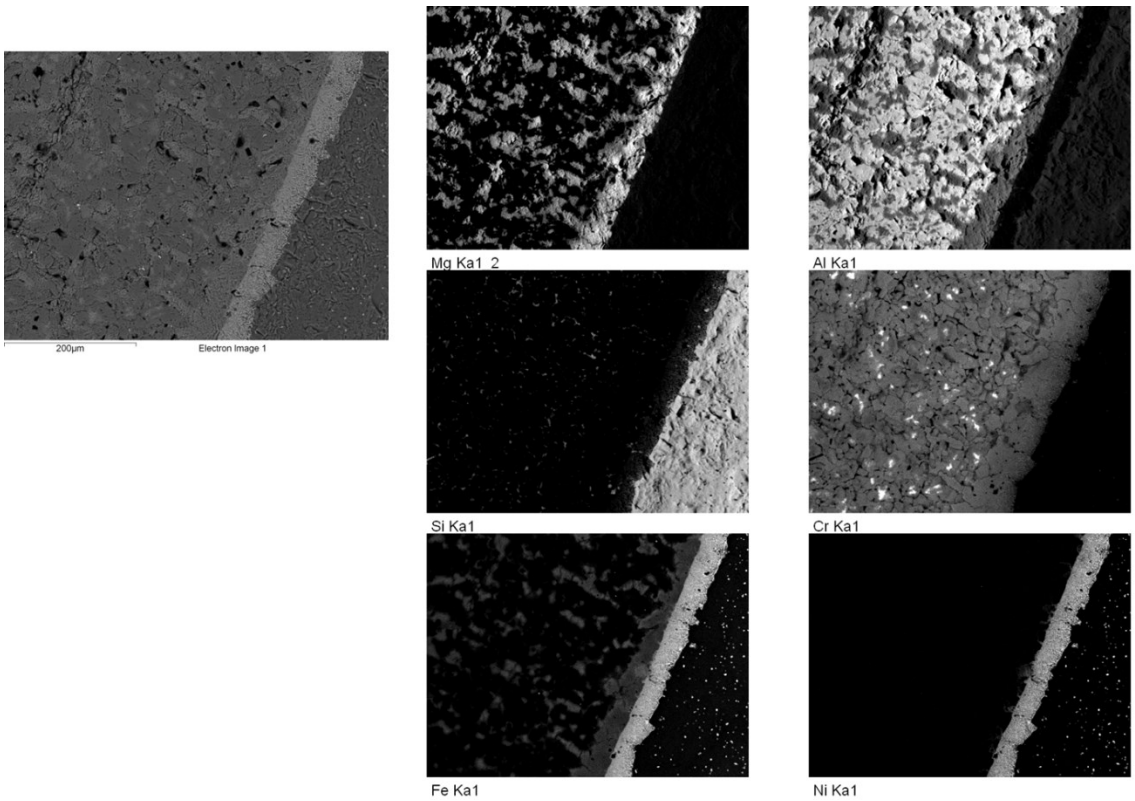

Figure D-3. Images of the a) and b) hot wall face and c) and d) cut face of a K-3 coupon immersed in CEF-2 SME after heat treatment for 24 hours. The regions measured for this study are shown as numbered lines.

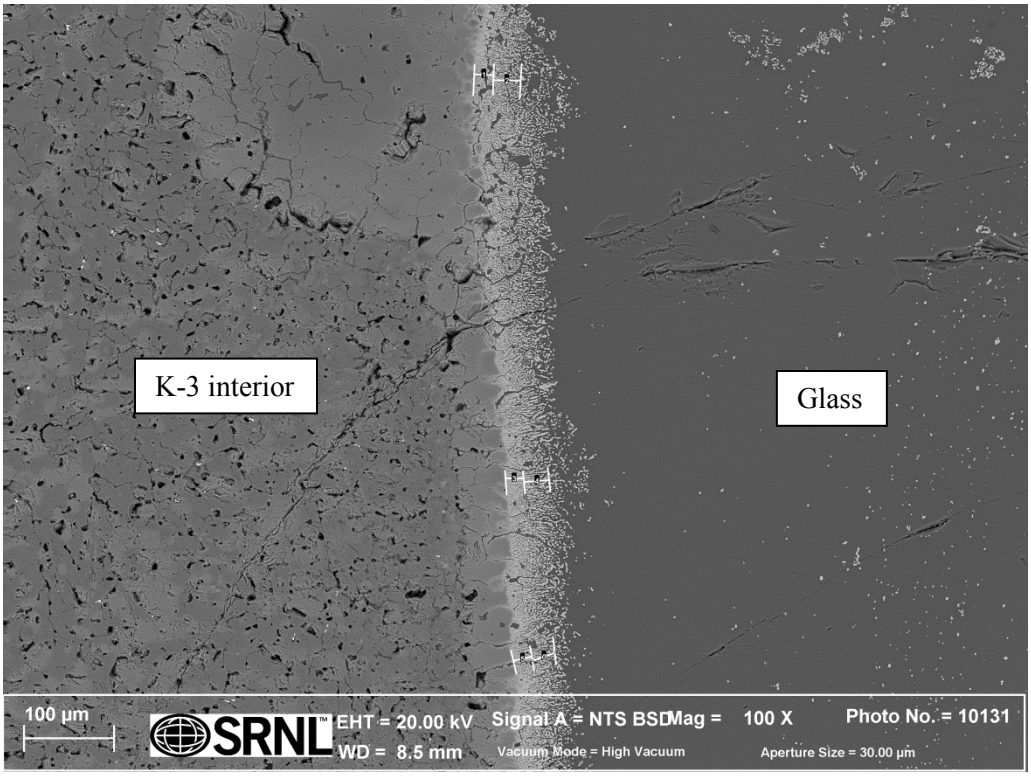

a)

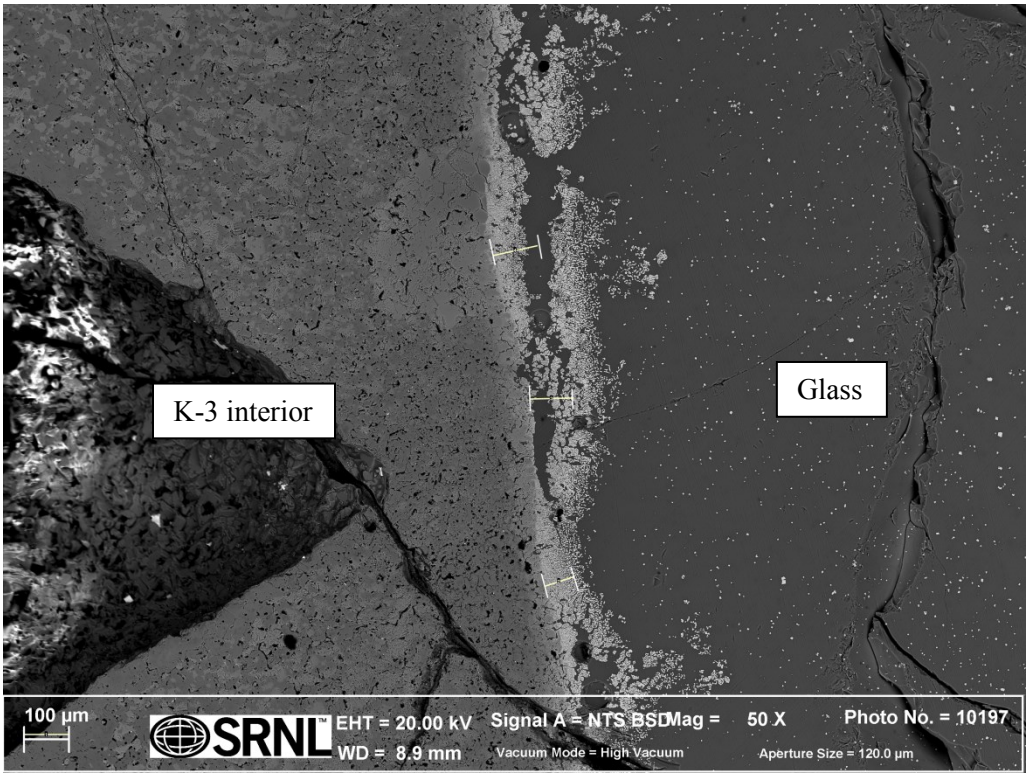

b)

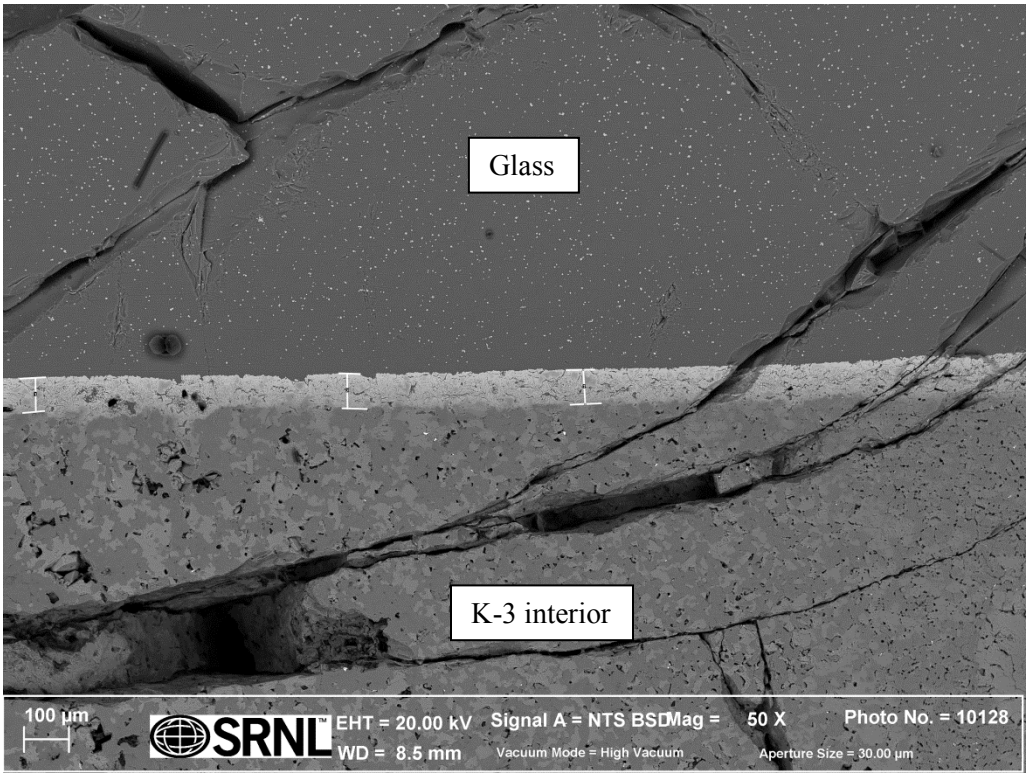
Glass
K-3 interior
100 µm
SRNL
EHT = 20.00 kV
WD = 8.5 mm
Signal A = NTS BSD
Vacuum Mode = High Vacuum
Mag = 50 X
Aperture Size = 30.00 µm
Photo No. = 10128

c)

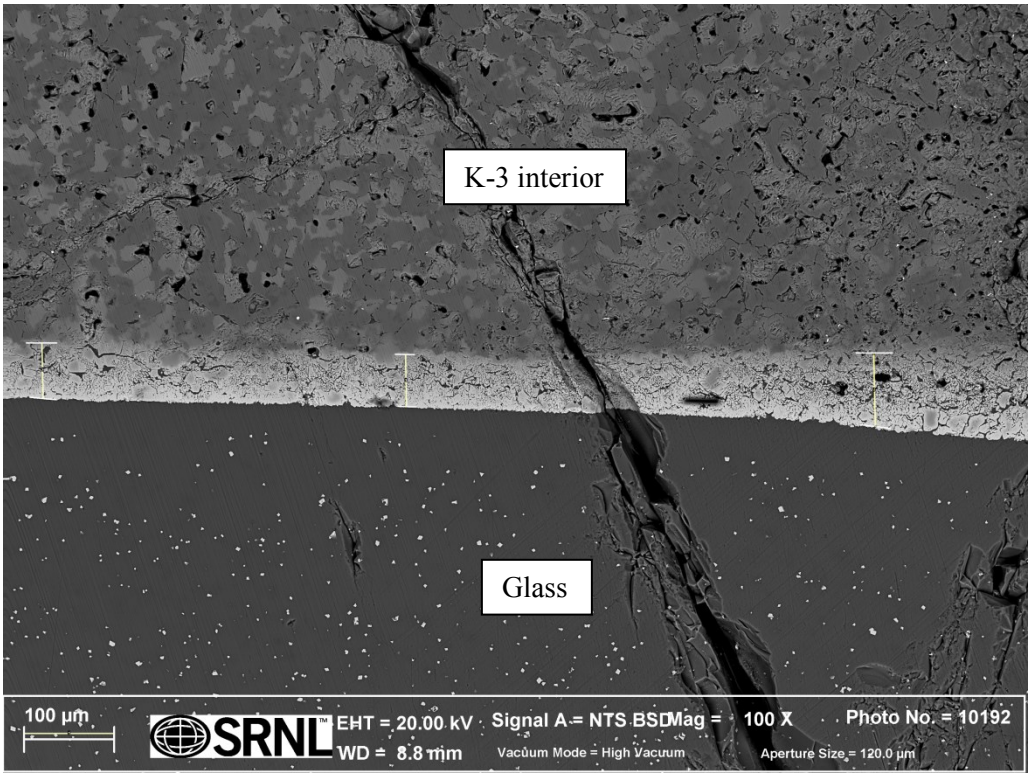
K-3 interior
Glass
100 µm
SRNL
EHT = 20.00 kV
WD = 8.8 mm
Signal A = NTS BSD
Vacuum Mode = High Vacuum
Mag = 100 X
Aperture Size = 120.0 µm
Photo No. = 10192

d)

Figure D-4. SEM Elemental Maps of K-3 Coupon Embedded CEF-2 SME Melter Feed for 24 Hours.

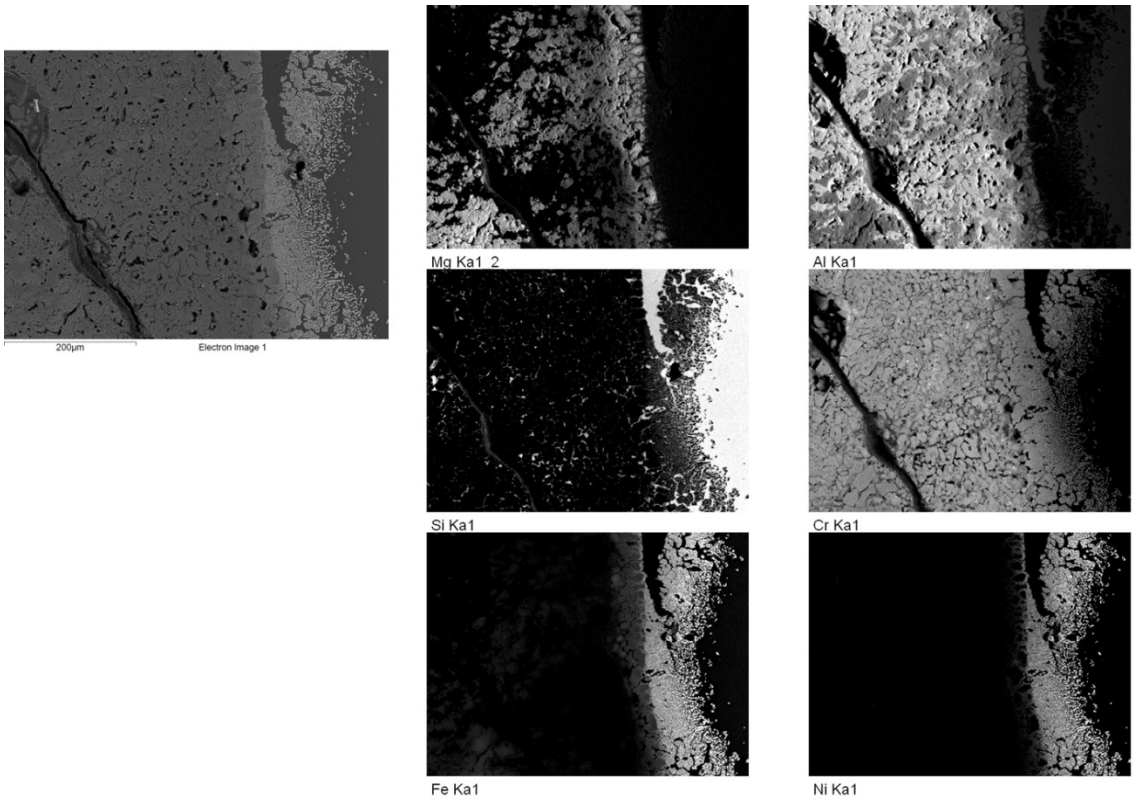

Figure D-5. Images of the a) and b) hot wall face and c) and d) cut face of a K-3 coupon immersed in CEF-2 SME after heat treatment for 120 hours. The regions measured for this study are shown as numbered lines.

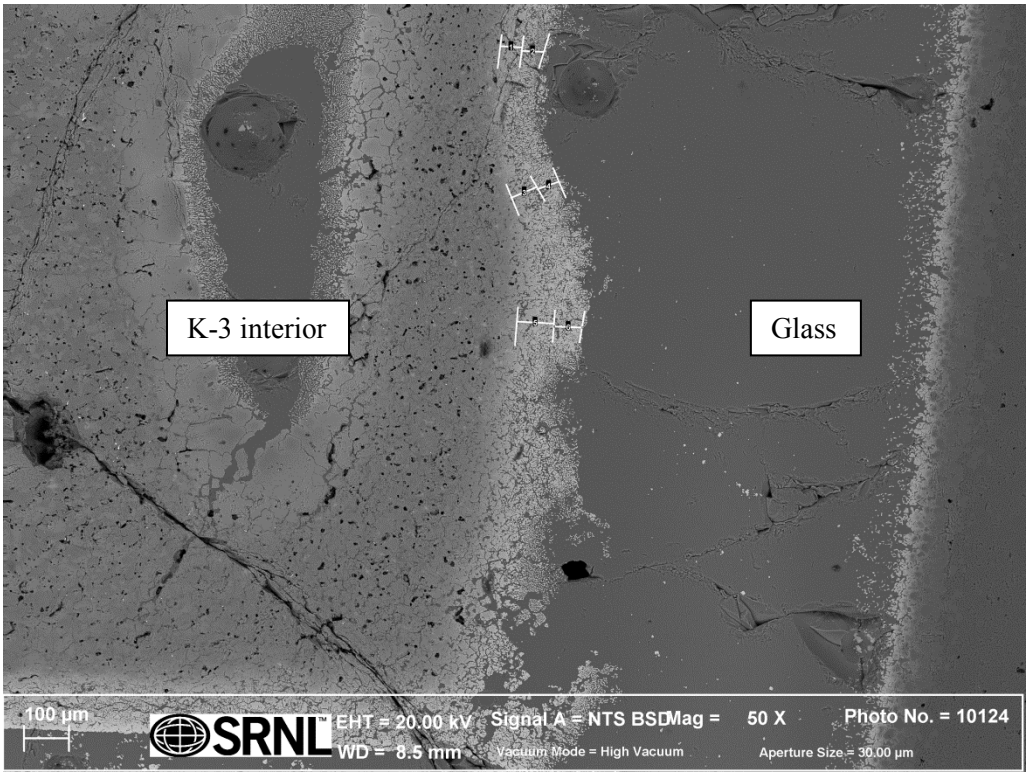

a)

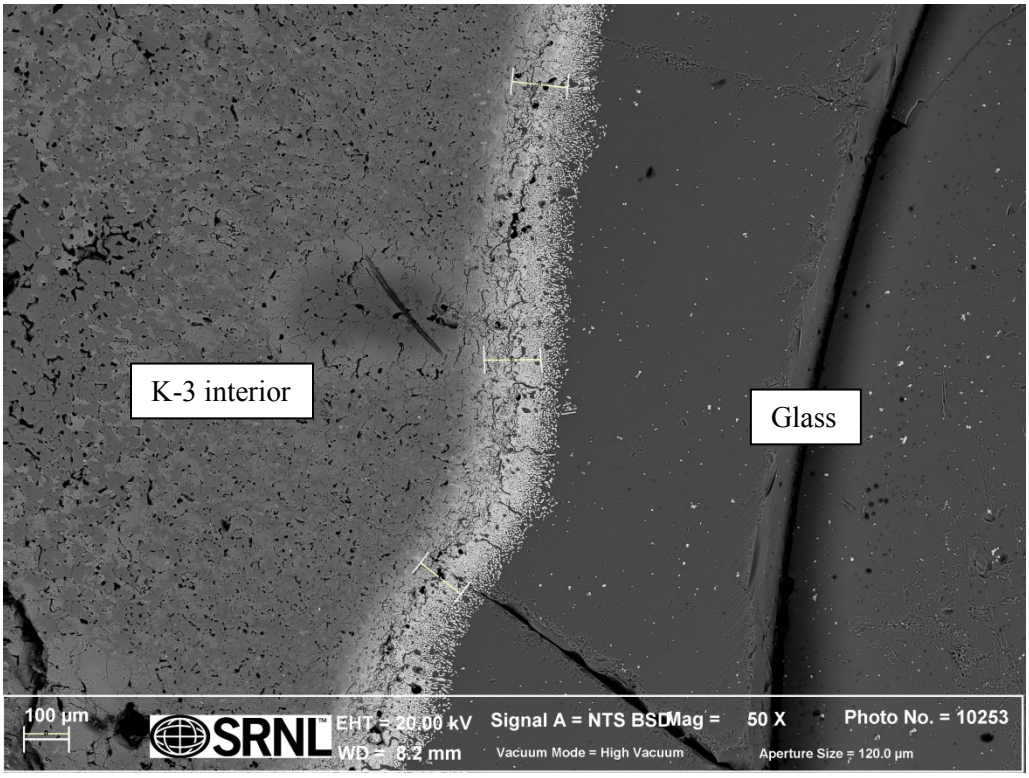

b)

c)

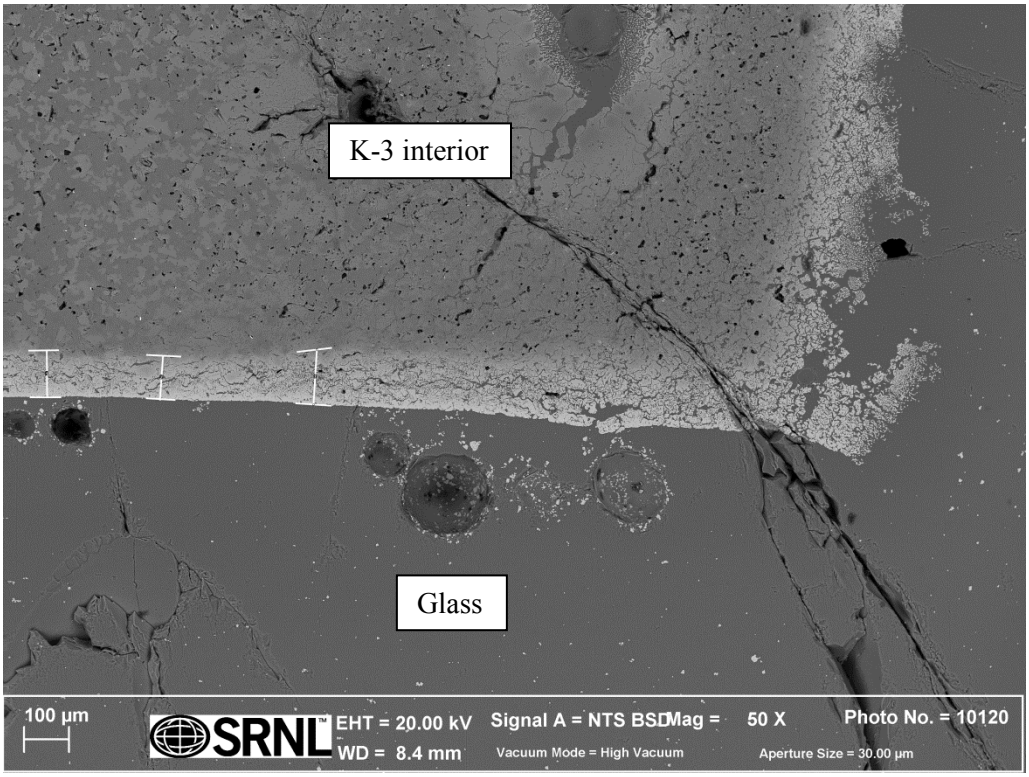
K-3 interior
Glass
100 µm
SRNL
EHT = 20.00 kV
WD = 8.4 mm
Signal A = NTS BSD
Vacuum Mode = High Vacuum
Mag = 50 X
Aperture Size = 30.00 µm
Photo No. = 10120

d)

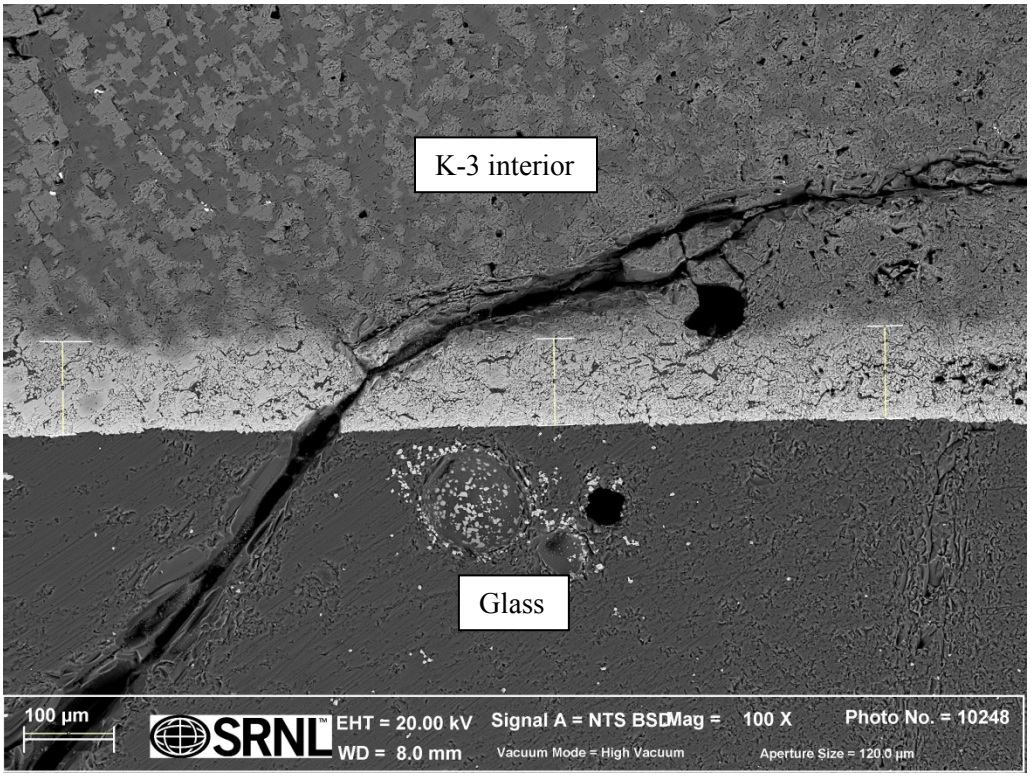
K-3 interior
Glass
100 µm
SRNL
EHT = 20.00 kV
WD = 8.0 mm
Signal A = NTS BSD
Vacuum Mode = High Vacuum
Mag = 100 X
Aperture Size = 120.0 µm
Photo No. = 10248

Figure D-6. SEM Elemental Maps of K-3 Coupon Embedded CEF-2 SME Melter Feed for 120 Hours.

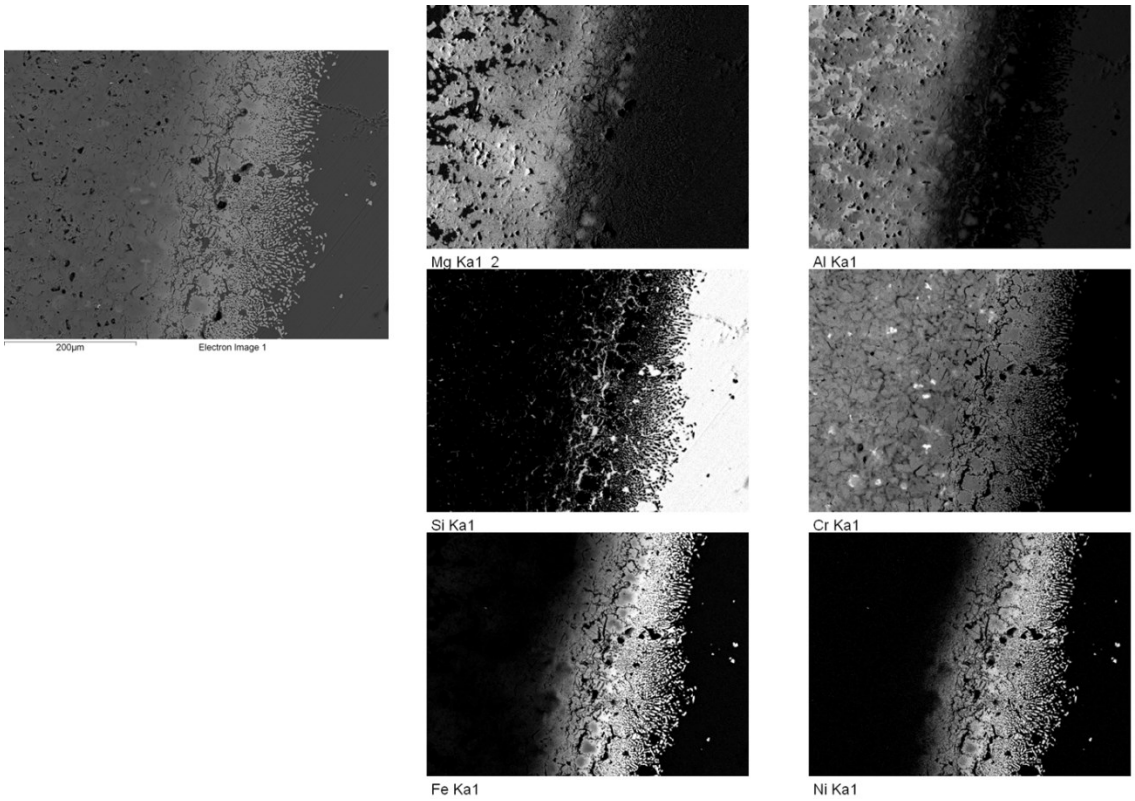

Appendix E. SEM Images of K-3 Coupons in GN78 Melter Feed.

Figure E-1. Images of the a) and b) hot wall face and c) and d) cut face of a K-3 coupon immersed in GN78 melter feed after heat treatment for 4 hours. The regions measured for this study are shown as numbered lines.

a)

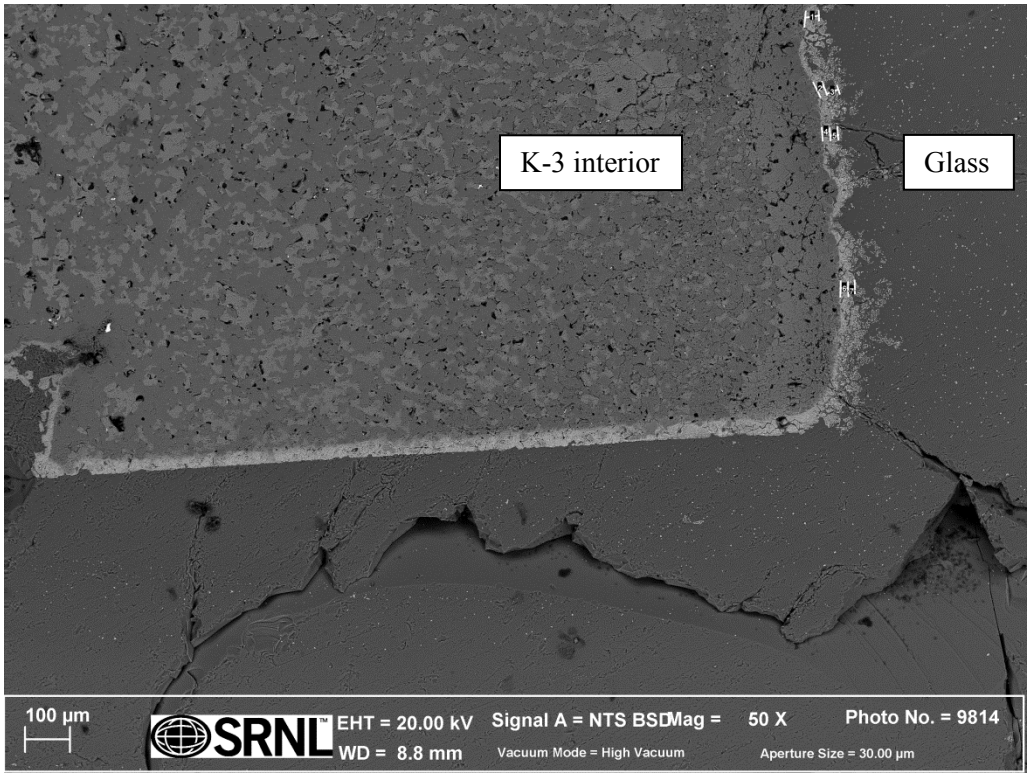

b)

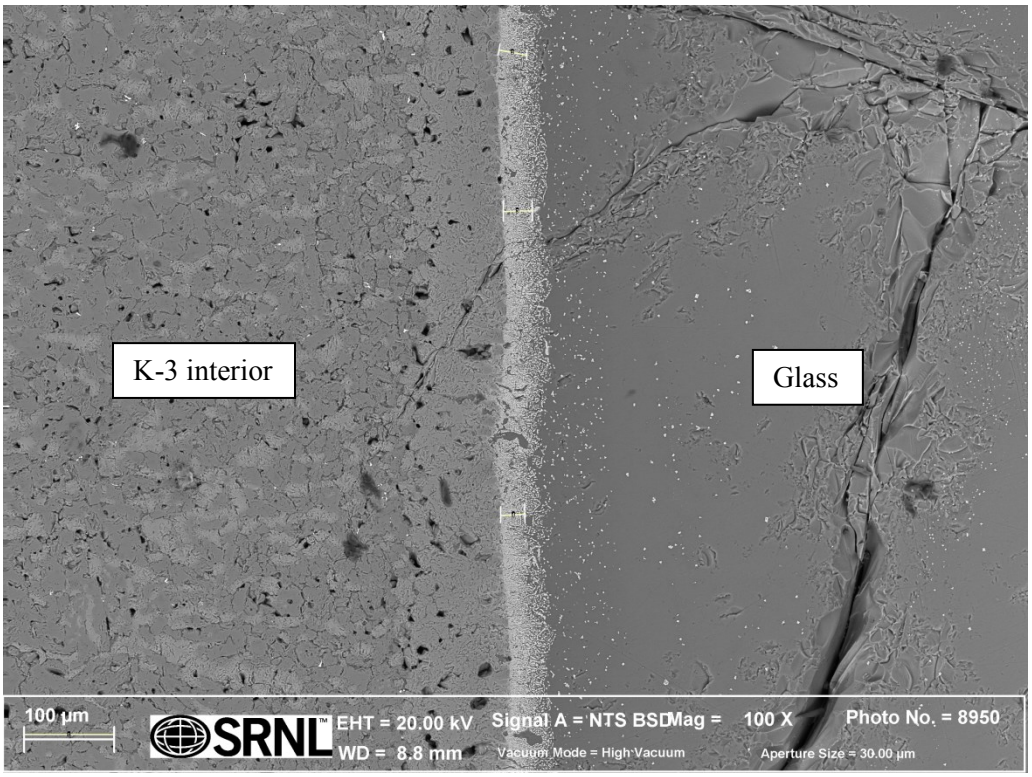
K-3 interior
Glass
100 µm
SRNL
EHT = 20.00 kV
WD = 8.8 mm
Signal A = NTS BSD
Vacuum Mode = High Vacuum
Mag = 100 X
Aperture Size = 30.00 µm
Photo No. = 8950

c)

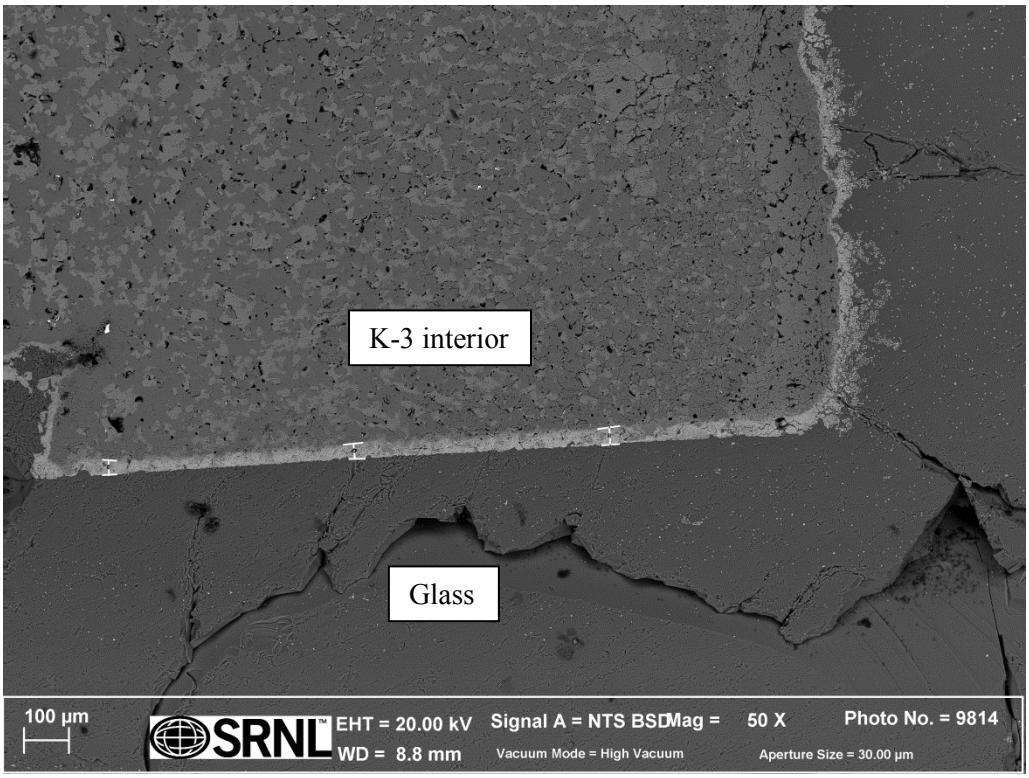
K-3 interior
Glass
100 µm
SRNL
EHT = 20.00 kV
WD = 8.8 mm
Signal A = NTS BSD
Vacuum Mode = High Vacuum
Mag = 50 X
Aperture Size = 30.00 µm
Photo No. = 9814

d)

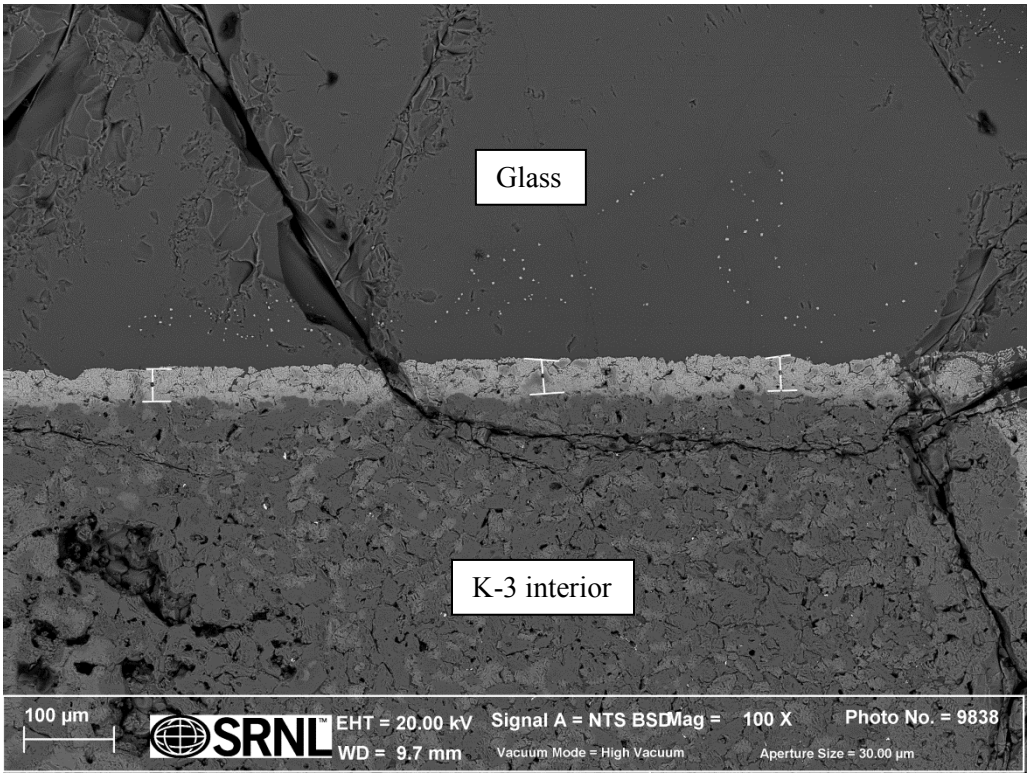

Figure E-2. SEM Elemental Maps of K-3 Coupon Embedded GN78 Melter Feed for 4 Hours.

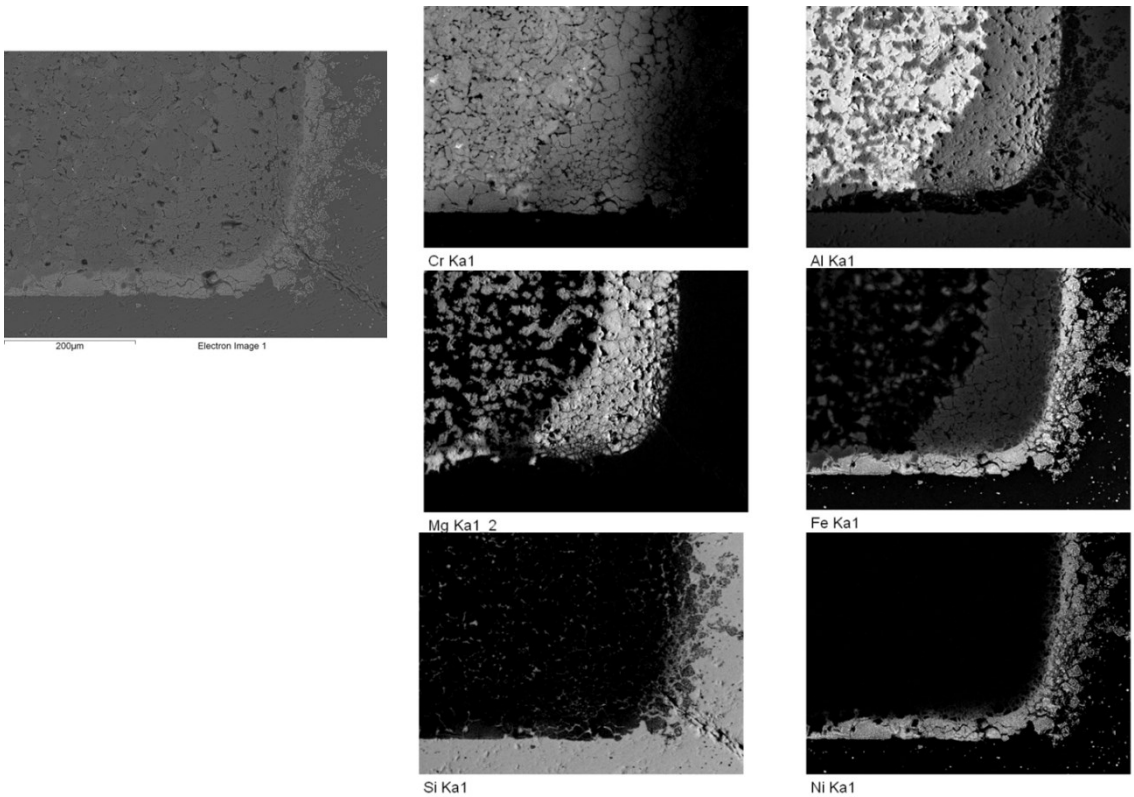

Figure E-3. Images of the a) and b) hot wall face and c) and d) cut face of a K-3 coupon immersed in GN78 melter feed after heat treatment for 24 hours. The regions measured for this study are shown as numbered lines.

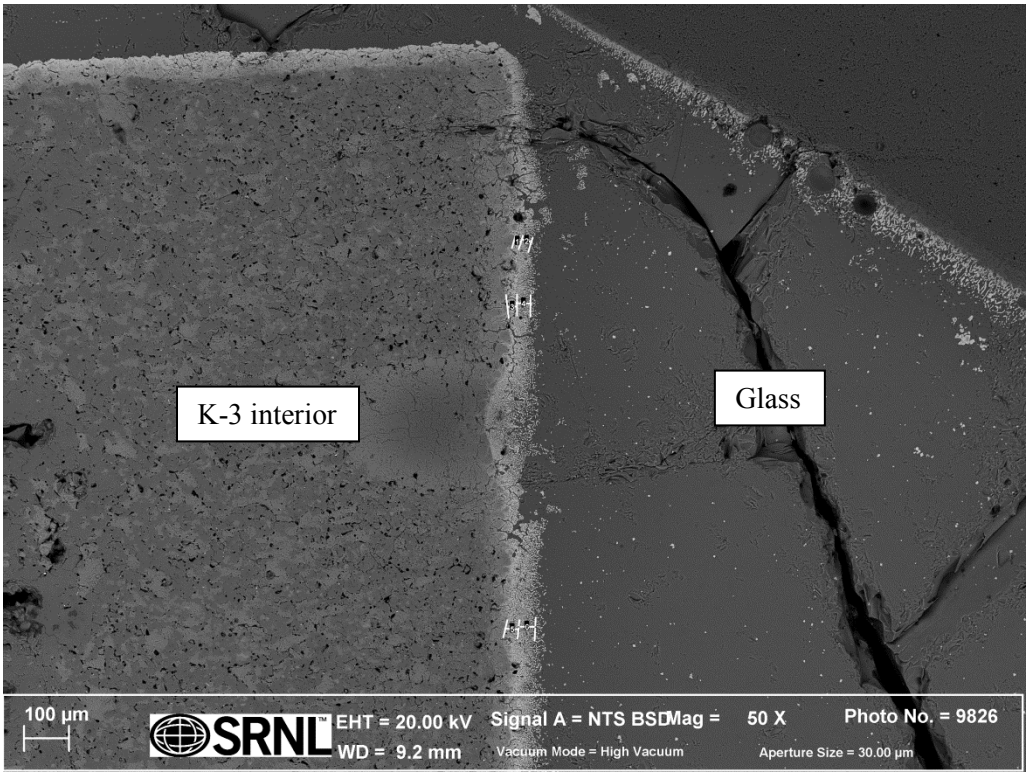

a)

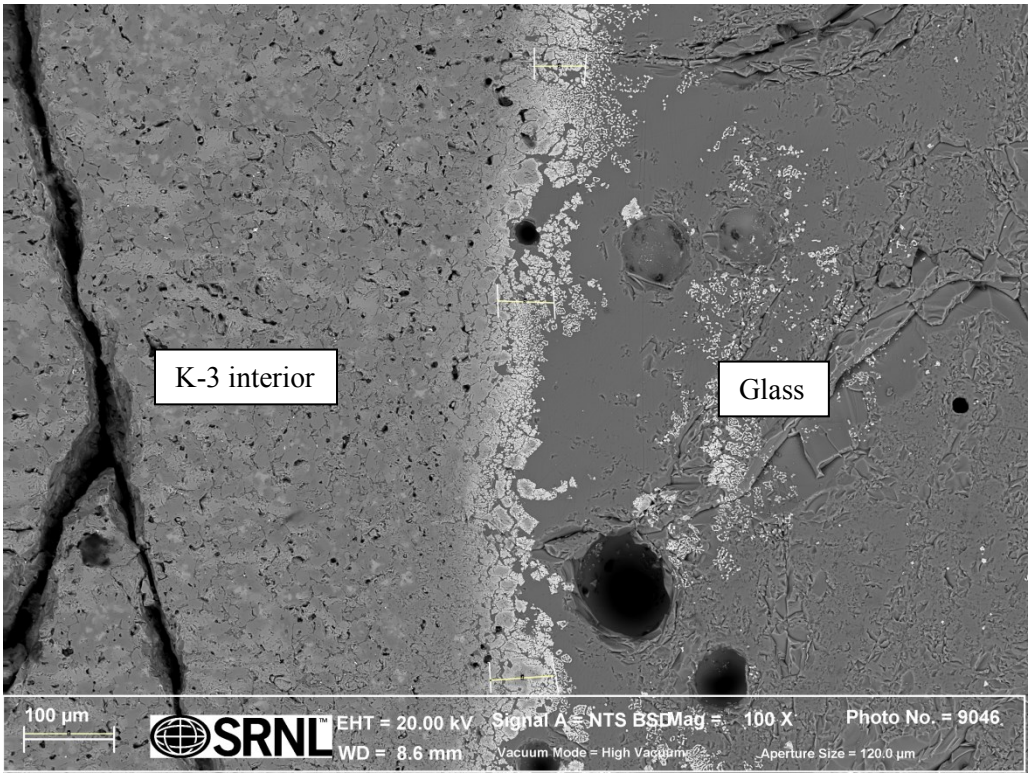

b)

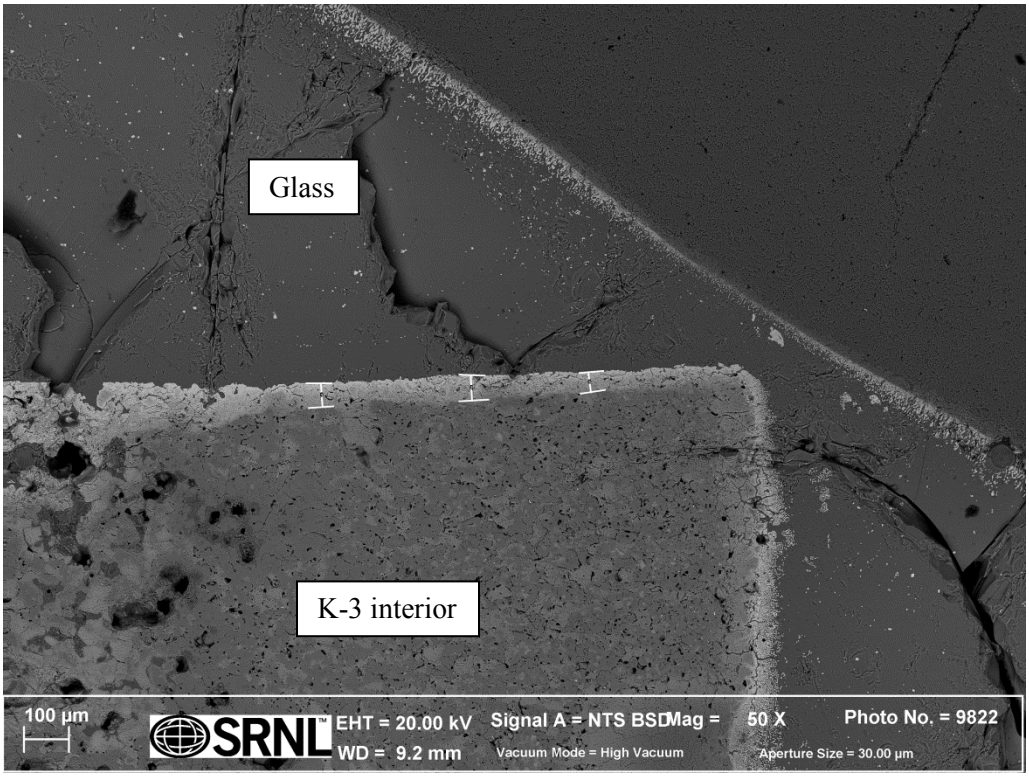
Glass
K-3 interior
100 µm
SRNL
EHT = 20.00 kV
WD = 9.2 mm
Signal A = NTS BSD
Mag = 50 X
Photo No. = 9822
Vacuum Mode = High Vacuum
Aperture Size = 30.00 µm

c)

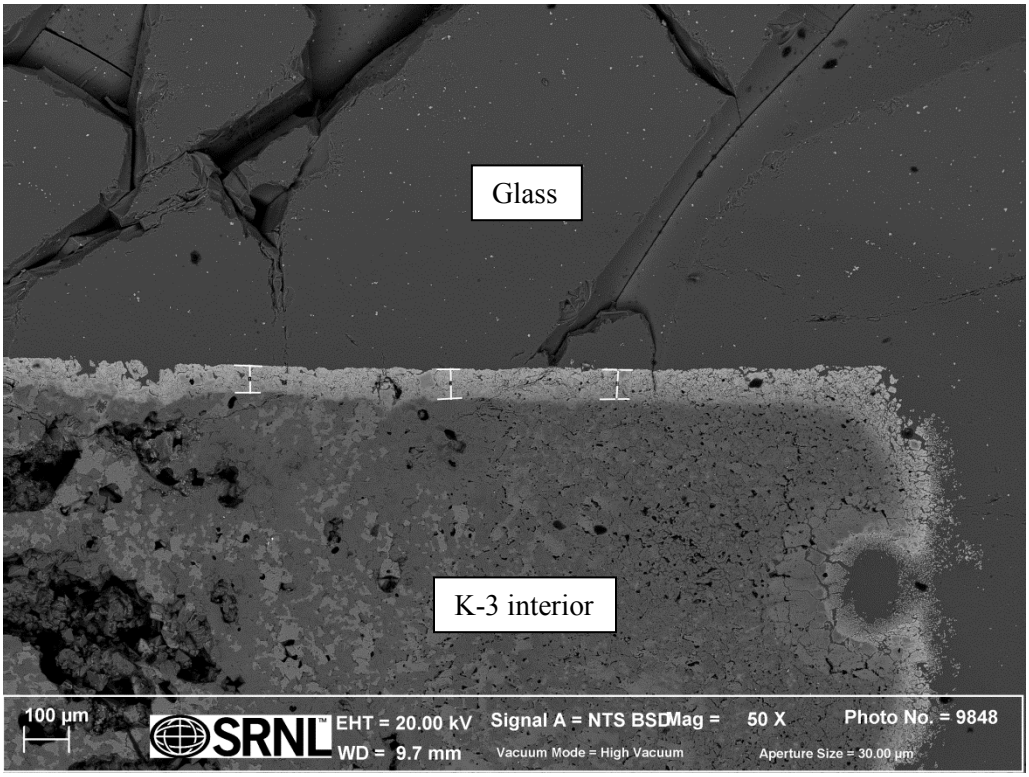
Glass
K-3 interior
100 µm
SRNL
EHT = 20.00 kV
WD = 9.7 mm
Signal A = NTS BSD
Mag = 50 X
Photo No. = 9848
Vacuum Mode = High Vacuum
Aperture Size = 30.00 µm

d)

Figure E-4. SEM Elemental Maps of K-3 Coupon Embedded GN78 Melter Feed for 24 Hours.

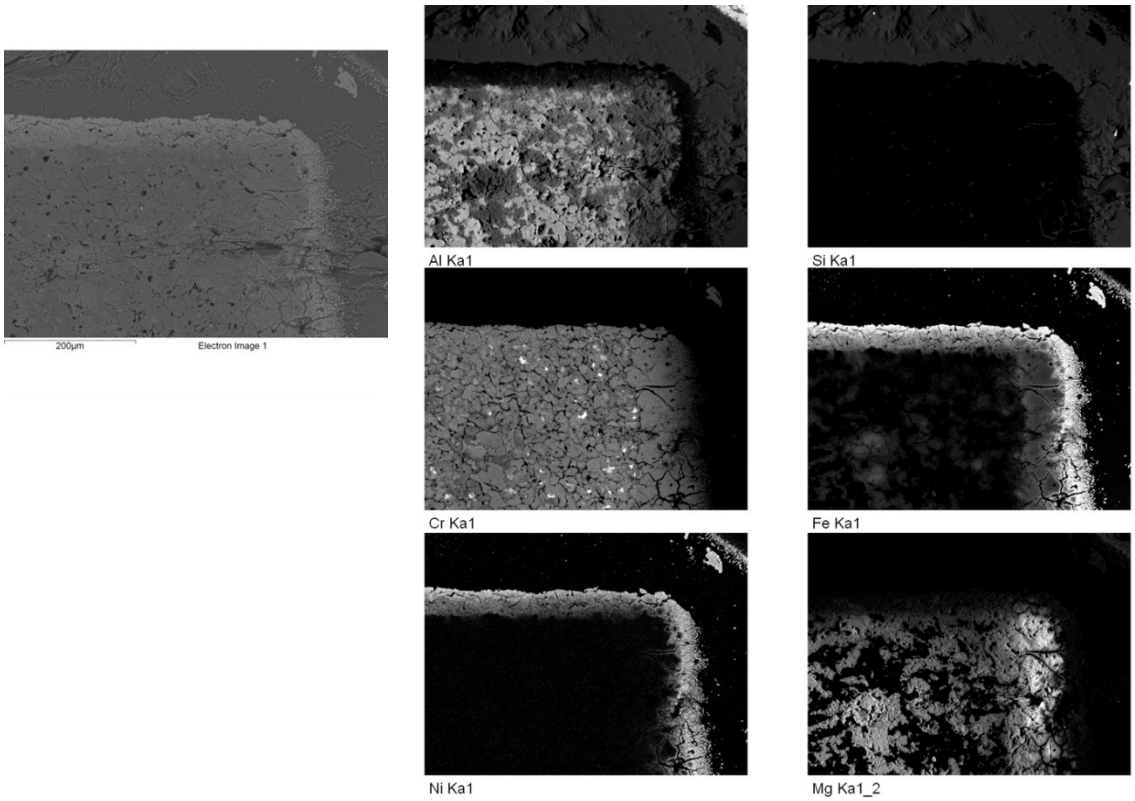

Figure E-5. Images of the a) and b) hot wall face and c) and d) cut face of a K-3 coupon immersed in GN78 melter feed after heat treatment for 120 hours. The regions measured for this study are shown as numbered lines.

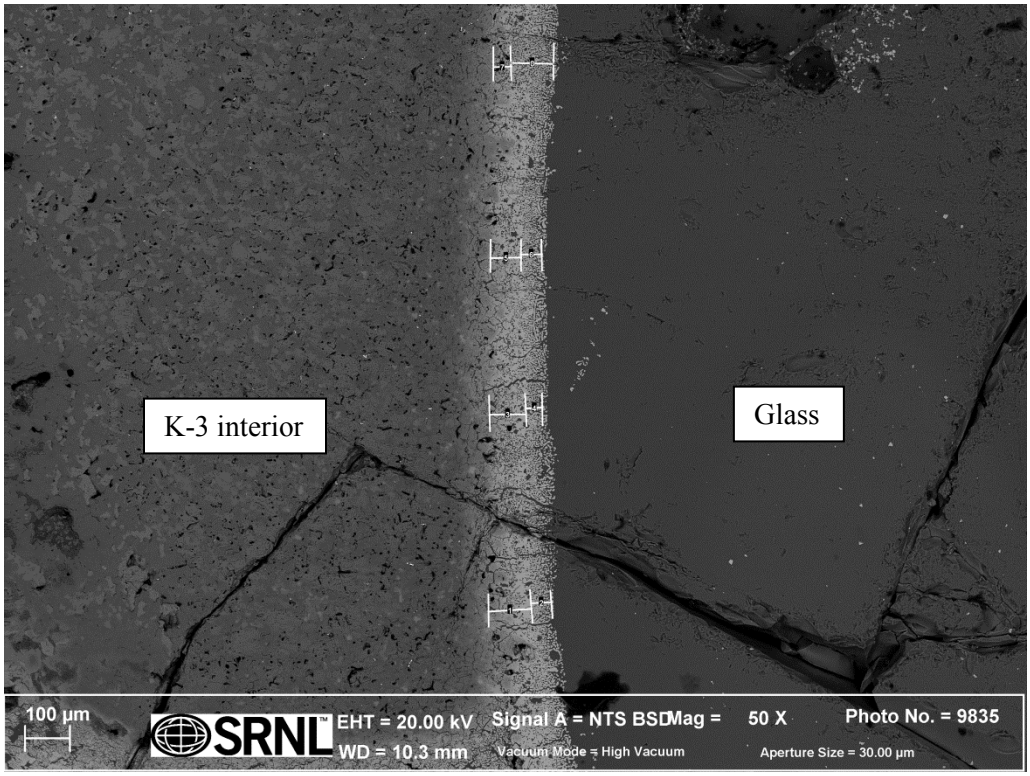

a)

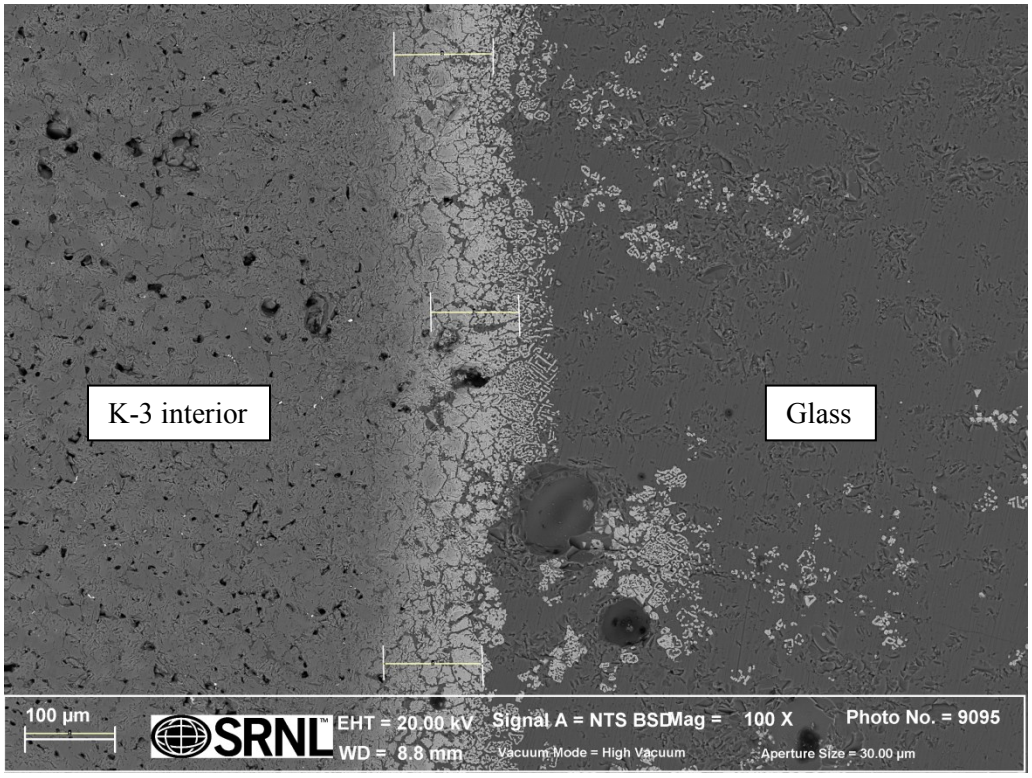

b)

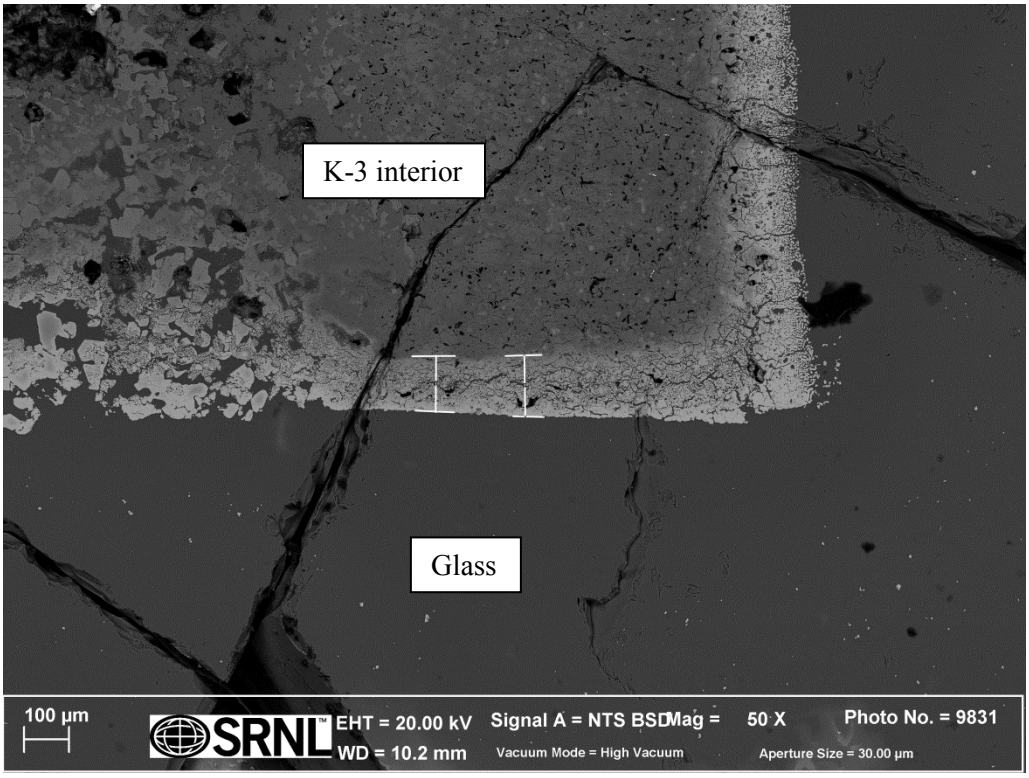
K-3 interior
Glass
100 µm
SRNL
EHT = 20.00 kV
WD = 10.2 mm
Signal A = NTS BSD
Mag = 50 X
Vacuum Mode = High Vacuum
Photo No. = 9831
Aperture Size = 30.00 µm

c)

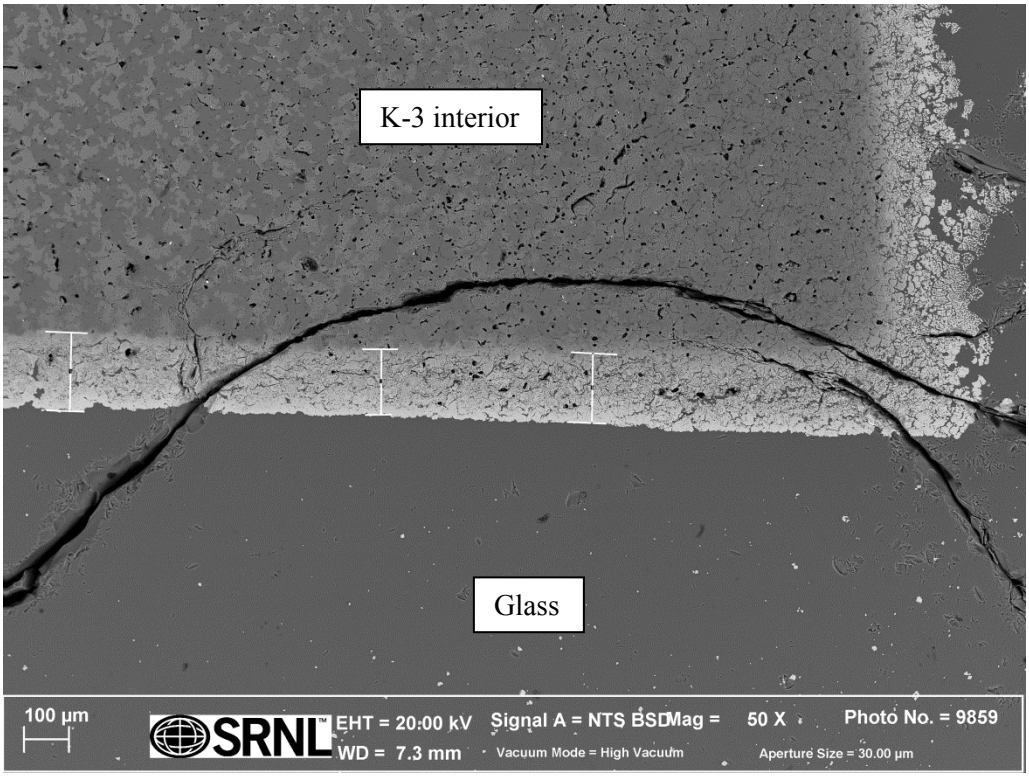
K-3 interior
Glass
100 µm
SRNL
EHT = 20.00 kV
WD = 7.3 mm
Signal A = NTS BSD
Mag = 50 X
Vacuum Mode = High Vacuum
Photo No. = 9859
Aperture Size = 30.00 µm

d)

Figure E-6. SEM Elemental Maps of K-3 Coupon Embedded GN78 Melter Feed for 120 Hours.

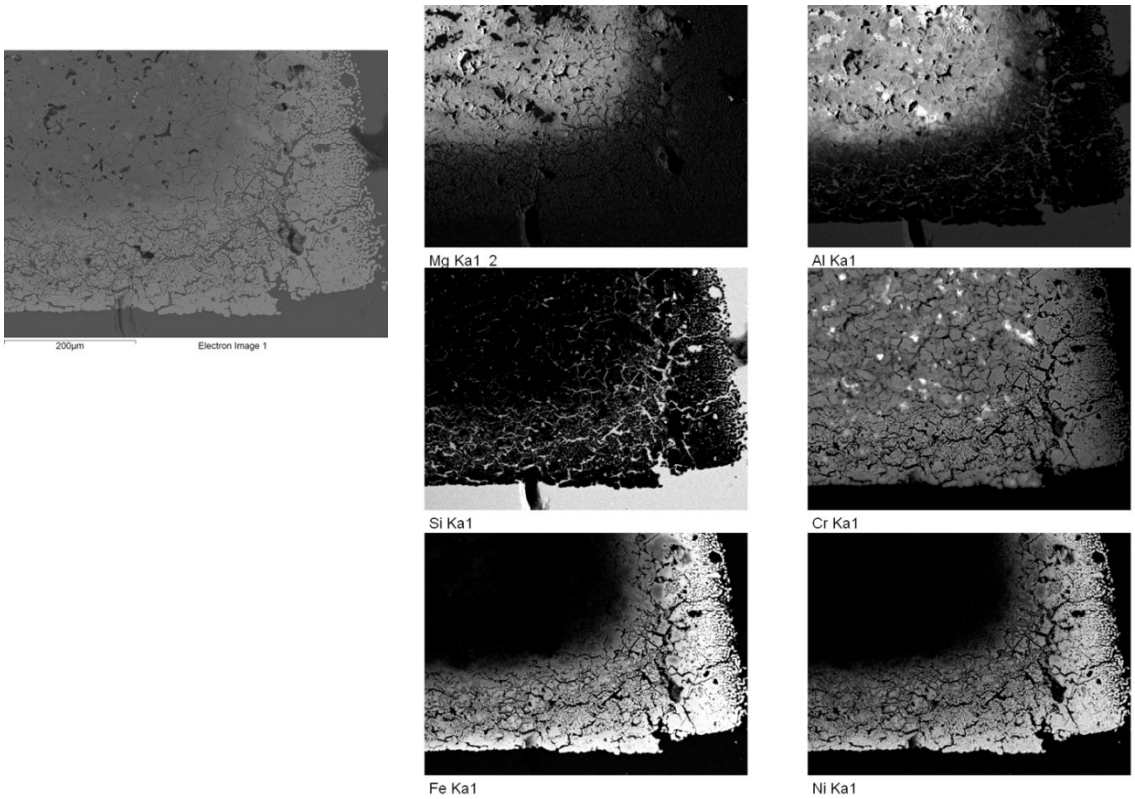

Appendix F. SEM Images of K-3 Coupons in GN79 Melter Feed.

Figure F-1. Images of the a) and b) hot wall face and c) and d) cut face of a K-3 coupon immersed in GN79 melter feed after heat treatment for 4 hours. The regions measured for this study are shown as numbered lines.

a)

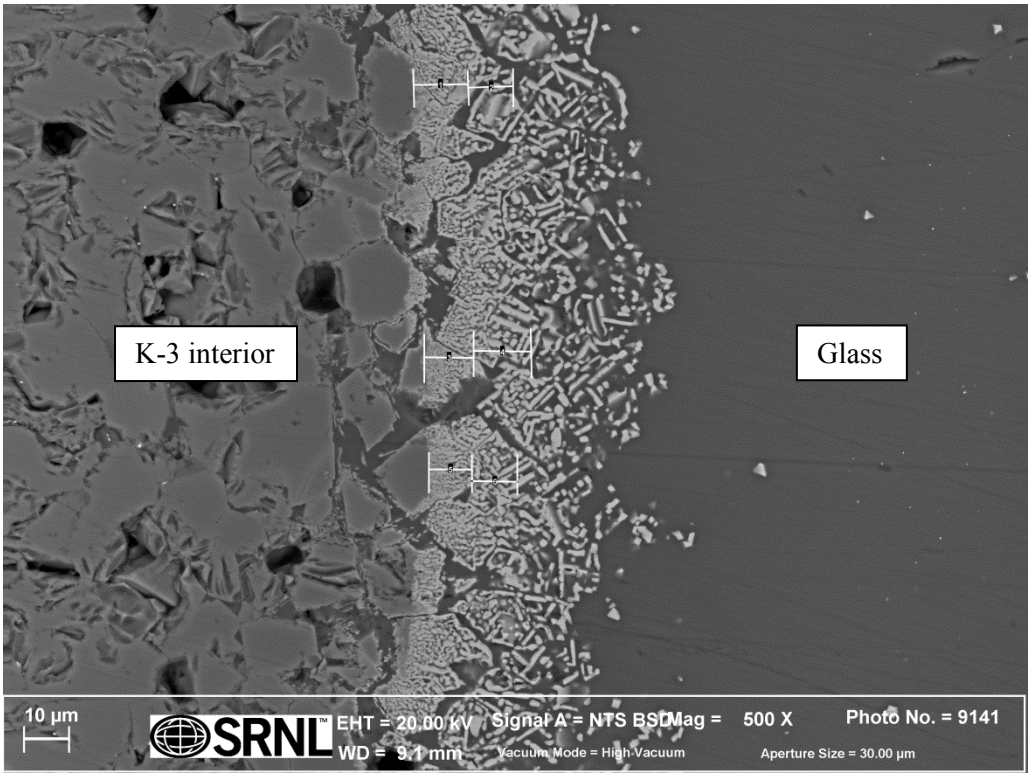

b)

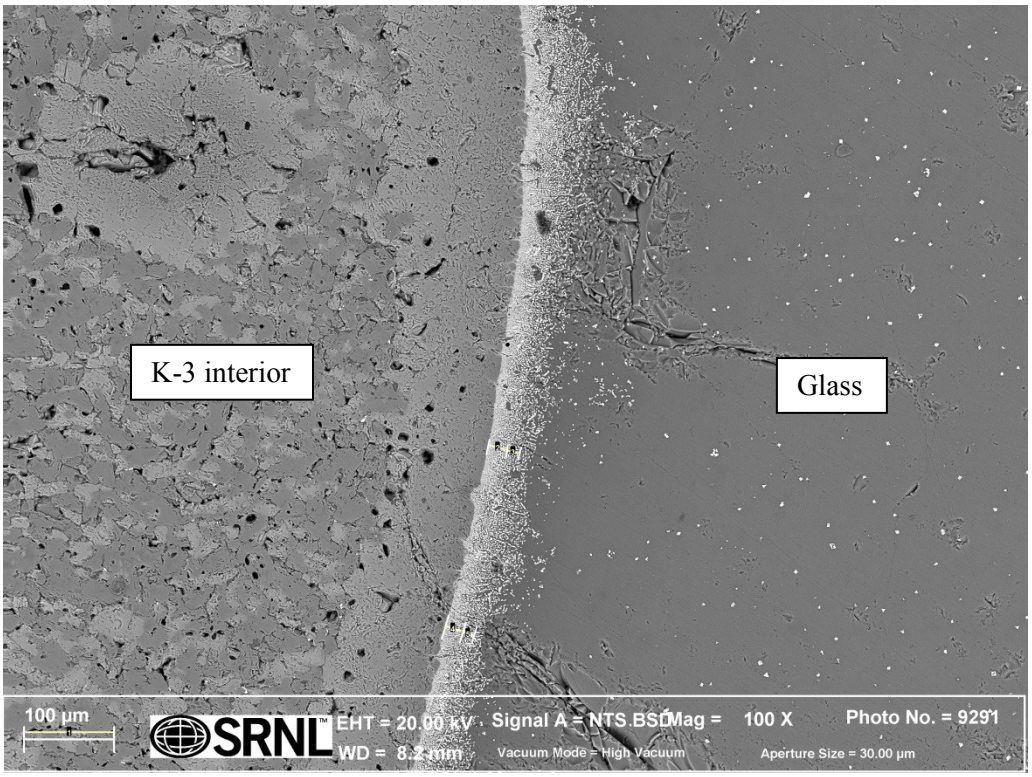
K-3 interior
Glass
100 µm
SRNL
EHT = 20.00 kV
WD = 8.2 mm
Signal A = NTS BSD
Mag = 100 X
Photo No. = 9291
Vacuum Mode = High Vacuum
Aperture Size = 30.00 µm

c)

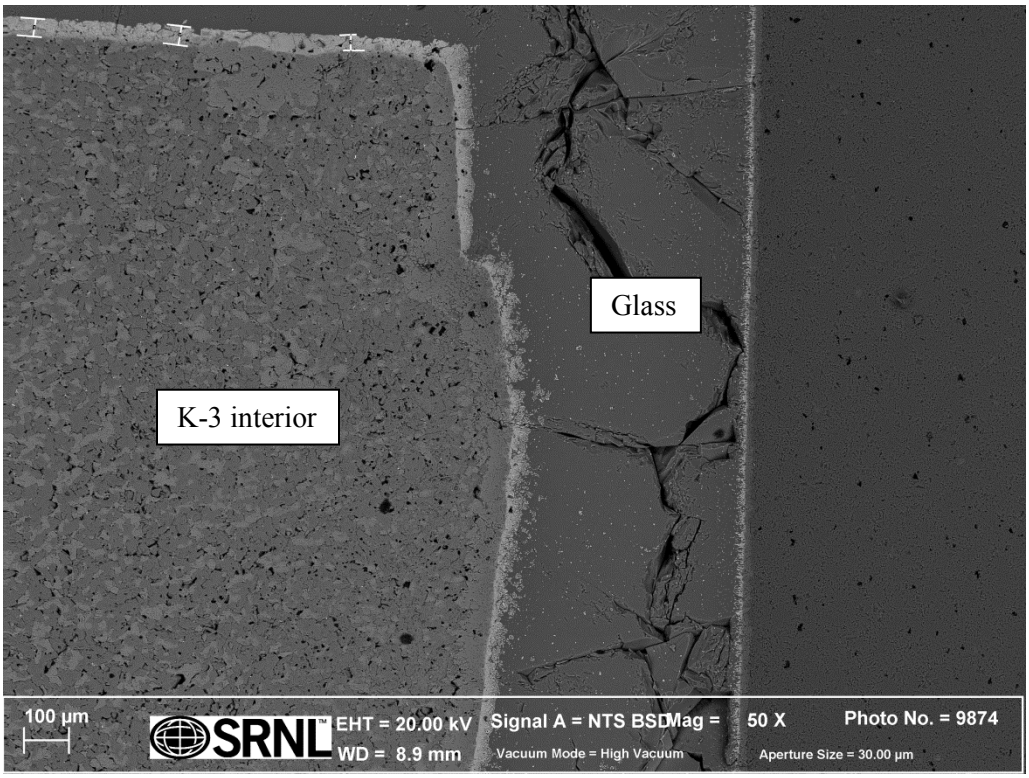
Glass
K-3 interior
100 µm
SRNL
EHT = 20.00 kV
WD = 8.9 mm
Signal A = NTS BSD
Mag = 50 X
Photo No. = 9874
Vacuum Mode = High Vacuum
Aperture Size = 30.00 µm

d)

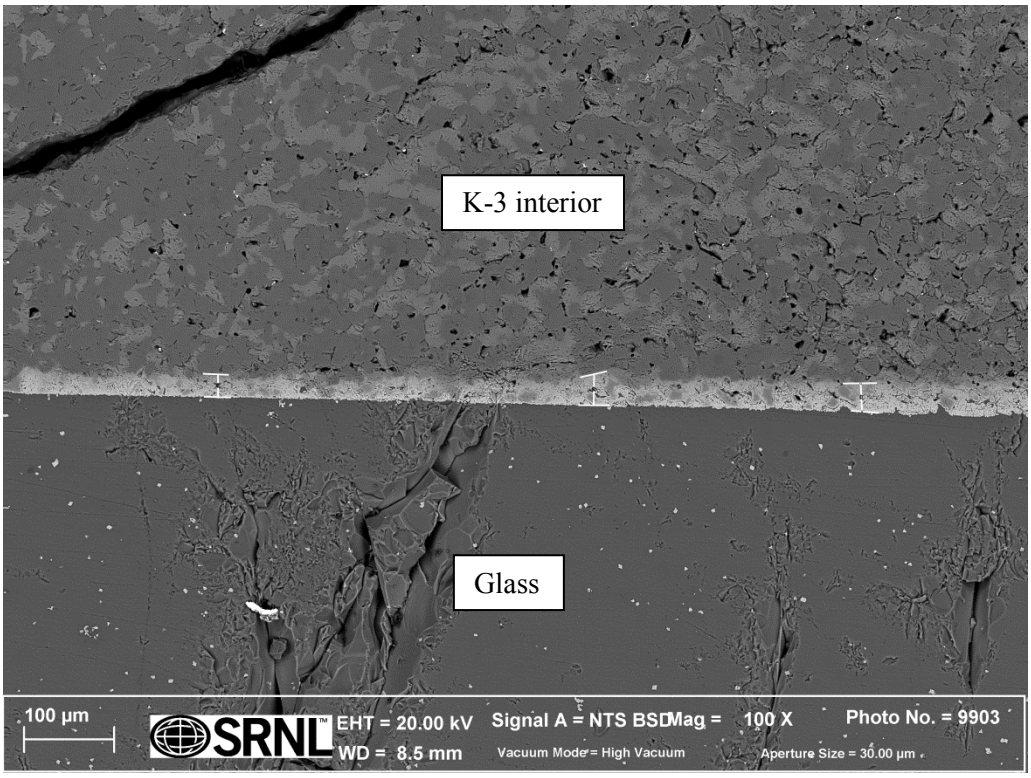

Figure F-2. SEM Elemental Maps of K-3 Coupon Embedded GN79 Melter Feed for 4 Hours.

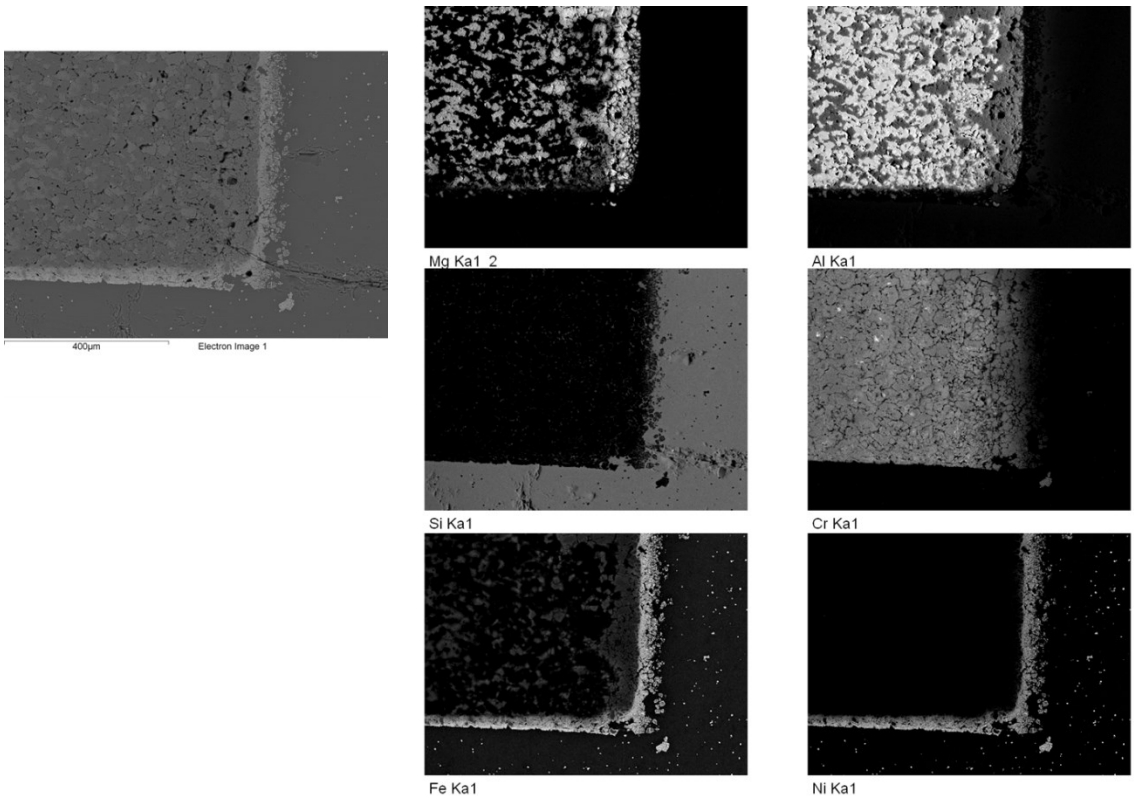

Figure F-3. Images of the a) and b) hot wall face and c) and d) cut face of a K-3 coupon immersed in GN79 melter feed after heat treatment for 24 hours. The regions measured for this study are shown as numbered lines.

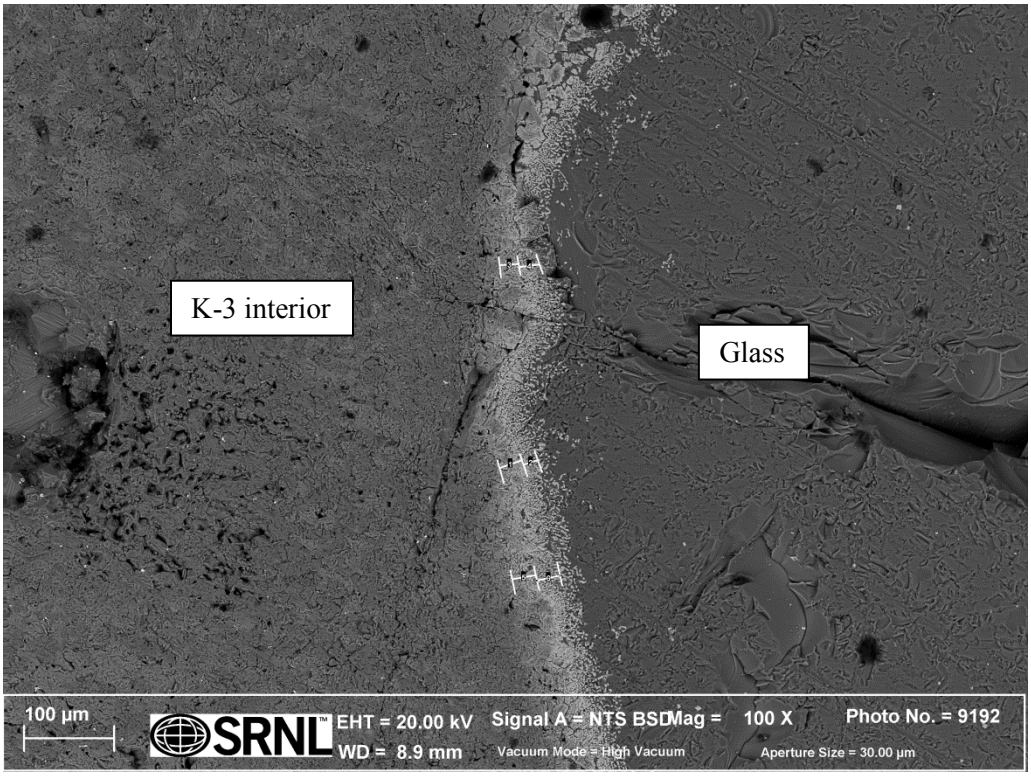

a)

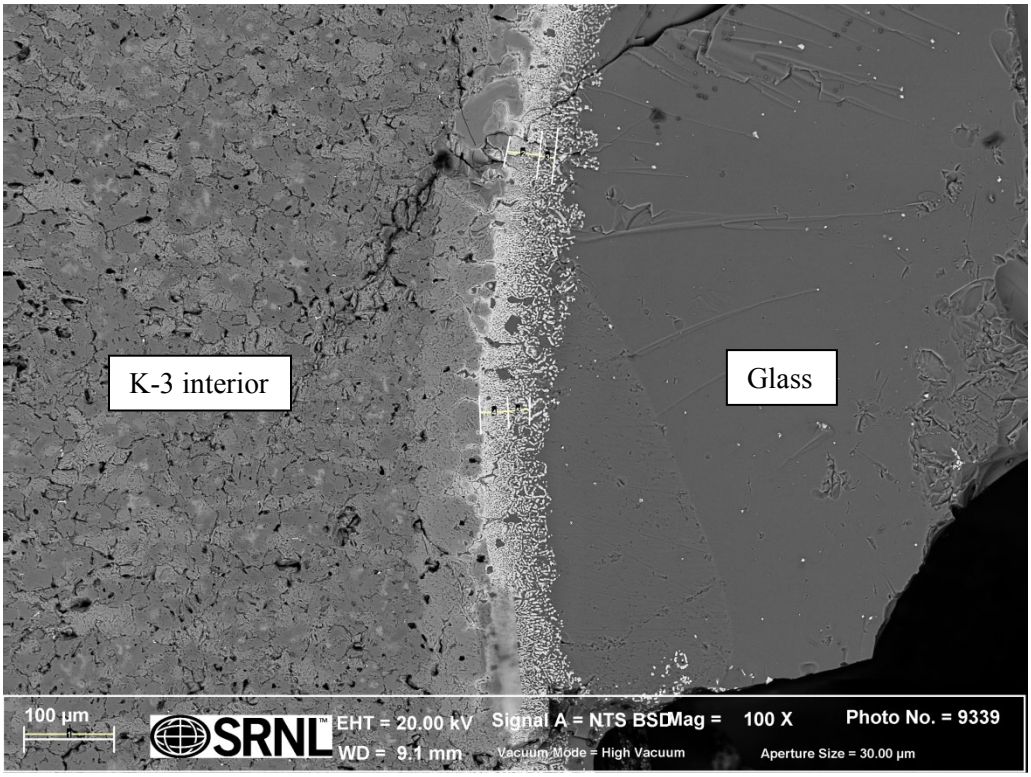

b)

c)

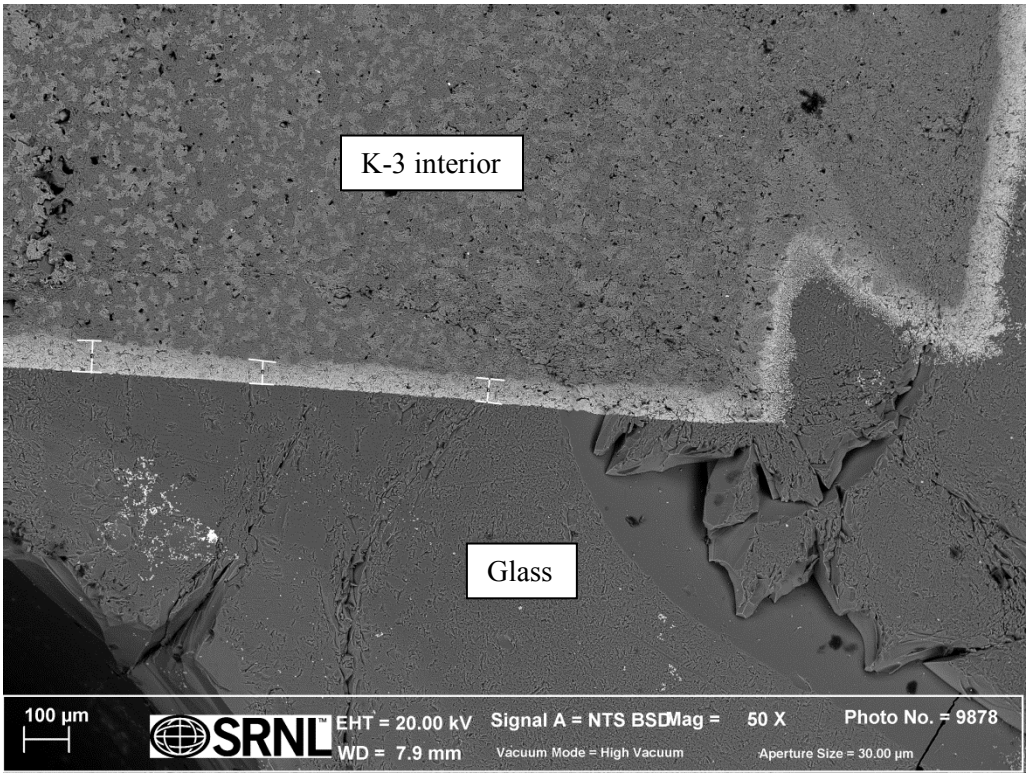
K-3 interior
Glass
100 µm
SRNL
EHT = 20.00 kV
WD = 7.9 mm
Signal A = NTS BSD
Mag = 50 X
Photo No. = 9878
Vacuum Mode = High Vacuum
Aperture Size = 30.00 µm

d)

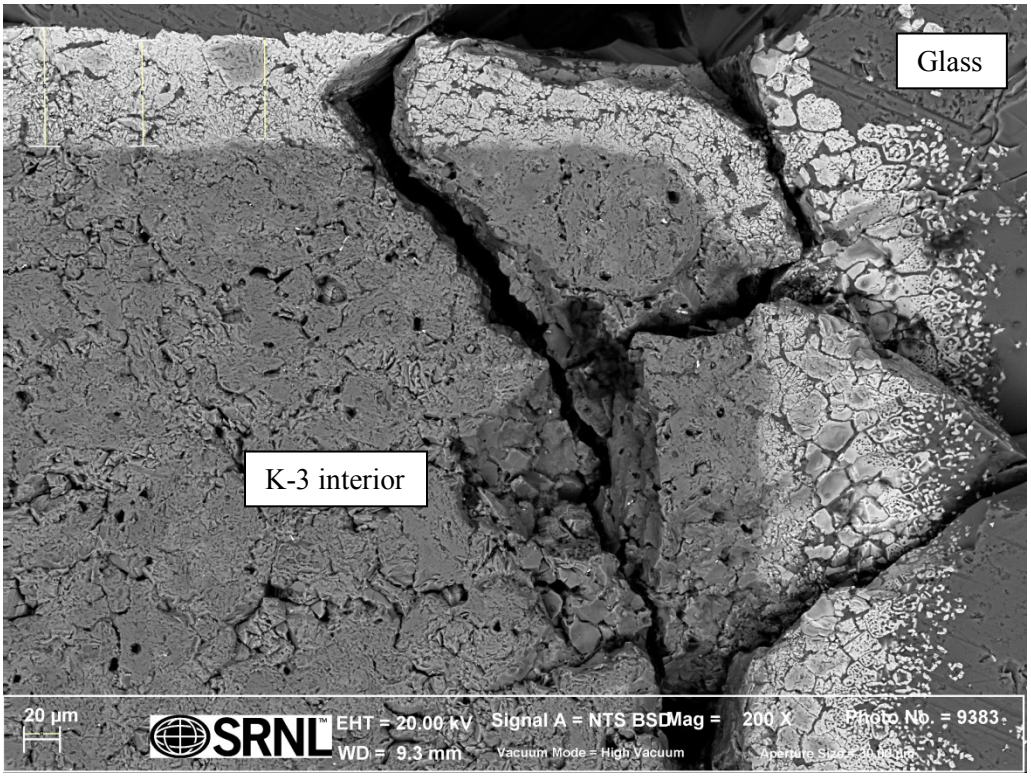
Glass
K-3 interior
20 µm
SRNL
EHT = 20.00 kV
WD = 9.3 mm
Signal A = NTS BSD
Mag = 200 X
Photo No. = 9383
Vacuum Mode = High Vacuum

Figure F-4. SEM Elemental Maps of K-3 Coupon Embedded GN79 Melter Feed for 24 Hours.

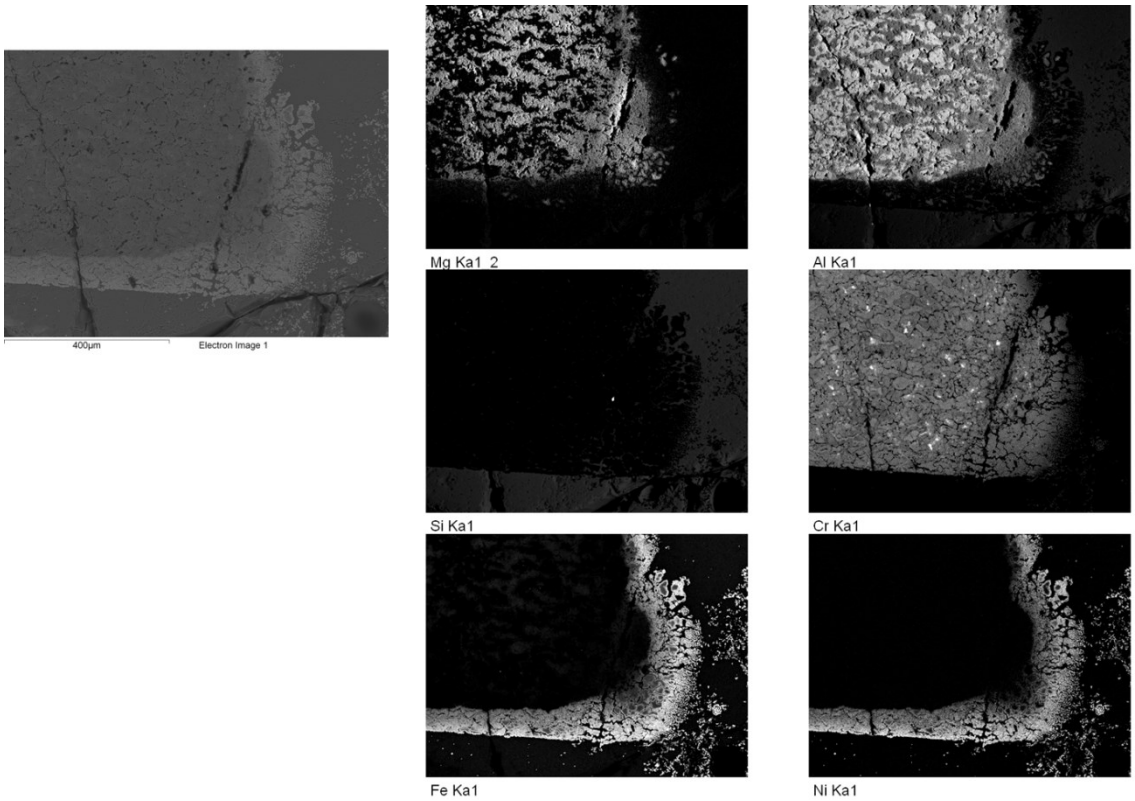

Figure F-5. Images of the a) and b) hot wall face and c) and d) cut face of a K-3 coupon immersed in GN79 melter feed after heat treatment for 120 hours. The regions measured for this study are shown as numbered lines.

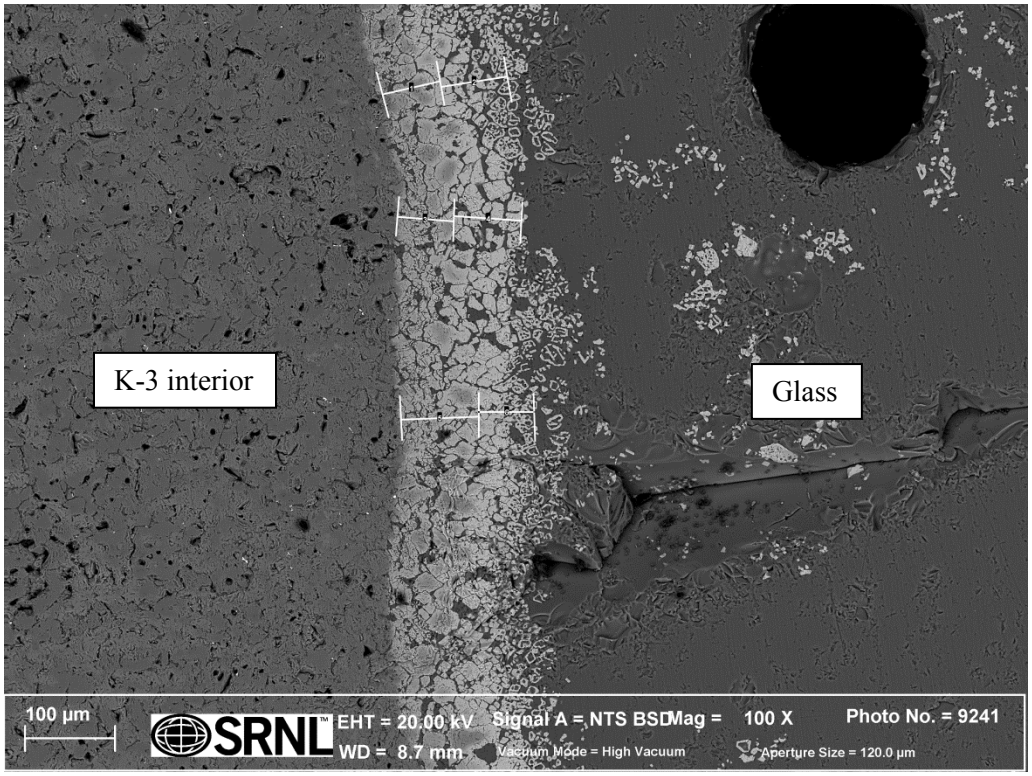

a)

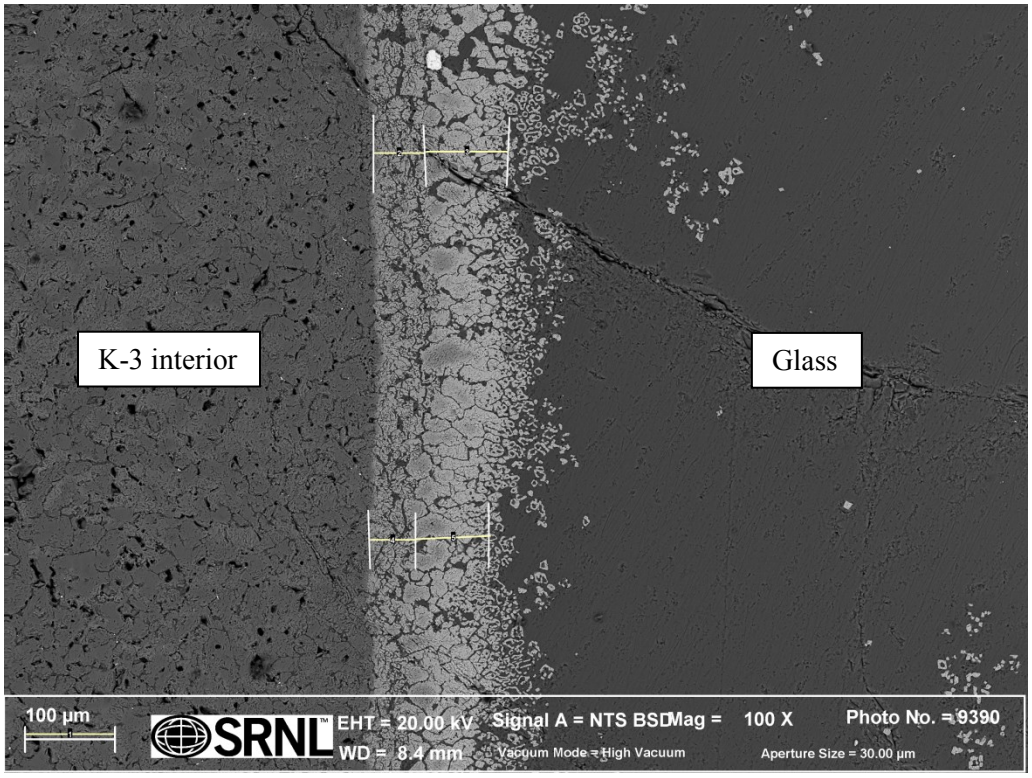

b)

c)

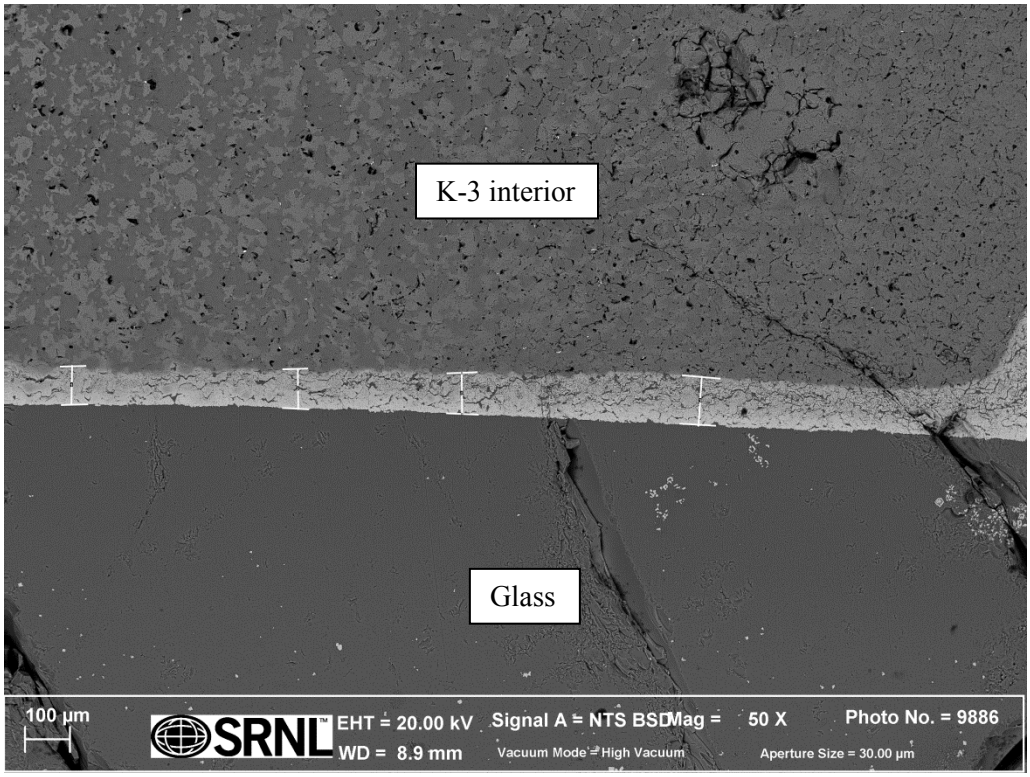
K-3 interior
Glass
100 µm
SRNL
EHT = 20.00 kV
WD = 8.9 mm
Signal A = NTS BSD
Vacuum Mode = High Vacuum
Mag = 50 X
Aperture Size = 30.00 µm
Photo No. = 9886

d)

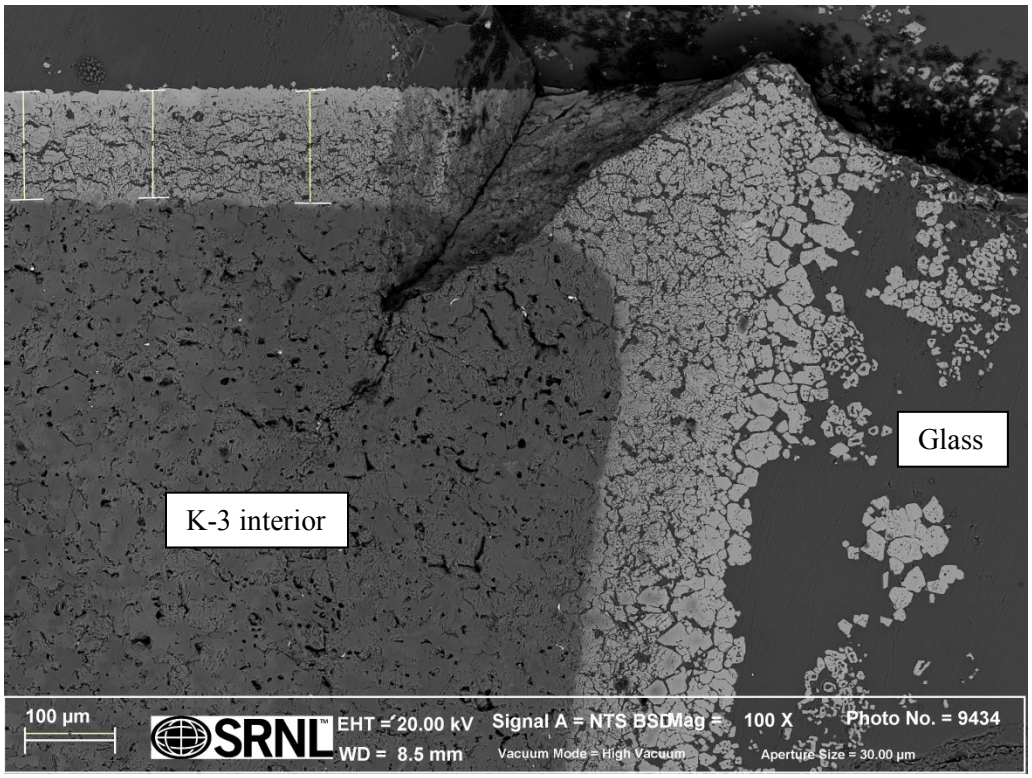
Glass
K-3 interior
100 µm
SRNL
EHT = 20.00 kV
WD = 8.5 mm
Signal A = NTS BSD
Vacuum Mode = High Vacuum
Mag = 100 X
Aperture Size = 30.00 µm
Photo No. = 9434

Figure F-6. SEM Elemental Maps of K-3 Coupon Embedded GN79 Melter Feed for 120 Hours.

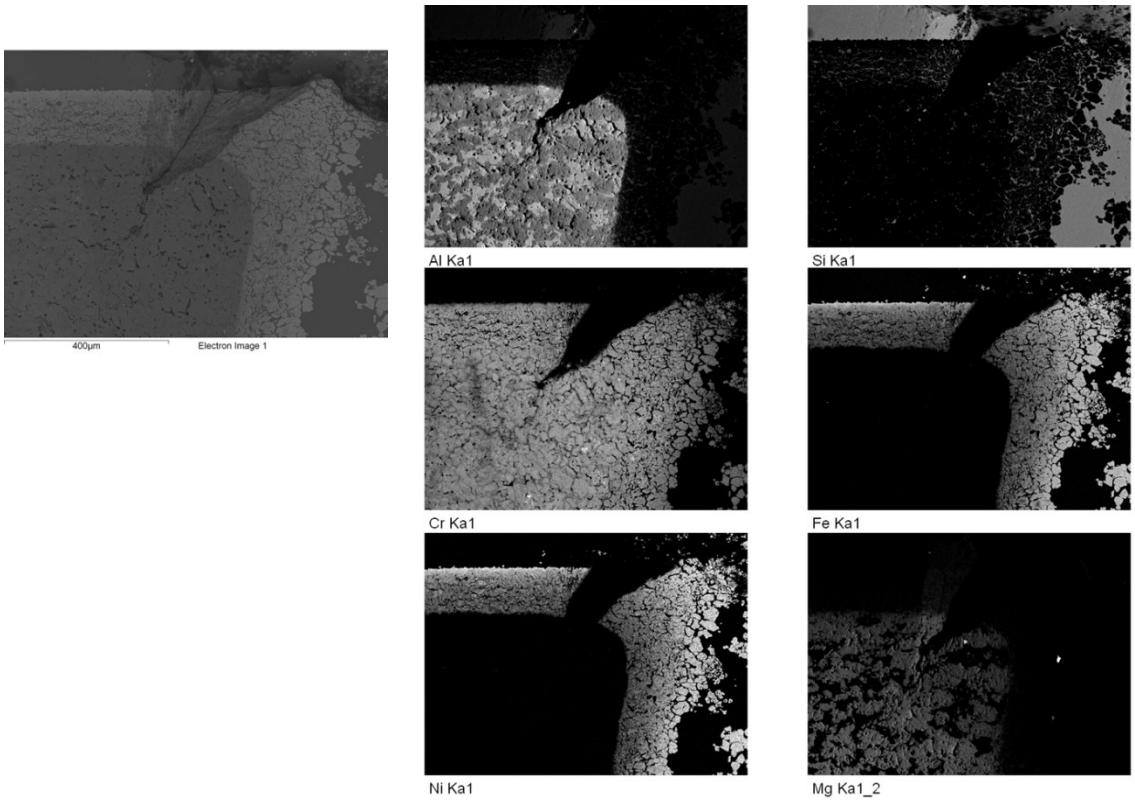

Distribution:

T. B. Brown, 773-A
M. E. Cercy, 773-42A
D. A. Crowley, 773-43A
A. P. Fellinger. 773-42A
S. D. Fink, 773-A
C. C. Herman, 773-A
D. T. Hobbs, 773-A
E. N. Hoffman, 999-W
J. E. Hyatt, 773-A
K. M. Kostelnik, 773-42A
B. B. Looney, 773-42A
D. A. McGuire,
T. O. Oliver, 773-42A
F. M. Pennebaker, 773-42A
G. N. Smoland, 773-42A
B. J. Wiedenman, 773-42A
W. R. Wilmarth, 773-A
Records Administration (EDWS)

H. P. Boyd, 704-27S
J. M. Bricker, 704-S
J. S. Contardi, 704-56H
T. L. Fellinger, 766-H
E. J. Freed, 704-S
J. M. Gillam, 766-H
B. A. Hamm, 766-H
E. W. Holtzscheiter, 766-H
J. F. Iaukea, 704-27S
V. Jain, 766-H
C. J. Martino, 999-W
J. W. Ray, 704-27S
P. J. Ryan, 704-26S
M. A. Rios-Armstrong, 766-H
H. B. Shah, 766-H
D. C. Sherburne, 249-8H
C. Sudduth, 707-7E

C. E. Brown, 773-A
P. E. O'Rourke, 773-A
H. M. Ajo, 773-A